Coupled heat and water transport in bare soils in semi-arid and arid regions

Thesis report

Thomas Berends

Soil Physics, Ecohydrology and Groundwater Management Group

Date: March 5, 2012
Supervisors: Dr. K. Metselaar, Dr. J.C. van Dam and MSc. E. Balugani

Thesis report

Coupled heat and water transport in bare soils in semi-arid and arid regions

Thomas Berends

March 5, 2012

Wageningen University
Soil Physics, Ecohydrology and Groundwater Management Group
Supervisors: Dr. K. Metselaar, Dr. J.C. van Dam and MSc. E. Balugani

Contents

List of Tables

List of Figures

Summary

For more than 50 years coupled heat and water transport is an interesting topic in the field of vadose zone hydrology. One basis is the theory by Philip & de Vries (1957) which couples the mass balance for water, the Richards equation, with a heat conservation equation based on Fickian diffusion process. In this thesis the contribution of water vapour flow to the total water movement on a daily time scale is analysed. At first the literature is reviewed, starting from the theory of Philip and de Vries and the many papers which have continued on this theory. Next to the theory also the literature on experiments associated to coupled transport is reviewed, distinguishing field and laboratory experiments. Data were collected during field work in Trabadillo, Spain under semi-arid weather conditions. Soil water pressure, soil water content and soil temperature were measured for 149 days on an hourly interval during the dry period. The soil hydraulic and soil thermal parameters are calibrated on this data in Hydrus-1D by using an inverse parameter estimated method. In the calibrated Hydrus model Monte Carlo simulations are performed to include the uncertainty in the parameters. Instantaneous fluxes of liquid water, isothermal water vapour and thermal water vapour flow are examined at multiple moments in time. Selecting fluxes for inclusion on an daily time basis in the SWAP model, the Hydrus 1-D isothermal water vapour flow is zero during night and day and is therefore not included in the SWAP model. A significant daily pattern is identified for the thermal water vapour flux and this flux is implemented in SWAP in addition to the standard isothermal liquid water flux. The cumulative net flux is computed for four different models, a Hydrus and SWAP model with only liquid water transport and a Hydrus and SWAP model with both coupled heat and water transport. Intercomparison between the four model versions showed that the contribution of water vapour flow is insignificant compared to the total transport of water. As a sensitivity analysis in addition to the soil hydraulic parameters from the field situation, simulations are also performed for a European set of soils from the HYPRESS project Wosten *et al.* (1999). The Hydrus model did not converge to a satisfactory numerical solution with a maximum spatial discretisation of 1 cm, which is advised by Simunek *et al.* (2008). In SWAP the contribution of water vapour movement to the total water transport is insignificant on a daily time scale for all the soil types. Finally a laboratory experiment design is proposed with the focus on coupled heat and water transport. The plan for the laboratory experiment will be based on the experience from the fieldwork and the literature study. Important components for this plan are the type of measurement devices, the spatial set-up of those devices and the boundary conditions. A model study is executed to look for the optimal measurement set-up for a laboratory experiment to liquid water and water vapour transport. Inverse modelling is used to determine the soil hydraulic and soil heat parameters from a selection of data and direct modeling is performed with the determined parameters to compare the accuracy of these parameters and so the data selection. The optimal laboratory design according to the model study includes measurements of soil temperature, soil water content and soil water pressure at depths of 5, 25 and 50 cm beneath the soil surface.

Acknowledgements

This thesis had all the elements which I wanted to do during my thesis. I've been on field work to Spain where I learned a lot about doing field experiments. Many issues like how to set up a field experiment, how to use the measuring devices, how to download the data, how to deal with problems about the experiment. But also about the external issues which arise by doing a field experiment. Field experiments seem not so complex to me as they were explained in lectures. However by really doing the field experiments I faced the problems with permissions. How to deal with the area your experiments takes place? How to deal with the animals? Always watch out for aggressive fighting bulls and dangerous land owners with rifles.
This thesis consist for the main part of modeling, which I prefer to do. In the programming language R I performed many simulations with the models Hydrus and SWAP and further all the processing I've done in R. The programming issues I faced were not annoying because I really like to solve these issues and let it work as it was suppose to work. The bottleneck of the modeling part was the Hydrus model. The two non-linear partial differential equations are solved numerically in an implicit way. This makes the model sensitive for mass balance errors, convergence problems, and wrongly calculated results. Because of my naivety I trusted the model results if the model converged, although I found later that the mass balance errors were unacceptably large. In the end every problem with the Hydrus model was solved in one way or another, and the learning point was clear to me; never trust a model based on one aspect, but investigate all the output critically.
I also want to thank my supervisors Dr. K. Metselaar and Dr. J. van Dam for supervising me during the entire thesis. Supportive feedback and advice help me to overcome the several problems I faced. The weekly meetings were very helpful and further I really appreciated the freedom they gave me to make this thesis my own thesis. More specifically I want to thank K. Metselaar for the opportunity to go on field work and for the creative and inspiring meetings. And J. van Dam for the support on the modeling part of this thesis, especially for the implementation of water vapour flow in SWAP. Further I want to thank my third supervisor MSc. E. Balugani for the advice for my problems, the extensive explanation of his laboratory and field experiments, the data collection and especially for all the guidance during the field trip. I had an interesting and great time in Salamanca and I learned a lot about the internal and external issues associated with field experiments.

1 Introduction

1.1 General

In the hydraulic cycle the vadose zone plays a central role, as it connects the atmosphere and the deeper groundwater. Many processes have an influence on the vadose zone, e.g. precipitation, evaporation, groundwater recharge, vegetation growth, irrigation, ploughing, diurnal heating, etc. These processes and many more will result in different kind of fluxes in the vadose zone with respect to water, heat and solutes. In this thesis the focus is on the first two, water and heat fluxes. The fluxes of heat, liquid water and water vapour are the major components in the energy and water balances in the subsurface. These fluxes are driven by soil water pressure gradients and temperature gradients. In semi-arid and arid regions the topsoil is often in an unsaturated condition with respect to soil water and the atmospheric conditions demand high evaporation rates. Water scarcity will easily occur in these regions which will result in problems for agriculture, drinking water supply and many other sectors. A good understanding of the vadose zone hydrology is crucial for good water management in these sectors. For them it is interesting to know the contribution of water vapour flow to the total water flux on a daily time scale for water balances. The small scale fluxes inside the soil are often not of their interest. According to the paper by Milly (1984) vapour movement contributes significantly to the total water flux in the soil in semi-arid and arid areas. Despite of the large amount of studies in the context of theories of vapour transport within the soil, coupled heat and water movement models are still not able to simulate the field situation properly. This thesis will try to draw a conclusion with respect to the contribution of water vapour flow to the evaporation fluxes.

1.2 Problem definition

Many models used for water management only deal with liquid water transport and neglect water vapour fluxes. Most of the time water vapour transport is neglected because of the lack of a model based on theory which is in correspondence with the measurements and the large amount of uncertainty about the contribution of water vapour flow. Almost every study about the coupling between heat and water movement in soils starts with the theory of Philip & de Vries (1957) and in many scientific papers, like in Jackson *et al.* (1974); Parlange *et al.* (1998); Saito *et al.* (2006) the researches refer to the theory from Philip and de Vries as *the theory*. The theory couples two partial differential equations, one mass conservation equation for water and one heat conservation equation. To solve these equations some additional parameters and variables need to known, but these parameters and variables are difficult to determine experimentally. Parameters like the pore-connectivity coefficient and the enhancement factor are still very inconvenient in research (Sakai *et al.*, 2009; Smits *et al.*, 2011; Webb & Ho, 1998). The importance of convective vapour flow relative to diffusive vapour flow is still uncertain. Parlange *et al.* (1998) argue in favour of convective vapour flow and diffusive flow. Whereas Rose (1968b) and Bittelli *et al.* (2008) note that only diffusive vapour flow occurs. In the paper by Smits *et al.* (2011) the assumption that water vapour and liquid water are in equilibrium is critically investigated. However often the most important issue is that the laboratory and field experiments don't result in measurements which are accurate enough to validate the developed theoretical models and to determine accurate parameter values. The discrepancy between experiments and models is most of the time corrected in the models by calibration of the inconvenient parameters like the enhancement factor (Sakai *et al.*, 2009). Without these vague calibrated parameters there is still not a distinctive model describing the complex processes of coupled heat and water movement in the soil which is in agreement with the experiments in the field.

1.3 Research objective

Given the above it is desirable to define a model which is in agreement with the field experiments on a daily time scale. To achieve that I set up multiple goals. First of all a literature study will be performed with the focus on the theory and the experiments on coupled heat and water movement in the soil. The literature will be the base for the modeling part. Subsequently the four fluxes (isothermal liquid flux, thermal liquid flux, isothermal vapour flux, thermal vapour flux) will be simulated from the acquired field data with the Hydrus-1D model (Simunek *et al.*, 2008). To do so the model has to be calibrated and the soil hydraulic properties will be estimated by an inverse parameter estimation method. Also the soil thermal properties will be fitted to the measurements. With the calibrated soil hydraulic properties and soil thermal properties the different fluxes will be investigated for the Hydrus model; the liquid water flux, the isothermal water vapour flux and the thermal water vapour fluxes. The fluxes which contribute the most to the total transport of water will be implemented into the SWAP model. The purpose of this new SWAP version is to be able to simulate combined vapour and liquid fluxes on a daily time scale and so determine the amount of evaporation. Thus in total four models will be used to explore the contribution of water vapour transport. Two models in SWAP and Hydrus with only liquid water movement and two coupled liquid water and water vapour transport models in Hydrus and SWAP. Due to a lack of experimental data the four models will be compared and conclusions will be drawn from simulations using these models. The ability to compare the developed coupled SWAP model with the coupled Hydrus model depends on the stability, accuracy and uniqueness of the coupled Hydrus model. Further simulations will be performed with the four models to discuss the contribution of water vapour flow in other types of soils. The soils from the HYPRESS project will be used for these simulations (Wosten *et al.*, 1999). Finally I will describe a plan for a laboratory experiment with the focus on the developed coupled SWAP model. Experience gained during the field work and knowledge from the literature study regarding the experiment will be used for the development of the laboratory experiment. Accuracy, type of measurement devices, spatial setup and boundary conditions are important components and issues for this experimental plan. A model study will be executed to find the optimal measurement depths and measurement types for a study on liquid water and water vapour transport in (semi-)arid conditions.

1.4 Research questions

Main question:

How important is water vapour movement in coupled heat and water flux models for bare soils in semi-arid and arid regions on a daily time scale?

Subquestions:

- Is the Hydrus-1D model able to simulate the field data?
- Can water vapour movement be implemented in the SWAP model to describe the coupled heat and water movement on a daily time scale?
- How to set up a laboratory experiment to measure accurately the variables for coupled heat and water movement models?

2 Theoretical framework from literature

2.1 Literature

2.1.1 Setup of theory by Philip and de Vries

The coupling between heat and water movement in the unsaturated soil has been an interesting topic for many researchers for many years. Bouyoucos (1915) was one of the first researchers who describes the coupling between heat and water movement. In 1957 an important theory of coupled heat and water movement was published by Philip & de Vries (1957) and till nowadays this theory is still the fundament for subsequent theories developed later in time. From now on in this thesis report *the theory* will refer to the theory by Philip & de Vries (1957). Philip and de Vries were the first who describe vapour diffusion in a porous media without neglecting the interaction between water vapour, liquid water and the solid media. With their theory, Philip and de Vries were able to predict the orders of magnitude and the general behaviour of the fluxes which were in agreement with their experimental data (Philip & de Vries, 1957). In the theory of Philip and de Vries equations based on Ficks law are introduced, which describe heat and water movement in porous media under moisture and temperature gradients. Four soil water content dependent diffusivity coefficients are used in the mass conservation equation which are related to the four fluxes, the thermal and isothermal liquid water flux, and the thermal and isothermal water vapour flux. According to Philip & de Vries (1957) the thermal fluxes have a maximum at an intermediate moisture content. In very dry and very wet media these fluxes are quite small. Thermal water fluxes are dependent on both matric potential and the air-filled pore space (Philip & de Vries, 1957). Finally an enhancement factor is defined for the thermal vapour flux. This enhancement factor takes two pore-scale processes into account; (a) the movement of water through a 'liquid island' in a soil pore where condensation takes place at one end and evaporation at the other end, and (b) a higher flux due to a significantly higher local temperature gradient in air-filled pores with respect to the average temperature gradient in the bulk soil (Philip & de Vries, 1957; Sakai *et al.*, 2009). This enhancement factor is hard to measure directly, but indirectly this parameter can be estimated based on the pressure head dependence of the thermal conductivity (Cass *et al.*, 1984).

An experiment was set up by Rose (1963) to estimate the four conductivity coefficients for different soil water content conditions from near saturation to dryness. The vapour conductivity coefficients were estimated from hydrogen diffusion in porous solids and the liquid conductivity coefficients were computed from pore size distributions and estimated from water transport experiments. Rose also defined six stages in the wetting of a porous media; adsorption, vapour transfer, distillation, surface creep (flow in surface films), unsaturated hydraulic flow and saturated hydraulic flow.

In 1968 Rose et al. (1968a; 1968b) did one of the first field studies to analyse coupled heat and water transfer in the soil. The observations show discrepancies compared to the calculated model results based on the model of Philip & de Vries (1957). Observations showed that the thermal liquid flux was very small compared to the isothermal liquid flux. Although the isothermal liquid flux has a dominant direction, the thermal vapour flux oscillates due to the diurnal heating effects. During the day the soil surface will heat up and higher temperature will be found on top. This results in a downward flux during the day. During the night the soil surface will cool down which result in lower soil temperatures in the topsoil, which result in an upward thermal vapour flux during night. And although Rose (1968b) found some evidence supporting the enhancement factor, it also results in uncertainties. Finally Rose et al. (1968b) also discussed the possibility of a convective air flow through the soil which could explain the discrepancy between observations and computations. However for the experimental conditions measured by Rose (1968b) this effect accounts for only 0.1% of the total vapour flux (Bittelli *et al.*, 2008).

The theory of Philip and de Vries was tested by Jackson *et al.* (1974) in a laboratory experiment. The thermal vapour diffusivity coefficient was calculated and the theory gives a good result with respect

to the laboratory observations for intermediate water contents. In very wet and very dry situations deviations were larger, but Jackson et al. stresses that this could be due to the inaccuracy of the diffusivity coefficients. These coefficients which are dependent on soil water content and soil temperature, must be accurately determined to get reasonable results. They also remark that hysteresis should be taken into account for the isothermal vapour flow.
Milly (1984) has simulated the theory (Philip & de Vries, 1957) for two climate conditions, the combinations cool and wet, and warm and dry. Specifically his study focuses on the four fluxes. The thermal liquid flux is the smallest flux compared to the others and also in an absolute sense this flux is very small. Neglecting this flux will result in an maximum error of 1% in the computed evaporation (Milly, 1984). Milly (1984) gives as physical explanation that the thermal liquid flux will induce an increase of the isothermal liquid flux with an almost identical amount. And the isothermal liquid flux flows in the opposite direction compared to the thermal liquid water flux. So the thermal liquid water flux won't affect the total water flux. If the thermal vapour flux is neglected, evaporation is overestimated during daytime and underestimated at night and these errors are most significant under dry conditions. These errors are probably due to the assumed equilibrium conditions at the soil surface. The relative humidity is assumed to be instantaneously in equilibrium with the soil water pressure head at soil surface, and to be only dependent on the surface temperature. Processes like the formation of dew are not taken into account. However in the study by Milly (1984) these over- and underestimation errors won't effect the calculation of the daily average evaporation. He also concludes from the results of the simulation of both climates that the isothermal vapour flux is higher than the thermal vapour flux. Milly also rewrote the coupled equations of Philip and de Vries using the matric potential as dependent variable in stead of the soil water content. This will help to get rid of some difficulties in case the soil profile is inhomogeneous. Finally Milly stresses the importance of vapour movement with respect to the total water flux in arid regions, because of very low soil moisture contents near the soil surface.

2.1.2 Assumptions and limitations of the theory by Philip and de Vries

In 1987 de Vries published a review of the present status of the Philip and de Vries theory (De Vries, 1987). De Vries concludes that the usefulness of the theory for describing laboratory and field experiments is proven, but there are doubts about the ability to predict liquid water and water vapour flow by using this theory. These doubts have two origins; (a) limitations of the theory, and (b) uncertainty about the experiments. The limitations of the theory are (De Vries, 1987):

- Hysteresis with respect to the relation between soil water content and soil water pressure is not taken into account.
- The medium has to be rigid.
- Macroscopically the medium has to be homogeneous and isotropic.
- Processes like freezing and thawing are not included.
- Surface phenomena on the interface between soil and liquid like the Knudsen force, are neglected.

Further de Vries mentioned eight important assumptions of the theory:

- No solutes are present.
- Liquid movement is viscous, influenced by capillary and adsorptive forces.

- Vapour movement by diffusion.
- In the gas phase free convection can be neglected.
- Total air pressure is uniform and constant.
- Thermodynamic equilibrium between liquid and water vapour.
- No heat transfer by radiation.
- Density of liquid water, the soil water pressure, latent heat of vaporization and the specific heat coefficient of liquid water are all not temperature dependent.

2.1.3 Extensions Philip and de Vries and other theories

Bear *et al.* (1991) wanted to compute coupled heat and water movement for a project related to thermal energy storage in the unsaturated soil. The project was especially important for semi-arid and arid regions mainly due to the occurrence of deep aquifers. Bear *et al.* (1991) used a modified theory of Philip and de Vries to calculate coupled heat and water movement with in addition convective water vapour flow. The equations were solved analytically requiring a number of assumptions. Not all of the assumptions are realistic, for example one assumption states that the net energy transfer by the isothermal and thermal liquid flux is zero as the thermal liquid flux is included in the model. This seems to be in contradiction to the study of Saito *et al.* (2006). According to them the amount of sensible heat transferred by the isothermal liquid water flux is significant. Bear *et al.* (1991) conclude a drying soil has a reduced thermal conductivity and thus will transfer less energy. Thermal energy storage is not possible in the unsaturated soil in semi-arid and arid regions consisting of coarse sands, because coarse sands have a low water holding capacity.
Nassar and Horton expand the theory, and coupled solute transport to the coupled heat and water movement theory of Philip and de Vries (Nassar & Horton, 1997). They remark that an increase in soil water content and to a lesser extent the increase in temperature will increase the liquid water diffusivities. Isothermal and thermal vapour diffusivity coefficients also increase with an increase in temperature, an increase in water content will at first result in higher vapour diffusivity coefficients until a certain value and then the vapour diffusivities will decrease with increase in water content. No explanation is given for this phenomenon. Nassar and Horton stress the need to have accurate knowledge about the parameters, to be able to simulate coupled heat & water movement with a model in an accurate way.
Parlange *et al.* (1998) note that a good agreement between theory and field results has not been found yet. They give two explanations for this lack of agreement; (a) most observations result from laboratory experiments with steady state boundary conditions and (b) only a few field experiments have been performed to test the theory. Parlange *et al.* (1998) give a new explanation for the difference between theory and field observations. Expansion and contraction of soil air occur due to diurnal warming of the land surface which will result in a convective movement of water vapour in the soil. According to Nassar & Horton (1997) convective water vapour movement can also occur due to changes in barometric pressure, temperature gradients or wind at the land surface. A convective flux of water vapour will change the concentration gradients within the soil. These changes in concentrations gradients influence also the other fluxes. In other scientific research tuning factors are used to increase the simulated water vapour flux by one order of magnitude in order to match the observed vapour flow. Thus according to Parlange *et al.* (1998) the assumption that convective vapour transport can be neglected, is wrong because it is the solution to overcome the difference between theory and measurements.
A land surface scheme is an important component of a general circulation model. It connects the surface with the atmosphere and the major components of a land surface scheme are the surface energy

balance and soil moisture balance. Jassal *et al.* (2003) combine heat and water movement in the soil to calculate the soil water content and temperature profiles accurately near the soil surface. The Bowen ratio which is the ratio of the sensible heat flux to the latent heat flux, is highly sensitive to the soil water content. Jassal *et al.* (2003) extended the model based on Philip and de Vries (1957) to compute the surface energy balance terms. Validation takes place using experimental measurements of those terms. The thermal liquid water flux is left out because it is negligible (Philip & de Vries, 1957; Jackson *et al.*, 1974). The convection of heat by the isothermal liquid water flux is also neglected and the enhancement factor is ignored because it leads to too low computed soil water contents near the surface. Jassal *et al.* (2003) conclude that models need sufficiently thin layers near the soil surface to be able to accurately simulate the soil energy balance and soil moisture balance which are important for general climate models.

A paper by Gowing *et al.* (2006) presents a theory different from the theories given above. They developed an isothermal model which divides the vadose zone into two layers, a liquid water layer (the lower part) and a water vapour layer (the upper part). On the interface, the evaporation front, a phase transition occurs. The model was in agreement with the observations from an isothermal laboratory experiment. Gowing *et al.* (2006) present different figures which show the lowering of the evaporation front after a longer time of evaporation or a higher evaporation demand. They acknowledge that the assumption about isothermal conditions is a crude simplification and extreme temperature gradients near the soil surface will lead to a more complex situation (Gowing *et al.*, 2006), but the advantage of this theory is the avoidance of forced parametrization of, for example, the gain factor and the enhancement factor.

Saito *et al.* (2006) have made the theory about coupled heat & water movement more 'user-friendly'. The movement of liquid water, water vapour and heat can be analysed by solving the system of equations for the conservation of mass and the conservation of energy. These equations are highly non-linear and coupled, so they need to be solved numerically. The Hydrus-1D code is developed which can solve the system of equations with the additional interactions, parametrizations and boundary conditions (Simunek *et al.*, 2008; Saito *et al.*, 2006). The surface energy balance terms were used as upper boundary conditions. Most of the time only standard daily meteorological data is provided by meteorological stations, although more detailed observations are required for the simulation. This paper presents seven equations to calculate the variables on the required time scale from the standard daily meteorological data (Saito *et al.*, 2006) The calculation of these variables is important for the top boundary conditions. Saito *et al.* (2006) note the overestimation of the evaporation flux if only an aerodynamic resistance is used in the calculation of the evaporation rate due to the assumption of thermodynamic equilibrium between liquid water and water vapour. An additional soil surface resistance is implemented which is especially important in dry conditions, to correct the evaporation rates to smaller values corresponding to the measurements.

Parlange *et al.* (1998) published a paper which attempts to clarify the discrepancy between the vapour flux calculated from theory and that observed in the field. The paper is based on the calculated vapour flux using the residual of the energy balance and the mass balance. This approach was validated by soil water content measurements. According to Bittelli *et al.* (2008) this conclusion is premature. Inaccurate soil water content measurements and calibration under variable temperature conditions could also support the theory of Parlange *et al.* (1998). Bittelli et al. believe that the discrepancy between model results and field observations occurs due to the incorrectness of the resistances, consisting of a soil surface resistance and an aerodynamic resistance. Bittelli *et al.* (2008) also discuss the water vapour flux within the soil. The vapour flux is higher closer to the soil surface as: (a) near the soil and atmosphere interface higher vapour concentration gradients exist, (b) larger thermal gradients near the soil surface will result in larger thermal fluxes and (c) a lower soil water content results in a higher air-filled porosity which is available space for vapour. The study by Bittelli *et al.* (2008) denotes that the soil surface resistance is a key parameter for the interface vadose zone and atmosphere as also is noticed by Saito *et al.* (2006). According to Bittelli *et al.* (2008) vapour movement is more affected

by boundary layer conditions than vapour enhancement processes in the porous media, such as convection of vapour flow (Rose, 1968b).
Steenpass *et al.* (2010) try to estimate the soil hydraulic parameters by inverse modeling using the soil surface temperature and measurements of soil water content. Like Bittelli *et al.* (2008) they use also the surface energy balance as upper boundary condition. According to Steenpass *et al.* (2010) however, the soil surface resistance should not be parametrized as Bittelli *et al.* (2008) did. The resistance to the vapour flux in the soil which reduces the vapour flux to the atmosphere, is explicitly taken into account, by an equation describing vapour density gradients and vapour diffusivity in the soil. The soil heat flux is defined by the conductive and convective heat fluxes and the latent heat flux caused by the vapour flow in the soil. In the situation of a very dry soil water conditions evaporation occurs in the soil profile and the surface energy balance only consist of the net radiation, the sensible heat flux and the soil heat flux. The latent heat flux is absent. In case of a wet soil the surface energy balance is defined by the net radiation, the sensible heat and the soil heat flux again plus the latent heat flux. When the water vapour flux is included in a soil water model and contributes significantly to the total evaporation, the surface temperature will become higher due to a higher soil heat flux (Steenpass *et al.*, 2010). The soil heat flux will become larger by the water vapour flux which provides energy for evaporation within the soil profile.
In the paper of Novak (2010) the theory of Philip and de Vries is used. But this time the finite element numerical simulation is done in a very fine grid at the top of the profile, so all interesting variables can be determined accurately. The grid size at the top was $10^{-5}m$ on top logarithmically increasing to $0.4m$ at the bottom of the profile. With this model they were able to analyse how diurnal cycles and continuous drying have influence on the dynamics of the evaporation zone. Instrumentation to measure these effects is presented by Heitman *et al.* (2008a,b) and for the first time the theory of Philip and de Vries could be validated exhaustively. However Novak didn't include in his model processes like convection, hysteresis and temperature dependency of the soil properties. That was why the entire theory as extended by the theories of Van Genuchten (1980); De Vries (1987); Parlange *et al.* (1998) is still not validated.
The objective of the paper by Deb *et al.* (2011) was to model the coupled movement of heat and water using Hydrus-1D for a specific field situation. Hysteresis effects in the soil water retention curve were neglected, because the field consists of a sandy soil (no shrinking and swelling) (Deb *et al.*, 2011). Deb et al. remark that the choice of the spatial discretization is difficult. On one hand a finer grid simulates most of the time better, on the other hand a finer grid may cause the model not to converge any more to a stable solution. Saito *et al.* (2006) and Deb *et al.* (2011) found a negligible small thermal liquid flux during a dry day, additionally Deb *et al.* (2011) noticed a small thermal liquid flux in the upward direction near the soil surface after a small water input. The thermal liquid flux is not only controlled by the temperature gradient, but is also affected by the thermal liquid hydraulic conductivity. According to Zeng *et al.* (2009) the thermal liquid flux is dominant during night and significant during day. Deb et al. stress that studies which showed insignificant thermal liquid fluxes most of the time did their studies under dry soil conditions and did not investigate the water vapour and liquid water fluxes after small water inputs of irrigation or precipitation (Deb *et al.*, 2011). After irrigation first the liquid water flux dominates and with an increase of soil drying the contribution of the vapour flux will increase. However Deb *et al.* (2011) do not mention which type of vapour flux will increase most.
In the paper by Smits *et al.* (2011) a theory is presented for coupled liquid water, water vapour and heat fluxes under varying temperature gradients with non-equilibrium liquid/gas phase change and vapour diffusion. Smits *et al.* (2011) address as many researchers the lack of validation of existing models and theories due to scarcity of field and laboratory data. Validation is necessary because the theory and experimental measurements still do not match. The observed water vapour flux is enhanced with respect to the water vapour flux calculated by Ficks law. Smits *et al.* (2011) give results of an extensive laboratory experiment, and a new theory is presented with a non-equilibrium

liquid-gas phase change. First of all Smits et al. comment on earlier published papers. According to them the theory by Philip & de Vries (1957) is a simplification as it does not take the convective transport of heat in the liquid water and water vapour fluxes, non-equilibrium liquid-gas phase change and sensible heat dispersion in the liquid phase into account. According to Smits *et al.* (2011) the enhancement factor is highly doubtful and pore-scale research has shown that the enhancement factor is not needed (Shokri *et al.*, 2009). Fick's law of diffusion can be used if capillary flow is included (in the isothermal liquid flux), in which case the enhancement factor is unnecessary. Smits et al. formulate even stronger doubts regarding the assumption water vapour and liquid water are always in equilibrium, in other words instantaneous vaporization (commonly used in vadose zone hydrology). Experiments in numerous studies have shown that it takes a long time to reach equilibrium between liquid water and water vapour (Benet *et al.*, 2009; Chammari *et al.*, 2008). Smits *et al.* (2011) note that water vapour can be made available by the volatilization of liquid water, with a specific volatilization time. This process is implemented in the mass conversation balance of liquid water as a sink term and in the mass conversation balance of water vapour as a source term. In this non-equilibrium approach a fourth partial differential equation is needed, the mass balance of the total gas phase. Bear *et al.* (1991) remark that a mass balance for the total gas phase is superfluous, because the total mass of the gas phase is negligible compared to that of the liquid phase. The source/sink term describes a finite liquid-gas phase change rate. Smits *et al.* (2011) neglected the thermal liquid flux in their model because Saito *et al.* (2006) showed that the thermal liquid flux was negligible with respect to the isothermal liquid flux. It is remarkable that in their paper Smits et al. use an enhancement factor while they first highly doubt the need of it. The enhancement factor is used for both the thermal vapour flux as introduced by Philip & de Vries (1957) and for the isothermal vapour flux. The enhancement of the isothermal water vapour flow based on pore-scale experiments that showed enhanced vapour diffusion without a temperature gradient (Webb & Ho, 1998). In addition due to the limited amount of experimental data a linear relationship is assumed by Smits *et al.* (2011) between the non-equilibrium phase change rate and the difference among the vapour pressure in the air and the equilibrium pressure at the liquid-vapour interface. The enhancement factor and the liquid-gas phase change rate contain unique parameters which need to be determined by fitting, for each different soil. At some intermediate water content the maximum phase change rate occurs because at that moment the largest differences occur between the actual and saturated vapour concentration and the corresponding phase change rate parameter is at his maximum (Smits *et al.*, 2011). Smits et al. compared the model of the non-equilibrium phase change with an equilibrium model, which has the assumption that liquid water and water vapour are always in equilibrium. When choosing one of the two models the availability of data should be considered. The equilibrium model needs evaporation rates as upper boundary condition, which can be calculated by obtained column weight observations. The non-equilibrium model is suitable for field situations because it can handle highly transient upper boundary conditions, but the relative humidity at the soil surface needs to be known. In addition also other variables need to be measured such as the wind speed and the surface roughness properties to be able to calculate the aerodynamic resistance. When both models have the same upper boundary condition the non-equilibrium model corresponds better with the observations, an underestimation of the cumulative evaporation rate after 30 days of circa 4%. The equilibrium model overestimates the cumulative evaporation rate after 30 days with circa 35% (Smits *et al.*, 2011). Unrealistic small soil water pressure heads at the soil surface are noticed by Smits *et al.* (2011) which are forced by the assumption of thermodynamic equilibrium. The larger soil water pressure gradient will result in an overestimation of the evaporation rate. In the studies by Saito *et al.* (2006) and Bittelli *et al.* (2008) which used equilibrium models, the overestimation of the evaporation rate was tried to correct by using a soil surface resistance. For the non-equilibrium model however the extra parameter for the liquid-vapour phase change rate needs to be fitted.

According to Zeng *et al.* (2011) an underestimated error of 33-55% on the first day after a rainfall event can be caused by neglecting the air flow in coupled models. A third mass balance equation for

dry air has to be added consisting of the dry air concentration gradient (diffusive movement) and the mixed soil air pressure gradient (convective movement). Zeng *et al.* (2011) noticed that barometric pressure variation can drive water vapour and dry air movements in and out of the soil. The model including the air flow process corresponds better to the measured evaporations than the model without air flow. For the day after an input of water by rainfall or irrigation an underestimated error of 33% was overcome by including air flow into the model. Note that thermal equilibrium was assumed between water vapour and liquid water.

2.2 Model for coupled heat and water movement

In this section a description of the system of equations is given for coupled heat and water movement based on theory by Philip & de Vries (1957) presented by Saito *et al.* (2006). The theory desribed by Saito *et al.* (2006) is chosen because this theory is also used in Hydrus-1D. This theory is not perfect and as seen in the section above. Saito *et al.* (2006) conclude a reasonable agreement is achieved between computed and measured soil water contents and soil temperatures, which doesn't sound very convincing. Deb *et al.* (2011) use the Hydrus model and explains the difference between simulations and measured by possible measurement errors for the top and bottom boundary conditions of the soil profile. In the paper by Saito *et al.* (2006) an independent experimental test of evaporation is lacking according to Bittelli *et al.* (2008). Nevertheless the theory of Saito *et al.* (2006) is selected because of the large amount of scientific research done into this theory and the availability of a widely scientifically-used model (Sakai *et al.*, 2009; Zeng *et al.*, 2009; Deb *et al.*, 2011). Due to these reasons I believe that this theory is a good starting point for this thesis.

2.2.1 Water flow

Saito *et al.* (2006) start with the mass conservation for water, given in equation (2.1). Their mass conservation equation for one dimensional flow is formulated for incoming and outgoing liquid water and water vapour fluxes in a storage control volume.

$$\frac{\partial \theta}{\partial t} = -\frac{\partial q_l}{\partial z} - \frac{\partial q_v}{\partial z} \tag{2.1}$$

where θ is the total soil moisture content ($m^3 \cdot m^{-3}$) , q_l and q_v are the flux densities of liquid water and water vapour ($m \cdot s^{-1}$), t is the time (s) and z is the spatial dimension positive in the upward direction (m). The total soil moisture content is the sum of the soil liquid water content and the soil water vapour content:

$$\theta = \theta_l + \theta_v \tag{2.2}$$

where θ_l and θ_v are respectively the soil liquid water content and the soil water vapour content ($m^3 \cdot m^{-3}$). Darcy's law is modified by Philip & de Vries (1957) to describe the flux density of liquid water, equation 2.3, which is the sum of the flux driven by pressure difference (isothermal) and the flux driven by a temperature difference (thermal).

$$q_l = q_{lh} + q_{lT} = -K_{lh}\left(\frac{\partial h}{\partial z} + 1\right) - K_{lT}\frac{\partial T}{\partial z} \tag{2.3}$$

where q_{lh} is the flux density caused by pressure differences ($m \cdot s^{-1}$) and q_{lT} is the flux density caused by temperature gradients ($m \cdot s^{-1}$), K_{lh} is the isothermal hydraulic conductivity coefficient for liquid water flow ($m \cdot s^{-1}$), K_{lT} is the thermal hydraulic conductivity coefficient for liquid water flow ($m^2 \cdot K^{-1} \cdot s^{-1}$), h is the soil water pressure head (m) and T is the temperature (K).

The flux density for water vapour flow is described by Philip & de Vries (1957) in equation 2.4 with again an isothermal part, caused by pressure differences, and an thermal part caused by temperature differences.

$$q_v = q_{vh} + q_{vT} = -K_{vh}\frac{\partial h}{\partial z} - K_{vT}\frac{\partial T}{\partial z} \tag{2.4}$$

where q_{vh} is the isothermal water vapour flux ($m \cdot s^{-1}$), q_{vT} is the thermal water vapour flux ($m \cdot s^{-1}$), K_{vh} is the isothermal hydraulic conductivity coefficient for water vapour flow (ms^{-1}) and K_{vT} is the thermal hydraulic conductivity coefficient for water vapour flow ($m^2 \cdot K^{-1} \cdot s^{-1}$). Equation 2.5 is the combination of equations 2.1, 2.3 and 2.4 and is a coupled liquid water and water vapour flow equation:

$$\begin{aligned}\frac{\partial \theta}{\partial t} &= \frac{\partial}{\partial z}[K_{lh}\frac{\partial h}{\partial z} + K_{lh} + K_{lT}\frac{\partial T}{\partial z} + K_{vh}\frac{\partial h}{\partial z} + K_{vT}\frac{\partial T}{\partial z}] \\ &= \frac{\partial}{\partial z}[K_{sh}\frac{\partial h}{\partial z} + K_{lh} + K_{sT}\frac{\partial T}{\partial z}]\end{aligned} \tag{2.5}$$

where K_{sh} ($m \cdot s^{-1}$) and K_sT ($m^2 \cdot K^{-1} \cdot s^{-1}$) are the total hydraulic conductivity coefficients for respectively isothermal and thermal flow, where:

$$K_{sh} = K_{lh} + K_{vh} \tag{2.6}$$

$$K_{sT} = K_{lT} + K_{vT} \tag{2.7}$$

2.2.2 Soil hydraulic properties

For the determination of the unsaturated isothermal hydraulic conductivity coefficient, $K_{lh}(h)$, the pore-size distribution model was used by Mualem (1976). This model combines the saturated hydraulic conductivity with the soil water retention curve of Van Genuchten (1980), equation 2.10.

$$K_{lh}(h) = K_s S_e^l \left[1 - (1 - S_e^{1/m})^m\right]^2 \tag{2.8}$$

where K_s is the saturated hydraulic conductivity coefficient ($m \cdot s^{-1}$), l and m are empirical parameters (dimensionless) and S_e is the effective saturation (dimensionless) which is defined as (Van Genuchten, 1980):

$$S_e = \frac{\theta - \theta_r}{\theta_s - \theta_r} \tag{2.9}$$

Mualem (1976) suggest a value of 0.5 for the parameter l and by using the analytical model of Van Genuchten (1980) the value of m can be determined by fitting against water retention data (Saito *et al.*, 2006).

$$\theta_l(h) = \begin{cases} \theta_r + \frac{\theta_s - \theta_r}{\left[1 + |\alpha h|^n\right]^m} & h < 0 \\ \theta_s & h \geq 0 \end{cases} \tag{2.10}$$

In equation 2.10 $\theta_l(h)$ is the liquid moisture content ($m^3 \cdot m^{-3}$) which depends on the pressure head, θ_s and θ_r are the saturated water content and the residual water content, respectively, α (m^{-1}), n (dimensionless) and m ($= 1 - 1/n$) are empirical shape parameters.

Equation 2.11 describes the thermal hydraulic conductivity coefficient:

$$K_{lT} = K_{lh}\left(hG_{wt}\frac{1}{\gamma_0}\frac{d\gamma}{dT}\right) \tag{2.11}$$

where G_{wT} is the gain factor which includes the temperature dependency of the soil water retention curve (dimensionless), γ is the surface tension of soil water ($J \cdot m^{-2}$) and γ_0 is the surface tension of soil water at 25 °C ($= 71.89 \quad g \cdot s^{-2}$) (Nimmo & Miller, 1986). The dependency of the surface tension on temperature is given in equation 2.12:

$$\gamma = 75.6 - 0.1425T - 2.38 \cdot 10^{-4}T^2 \tag{2.12}$$

In equations 2.13 and 2.14 the isothermal and thermal hydraulic conductivity coefficients for vapour flow are presented as defined by Nassar & Horton (1989).

$$K_{vh} = \frac{D}{\rho_w}\rho_{sv}\frac{Mg}{RT}H_r \tag{2.13}$$

$$K_{vT} = \frac{D}{\rho_w}\eta H_r\frac{d\rho_{sv}}{dT} \tag{2.14}$$

Here D is the vapour diffusivity in the soil ($m^2 \cdot s^{-1}$), ρ_w is the density of liquid water ($kg \cdot m^{-3}$), ρ_{sv} is the density of saturated vapour ($kg \cdot m^{-3}$) which is temperature dependent, M is the molecular weight of water ($= 0.018015 \quad kg \cdot mol^{-1}$), g is the gravitational constant ($= 9.81 \quad m \cdot s^{-2}$), R is the universal gas constant ($= 8.314 \quad J \cdot mol^{-1} \cdot K^{-1}$), η is the enhancement factor by Cass *et al.* (1984) (dimensionless) and H_r is the relative humidity (dimensionless). In equation 2.15 the vapour diffusivity factor is described as:

$$D = \tau\theta_a D_a \tag{2.15}$$

where τ is the tortuosity factor as defined in equation 2.16, the variable θ_a is the air-filled porosity ($m^3 \cdot m^{-3}$) and D_a is the diffusivity of water vapour in air ($m \cdot s^{-2}$) which is dependent on the temperature (T) as defined in equation 2.17.

$$\tau = \frac{\theta_a^{7/3}}{\theta_s^2} \tag{2.16}$$

$$D_a = 2.12 \cdot 10^{-5}\left(\frac{T}{273.15}\right)^2 \tag{2.17}$$

In equation 2.18 the definition is given for the saturated vapour density as function of the temperature (T):

$$\rho_{sv} = 10^{-3}\frac{exp\left(31.3716 - \frac{6014.79}{T} - 7.92495 \times 10^{-3}T\right)}{T} \tag{2.18}$$

A thermodynamic relationship between liquid water and water vapour in the soil is used to calculate the relative humidity from the soil pressure head, h, as can be seen in equation 2.19 (Philip & de Vries, 1957):

$$H_r = exp\left(\frac{Mgh}{RT}\right) \tag{2.19}$$

The enhancement factor is defined by Cass *et al.* (1984) to describe the increase in the thermal vapour flux.

$$\eta = 9.5 + 3\frac{\theta}{\theta_s} - 8.5exp\left\{ -\left[\left(1 + \frac{2.6}{\sqrt{f_c}}\right)\frac{\theta}{\theta_s}\right]^4\right\} \tag{2.20}$$

where f_c is the mass fraction of clay in the soil (dimensionless).

2.2.3 Heat flow

The movement of heat in a variably saturated porous media is described by the heat conservation equation:

$$\frac{\partial S_h}{\partial t} = -\frac{\partial q_h}{\partial z} - Q \tag{2.21}$$

where S_h is the storage of heat in the soil ($J \cdot m^{-3}$), q_h represents the total heat flux density ($J \cdot m^{-2} \cdot s^{-1}$) and Q is the term for the sources and sinks of energy ($J \cdot m^{-3} \cdot s^{-1}$). Heat storage, S_h, is described by equation 2.22:

$$\begin{aligned} S_h = C_n T\theta_n + C_w T\theta_l + C_v T\theta_v + L_0\theta_v = (C_n\theta_n + C_w\theta_l + C_v\theta_v)T + L_0\theta_v \\ = C_p T + L_0\theta_v \end{aligned} \tag{2.22}$$

where θ_n is the volumetric fraction of the solid phase ($m^3 \cdot m^{-3}$), C_n, C_w, C_v and C_p are volumetric heat capacities ($J \cdot m^{-3} \cdot K^{-1}$) of respectively the solid, liquid water, water vapour phase and the 'total' moist soil and L_0 is the volumetric latent heat of the vaporization of liquid water ($J \cdot m^{-3}$) which is described by:

$$L_0 = L_w\rho_w \tag{2.23}$$

where L_w is the gravimetric latent heat of the vaporization of liquid water ($= 2.501 \cdot 10^{-6} - 2369.2T$). In equation 2.24 the total heat flux density, q_h, is defined as the sum of the sensible heat conduction through the soil described by Fourier's law, the convection of sensible heat by liquid water and water vapour, and the latent heat transported by vapour flow (De Vries, 1987):

$$q_h = -\lambda(\theta)\frac{\partial T}{\partial z} + C_w T q_l + C_v T q_v + L_0 q_v \tag{2.24}$$

where $\lambda(\theta)$ is the soil apparent thermal conductivity ($J \cdot m^{-1} \cdot s^{-1} \cdot K^{-1}$). The combination of equations 2.21, 2.22 and 2.24 results in the following equation for heat movement (Nassar & Horton, 1992):

$$\frac{\partial C_p T}{\partial t} + L_0\frac{\partial \theta_v}{\partial t} = \frac{\partial}{\partial z}\left[-\lambda(\theta)\frac{\partial T}{\partial z}\right] - C_w\frac{\partial q_l T}{\partial z} - L_0\frac{\partial q_v}{\partial z} - C_v\frac{\partial q_v T}{\partial z} - C_w S T \tag{2.25}$$

where the term $C_w ST$ describes the loss of energy due to root water uptake. Because this thesis is about the movement of heat in a bare soil, this term can be abolished.

2.2.4 Soil thermal properties

The soil thermal apparent conductivity, $\lambda(\theta)$, is a combination of the conduction of heat through the porous medium without liquid water, water vapour, or air movement and the macrodispersivity.

The latter is the energy flux created by spatial variations in local convective fluxes of liquid water which is in equation 2.26 defined and is assumed to be a linear function of the velocity:

$$\lambda(\theta) = \lambda_0(\theta) + \beta C_w |q_l| \tag{2.26}$$

where β is the thermal dispersivity (m). Macrodispersivity is only significant if the liquid water flux is large and thus for (semi-)arid conditions this term can be neglected. Further the apparent thermal conductivity of the soil is equal to the thermal conductivity of the porous medium which can be defined as:

$$\lambda_0(\theta) = b_1 + b_2\theta + b_3\theta^{0.5} \tag{2.27}$$

where b_1, b_2 and b_3 are empirical parameters ($W \cdot m^{-1} \cdot K^{-1}$). In the Hydrus-1D code the values for different soil types are already included. Saito *et al.* (2006) note the soil water content has more influence on the soil thermal properties than the textural differences among soil types since the thermal properties of the different minerals in the variety of soil types are all in the same order of magnitude.

2.2.5 Surface energy balance

The upper boundary conditions for the coupled heat and water movement model are precipitation, irrigation, evaporation and heat fluxes. The surface energy balance by Van Bavel & Hillel (1976) can be used to calculate the latter two terms:

$$R_n - H - L_w E - G = 0 \tag{2.28}$$

where R_n is the net radiation ($W \cdot m^{-2}$), H is the sensible heat flux ($W \cdot m^{-2}$), LE is the latent heat flux ($W \cdot m^{-2}$) and G is the soil surface heat flux ($W \cdot m^{-2}$). L_w is the latent heat ($J \cdot kg^{-1}$) and E is the rate of evaporation ($kg \cdot m^{-2} \cdot s^{-1}$). In which H and LE are positive in the upward direction and R_n and G are positive downward. The net radiation is defined as the sum of the net shortwave radiation and the net longwave radiation:

$$R_n = R_{ns} + R_{nl} = (1-a)S_t + (\varepsilon_s R_{ld\downarrow} - R_{lu\uparrow}) \tag{2.29}$$

where R_{ns} and R_{nl} are respectively the net shortwave and the net longwave radiation ($W \cdot m^{-2}$), a is the albedo of the surface (dimensionless), S_t is the incoming global shortwave solar radiation ($W \cdot m^{-2}$), ε_s is the soil surface emissivity (dimensionless) which is the reflection coefficient at the soil surface for the longwave incoming radiation and it depends on the soil water content in the surface layer, $R_{ld\downarrow}$ is the incoming longwave radiation (positive downwards) and $R_{lu\uparrow}$ is the outgoing longwave radiation (positive upwards), both in $W \cdot m^{-2}$. The albedo of the soil surface, a, depends primary on the soil water content. A simple formula is proposed by Van Bavel & Hillel (1976) to calculate the albedo from the soil water content in the top layer:

$$\begin{array}{ll} a = 0.25 & \theta_{top} < 0.1 \\ a = 0.10 & \theta_{top} \geq 0.25 \\ a = 0.35 - \theta_{top} & 0.1 \leq \theta_{top} < 0.25 \end{array} \tag{2.30}$$

where θ_{top} is the soil water content in the surface layer. The net longwave radiation can be rewritten using the law of Stefan-Boltzmann (Monteith & Unsworth, 1990):

$$R_{nl} = \varepsilon_s R_{ld\downarrow} - R_{lu\uparrow} = \varepsilon_s \varepsilon_a \sigma T_a^4 - \varepsilon_s \sigma T_s^4 \tag{2.31}$$

where ε_a is the emissivity (dimensionless) of the atmosphere which depends on the air temperature and the humidity, T_a and T_s are respectively the air temperature and the soil surface temperature (K).

Equation 2.32 is presented by Van Bavel & Hillel (1976) for the soil surface emissivity which depends on the soil water content:

$$\varepsilon_s = min(0.9 + 0.18\theta_{top}; 1.0) \tag{2.32}$$

Idso (1981) proposed the following equation for the calculation of the atmospheric emissivity, ε_a:

$$\varepsilon_a = 0.7 + 5.95 \cdot 10^{-5} e_a exp\left(\frac{1500}{T_a}\right) \tag{2.33}$$

where e_a is the vapour pressure (kPa) in the atmosphere which depends on the air temperature and can be calculated by equation 2.34:

$$e_a = 0.611 exp\left(\frac{17.27(T_a - 273.15)}{T_a - 35.85}\right) H_r \tag{2.34}$$

Monteith & Unsworth (1990) presented equation 2.35 for the calculation of the incoming long-wave radiation from a sky partially covered by clouds:

$$R_{ld\downarrow} = \left[(1 - 0.84c)\varepsilon_a + 0.84c\right]\sigma T_a^4 \tag{2.35}$$

where c is the fraction of sky covered by clouds (dimensionless). This factor, c is estimated by Campbell (1985) from the atmospheric transmission coefficient for solar radiation, T_t:

$$0 \leq c = 2.33 - 3.33T_t \leq 1 \tag{2.36}$$

The position of the sun must be taken into account to determine the amount of incoming shortwave radiation, S_t, at any time and location (Campbell, 1985):

$$S_t(t) = max(G_{sc} T_t \sin e; 0) \tag{2.37}$$

where G_{sc} is the solar constant (1360 $W \cdot m^{-2}$), and the atmospheric transmission coefficient, T_t, is described by the ratio of the measured daily global solar radiation S_{tm} ($W \cdot m^{-2}$) and the potential daily global radiation at the top of the atmosphere, R_a ($W \cdot m^{-2}$):

$$T_t = \frac{S_{tm}}{R_a} \tag{2.38}$$

The term $\sin e$ is the solar elevation angle (rad) defined by Monteith & Unsworth (1990) as:

$$\sin e = \sin\phi \sin\delta + \cos\phi \cos\delta \cos\frac{2\pi}{24}(t - t_0) \tag{2.39}$$

where ϕ is the local latitude, δ is the declination of the sun, t_0 is the time of solar noon and t is the local time within a day. The sensible heat flux, H is described by Van Bavel & Hillel (1976) as:

$$H = C_a \frac{T_s - T_a}{r_H} \tag{2.40}$$

where C_a is the volumetric heat capacity of air ($J \cdot m^{-3} K^{-1}$) and r_H is the aerodynamic resistance for heat transfer ($s \cdot m^{-1}$). Equation 2.41 can be used to calculate the evaporation at the soil surface. The equation accounts for the atmospheric conditions, soil water content in the top layer and soil moisture movement in the topsoil.

$$E = \frac{\rho_{vs} - \rho_{va}}{r_v + r_s} \tag{2.41}$$

where ρ_{vs} and ρ_{va} are respectively the water vapour density at the soil surface and the atmospheric vapour density, both in $kg \cdot m^{-3}$. The aerodynamic resistance for water vapour flow is represented in r_v ($s \cdot m^{-1}$) and r_s is the soil surface resistance term to water vapour flow ($s \cdot m^{-1}$). The soil surface resistance is an additional resistance which is especially important for dry soils. In dry soils the water vapour is dynamically transported through the larger pores towards the atmosphere and than the density of the water vapour in the larger pores is not in equilibrium with the density of water vapour in the porous medium, thus the assumption about thermodynamic equilibrium is not valid at the soil surface in these dry conditions. Without this soil surface resistance term, r_s, the rate of evaporation will be overestimated (Camillo & Gurney, 1986). The following equation by Camillo & Gurney (1986) is used to calculate the soil surface resistance:

$$r_s = -805 + 4140(\theta_s - \theta_{top}) \tag{2.42}$$

where θ_s is the saturated water content and θ_{top} is the soil water content at the soil surface. Already for a long time is assumed that the aerodynamic resistance for heat transfer, r_H, is equal to the aerodynamic resistance for vapour flow, r_v (Van Bavel & Hillel, 1976).

$$r_H = r_v = \frac{1}{U^* k}\left[ln\left(\frac{z_{ref} - d + z_H}{z_H}\right) + \psi_H\right] \tag{2.43}$$

where k is the von Karman constant ($= 0.41$), z_{ref} is the reference height at which the temperature measurements are taken (m), z_H is the surface roughness of the heat flux (m), d is the zero-plane displacement height (m), ψ_H is a correction factor for the heat flux related to the atmospheric stability (dimensionless) and U^* is the friction velocity ($m \cdot s^{-1}$) and is defined by Campbell (1985) as:

$$U^* = uk\left[ln\left(\frac{z_{ref} - d + z_m}{z_m}\right) + \psi_m\right]^{-1} \tag{2.44}$$

where u is the mean wind speed at height z_{ref} ($m \cdot s^{-1}$), z_m is the surface roughness for the momentum flux (m) and ψ_m is a correction factor (dimensionless) for the momentum flux related to the atmospheric stability. For bare soils typical values for the above parameters are; 0 meter for d and 0.001 meter for the roughness factors z_H and z_m. Camillo & Gurney (1986) presented an approximation to calculate the stability correction factors.

Saito *et al.* (2006) stress that at the first glance the system of equations for coupled liquid water, water vapour and heat movement seems to need a lot of information about different parameters. But they note that this is actually not true. The soil hydraulic properties are described by six parameters in total; θ_s, θ_r, α, n, K_s and l. These six parameters are needed to simulate isothermal liquid water flow by using the Richards equation. The addition of thermal liquid water flow, thermal water vapour flow and isothermal water vapour flow do not need extra input parameters. The parameters $K_l T$, $K_v h$, $K_v T$ and Sh from equations 2.11, 2.13, 2.14 and 2.22 respectively, can be defined by using values from the literature for the several properties, like surface tension, water vapour diffusivity and heat capacities (Saito *et al.*, 2006). The soil thermal properties are based on three different b-parameters.

2.3 Discussion of theoretical framework

The short literature review presented above, shows a brief 'picture' of the theories about coupled heat and water movement through time. Almost every paper starts with the fundamental theory of Philip & de Vries (1957), only the papers by Gowing *et al.* (2006) and Smits *et al.* (2011) use another starting point in their research. Gowing *et al.* (2006) made the assumption of isothermal conditions which makes the model much easier. Smits *et al.* (2011) use three mass balances for liquid water, water vapour and total gas, and an energy balance for the heat fluxes. The theory by Philip & de Vries (1957) including the extensions is still not validated. Novak (2010) presented a method with a very

fine grid near the soil surface which is accurate enough to validate the theory. But he didn't implement a couple of important processes which makes the result of the validation by Novak (2010) incomplete. What many studies recognize, is the discrepancy between calculated results from the theory and the observations from the field. However on the causes of this discrepancy isn't an uniform agreement. Most researches argue that the processes are not well understood. One of the processes is the enhancement of water vapour flow introduced by Philip & de Vries (1957), who used an enhancement factor for the thermal vapour flux. Smits *et al.* (2011) use this factor for the thermal and isothermal vapour fluxes. Shokri *et al.* (2009) however, have published a paper which addresses arguments against the use of the enhancement factor. Another process under discussion is the convective vapour flux introduced by Rose (1968b). Later Parlange *et al.* (1998) published a paper about this convective movement due to contraction and expansion of the soil by diurnal warming of the soil surface, as the solution for the discrepancy between simulation results and observations. Nassar & Horton (1989) provide more arguments for a convective water vapour flux. Bittelli *et al.* (2008) question the conclusions of the paper by Parlange *et al.* (1998) and note that the difference between simulations and observations is due to the inaccurate soil surface resistance and aerodynamic resistance. Another point of discussion is the thermal liquid flow. In some papers the thermal liquid flow is neglected due to it's insignificance (Saito *et al.*, 2006; Smits *et al.*, 2011) while Deb *et al.* (2011) remark that in dry conditions the thermal liquid flow is negligible, although after a small input of water the thermal liquid flux is important (Zeng *et al.*, 2009). Milly (1984) also notes that the thermal liquid flux is insignificant and the thermal vapour flux can be neglected by evaporation calculations on a daily time scale due to the diurnal heating effect. The highest vapour fluxes occur at an intermediate soil water content (Philip & de Vries, 1957; Milly, 1984; Nassar & Horton, 1997; Bittelli *et al.*, 2008). Also because the two vapour diffusivity coefficients have their maximum value at that water content condition, which can be seen in figure 3 of the paper by Nassar & Horton (1997). According to Bittelli *et al.* (2008) near the soil surface the water vapour flux has the largest values because of; (a) the highest vapour gradient occurs at the soil surface, (b) the largest temperature takes gradients exist at the top of the soil profile, and (c) in semi-arid and arid regions a lower soil water content occurs near the soil surface which results in a higher air-filled porosity.

In the development of a new model which can determine the daily evaporation rate, the above theory will be used. The theory by Smits *et al.* (2011) is the most detailed one with the four partial differential equations; three mass conservation equations for liquid water, water vapour and total gas, and a heat conservation equation. But these equations are difficult to describe in a numerical code and a large amount of accurate data is necessary to calculate all the parameters. Besides of that Bear *et al.* (1991) remark that a mass balance for the total gas phase is superfluous, because the total mass of the gas phase is negligible compared to that of the liquid phase.. For the development of a coupled SWAP model, the theory by Philip & de Vries (1957) is well-described fundament. I appreciate the descriptions of the components; the four fluxes, the different diffusivity coefficients, the transfer of heat through the porous media, by water vapour and liquid water. From the analyses of the field data in the Hydrus-1D model the assumptions can be proposed for the SWAP model and the contribution of the different fluxes can be assessed. For example Milly (1984) concludes that the thermal liquid flux is negligible and the thermal vapour flux can be ignored on a daily time scale. An implementation of this thermal water vapour flux can be used to test the contribution of this flux on a daily time scale. And in this way a model can be developed which can simulate the daily evaporation rates accurately.

3 Experimental framework from literature

3.1 Laboratory experiments

3.1.1 Soil water content, soil pressure head and temperature profiles

In this section a number of laboratory experiments measuring soil water content, soil pressure head and soil temperature profiles will be presented and discussed with the objective to give a overview about the experiments performed in research. This overview serves a start for the design of a laboratory experiment in chapter 7. Rose (1968a) has taken soil samples at the depth of 1-5 cm and at 15 cm depth. The dependency of the soil water content on the matric potential was analysed in a laboratory with soil suction equipment for a potential up till -500 cm and with a pressure membrane for lower pressures. In this way the entire soil water retention curve can be determined. Jackson *et al.* (1973) used a similar gravimetric technique to determine the soil water content. Gowing *et al.* (2006) perform an isothermal experiment. Two soil columns are used, one of 45 cm and one of 70 cm deep. The tubes have a diameter of 20 cm and are made of PVC, upward from the bottom a layer of 5 cm is filled with ceramic grains. Soil water contents were measured with nine thermal conductivity probes between 1 cm and 29 cm from the top. The probes are produced for continuously monitoring in a fine spatial resolution; the specific resolution, however, is not mentioned. Sakai *et al.* (2009) performed a different column experiment with respect to other studies. In this study moist hot air is flowing over six dry soil columns with a height of 10 cm and a diameter of also 10 cm; water vapour is diffusing into the column due to a difference in vapour density. The vapour is assumed to condensate at the cold bottom. Subsequently a liquid water flow is going up due to pressure gradients. The sides of the columns were isolated with foam polystyrene, to achieve a one-dimensional heat flow. The temperature is measured with thermocouples at 0, 2, 5, 8 and 10 cm from the top. After 2, 5, 10, 16, 21 and 30 days soil sections of 1-2 cm thick were measured gravimetrically to determine the soil water contents. This procedure implies multiple sets of 6 samples are needed, because gravimetric sampling is destructive. Smits *et al.* (2011) remark that although destructive sampling mostly results in accurate soil water content measurements, the requirement of different samples can easily result in large errors due to the variability among the samples. Smits *et al.* (2011) use a large column with a height of 120 cm in their experiment and a diameter of 10.2 cm. Temperature, soil water content and soil water pressure head were measured for every 10 cm with respectively temperature probes (EC-T), dielectric soil moisture sensors ECH$_2$O EC-5 and tensiometers. The entire soil column was put on a scale to weigh the column continuously. The column was isolated with 5 cm thick fiberglass to avoid radial heat flow due to heat loss by the wall. When the heat loss at the wall is negligible a one-dimensional heat flow can be assumed. In intervals of 10 minutes the column weight, the relative humidity at the soil surface, soil water pressure, soil water content and soil temperature were measured.

3.1.2 Initial and boundary conditions

In this section information is given about the boundary conditions used in the different laboratory experiments. Gowing *et al.* (2006) kept the surrounding temperature around the 40 °C, to maintain the column in isothermal conditions. The relative humidity was between 0.15 and 0.3 which resulted in a very large evaporation rate of circa 24 mm per day. At 3 cm from the bottom of the column two T-joints were connected to a Mariotte siphon, which was installed to maintain a constant water table depth. The amount of water supplied to the column was also measured. The initial water content of the column was brought in an equilibrium condition. Sakai *et al.* (2009) exposed a soil column in a chamber with a constant air temperature of 37 °C and a relative humidity between the 85 and 90%. The bottom temperature of the soil column was maintained at a temperature of 20 °C using a water pump and an bath. The initial soil water content was near dryness at 0.0045 and the initial temperature throughout the soil was assumed to be 23.5 °C, the temperature of the room before the

experiment started. Smits *et al.* (2011) started from a fully saturated profile with the water supplied from below. They measured the relative humidity using a relative humidity probe installed at the soil surface in close contact with the grains. This relative humidity is important as upper boundary condition. An infrared heating element was installed above the soil column and connected to a non-infrared non-contact temperature sensor, which measured the soil surface temperature. A control mechanism maintained the temperature between the 56-60 °C.

3.1.3 Parameters

This section will provide insight in the measurement of parameters required to model coupled heat and water movement in the soil. The soil hydraulic properties used in the study by Gowing *et al.* (2006) were acquired from literature. Additional parameters can be calculated by the already measured quantities; note that a simple model is used with a limited amount of parameters. Rose (1963) determined the gaseous diffusion coefficient for two types of building stones and four types of soils. From near saturation till dryness the diffusion rate was measured for hydrogen by use of the Currie method (Currie, 1960). The assumption is made that the diffusion rate for hydrogen is equal to the diffusion rate for water vapour. Near dryness the diffusion rates were at their maximum for all six media due to the highest amount of free pore space. Cass *et al.* (1984) did an experiment to measure the change in vapour diffusion by a change in pressure as function of soil water content and temperature. The differential of vapour over pressure is needed to calculate the enhancement factor. In the experiment soil in a pressure cell is first brought in one bath at a certain temperature till an equilibrium temperature in the soil is reached and then put into another bath with a different temperature. This action is repeated for different pressures. Two copper constantan thermocouples were installed, one in the middle of the pressure cell and one just outside the cell. The thermal diffusivity is calculated from the temperature responses of the thermocouple by using an approximation of the radial heat flow equation (Cass *et al.*, 1984). Shokri *et al.* (2009) have done two kinds of experiments to determine the pathways and transport rates of water in a soil column. These phenomena are important to investigate the processes explaining the enhancement factor. In one experiment blue dye was dissolved in water for three purposes; (a) to distinguish a clear contrast between the unsaturated and saturated part, (b) to provide insight regarding the transport mechanisms at high and intermediate soil water content conditions and (c) detection of a secondary drying front. The second experiment uses X-ray radiation to show the soil water content in a soil column. Measured X-ray attenuation values can distinguish the solid media, liquid water and gas phase in a soil column. Based on these two experiments Shokri *et al.* (2009) concluded the enhancement factor is unnecessary, because capillary flow and Ficks diffusion are sufficient to describe vapour movement in a soil. Sakai *et al.* (2009) use the falling head-method to determine the saturated hydraulic conductivity of the soil material. The soil hydraulic properties were determined from water retention curves measured with TDR probe and tensiometer in a soil column of 2 cm deep with an installed pressure transducer. Saito *et al.* (2006) measured the soil water retention curve in a laboratory. A Tempe cell was used to measure the matric potential down to -800 cm and a pressure chamber was used for the lower heads till -15000 cm. The soil hydraulic properties were determined from the soil water retention curve. The soil bulk density is often determined by the core method (Novak, 2010; Deb *et al.*, 2011). Deb *et al.* (2011) used the constant head method to determine the saturated hydraulic conductivity and the pressure chamber method was performed to define the soil water retention curve. Thus a large variety of methods is used to calculated the different parameters.

3.2 Field experiments

3.2.1 Soil water content, soil pressure head and temperature profiles

This section reviews measurements of soil water content, soil pressure head and soil temperature performed in field experiments focusing on water vapour transport. Rose (1968a) determined the soil water content gravimetrically by taking soil samples in the field. The samples were taken of 1-5 cm depth and at a depth of 15 cm and analysed in a laboratory. The experimental site was assumed to be homogeneous, therefore it was argued to be acceptable to measure soil temperature at two other spots using thermistors at depths of 0, 0.4, 1, 2, 4, 7 and 13 cm. The thermistors were installed at those depths by inserting a vertical face with thermistors into the soil. The measurements lasted for six days, starting from a fully saturated situation. Jackson *et al.* (1973) measured the amount of evaporation by using lysimeters in the field. In both situation only upward flow of liquid water and water vapour was assumed and the assumption was made that the field is homogeneous.
Parlange *et al.* (1998) measured soil water contents and soil temperatures every 20 minutes. TDR probes at depths of 10, 20 and 30 cm were used for the soil water content measurements and platinum resistance temperature detectors were installed at depths of 2, 4, 7, 10 en 15 cm. These measurements were used to calculate the vapour fluxes. Bittelli *et al.* (2008) measured the soil water content by using ECH_2O probes. At depths of 2 and 5,5 cm the probes were installed in the soil. At a daily time scale soil samples were taken and gravimetrically measured to calibrate the ECH_2O probes. The ECH_2O probes were measuring continuously. At 1, 3 and 7 cm beneath the soil surface thermocouples were installed to measure the soil temperature. Steenpass *et al.* (2010) investigated a different topic, the estimation of the soil hydraulic properties by soil water content and soil temperature measurements. However the experiment is useful because a coupled heat and water movement model is used. Steenpass *et al.* (2010) measured soil water contents with TDR probes at 36 locations at depths of 7 and 15 cm below the soil surface. The monitoring was done on a time scale of a half-hour. On each location the soil temperature was also measured with thermocouples at depths of 3 and 6 cm every 6 hours manually.
Zeng *et al.* (2009) measured the soil water content, soil temperature and matric potential in the field for 17 days to quantify the effective infiltration of water in the soil. The soil water content and the soil temperature were measured with profile sensors which are especially appropriate devices for easily collapsing sandy soils (Fares & Polyakov, 2006). Another advantage of a profile sensor is the ability to measure gradients while normally two devices are needed with their own deviations in the measurements. The matric potential was measured with pF-meters installed at the same depths as the profile sensors. A pF-meter measures the molar heat capacity of the ceramic cup which is in contact with the soil. The pF-meters were installed at depths of 20, 30, 40 and 50 cm below the soil surface.
In the study by Saito *et al.* (2006) TDR probes and thermocouples were installed horizontally to measure respectively soil water contents and soil temperatures in the soil at depths of 2, 7 and 12 cm. Temperature in time and space was measured every half hour by Novak (2010) with copper constantan thermocouples and FD-300 diode thermometers at 30 depths 0.002 - 1.05 meter below the soil surface. The soil water content up to 21 cm depth was measured gravimetrically with a core sampler every 2 days and up to a depth of 100 cm every 3-10 days. The soil water contents were interpolated to obtain half-hour values. Deb *et al.* (2011) measured the soil water contents and soil temperatures with TDR probes and temperature sensors. The devices were installed at depths of 5, 10, 20 and 50 cm below the soil surface in duplo. The measurements were recorded every 15 or 30 minutes.

3.2.2 Initial and boundary conditions

In this section the initial and boundary conditions of field experiments are summarized which are described in papers. These conditions will be used for determining the boundary conditions for the laboratory experiment set-up which will be explained in section 7. Rose (1968a) brought the experi-

mental site first at saturation before starting the measurements. Parlange *et al.* (1998) remarkably do not present their initial conditions, maybe because they focussed in their study only on the changes in moisture content and not on the absolute values. Parlange *et al.* (1998) also did not define the boundary conditions in their study. Bittelli *et al.* (2008) set up an experimental station to measure the air temperature and the relative humidity on a hourly basis. Wind speed, precipitation and solar radiation were measured at a meteorological station nearby, also on a hourly time scale. Bittelli *et al.* (2008) started their experiment with a short irrigation event of 100 mm. After this irrigation event the soil water content was 0.49 at a depth of 2 cm and 0.33 at a depth of 5 cm. An infrared camera was installed in the field by Steenpass *et al.* (2010) to measure the soil surface temperature every 5 minutes. The meteorological data used in the model, had a half-hour time interval. Some distance from the experimental plot soil water content and soil temperature were measured with TDR and temperature probes. The measurements were taken at depths of 45, 60, 90 cm for soil water content measurements and at depths 15, 45, 60 and 90 cm soil temperatures were measured. These measurements were only needed for the initial conditions of the model. The soil water content measurements at depths of 7 and 15 cm were used for the inverse optimization to determine the soil hydraulic parameters.

Milly (1984) performed a study with two hypothetical soils in two different climates. For the upper boundary condition however real measured meteorological data was used. For both stations the 3- and 6-hourly meteorological data was interpolated to compute hourly data which is the time scale for the model. The total model run was 31 days. The meteorological data consisted of air temperature, wind speed and precipitation rate. The absolute humidity is computed by using temperature and dewpoint. Solar radiation is defined by solar angle, cloud cover and atmospheric turbidity and atmospheric radiation is calculated by air temperature and cloud cover. All of these parameters are required to calculate the evaporation rate at the soil surface which is the upper boundary condition in the model of Milly (1984). Because the water table is more than 2 meters below the soil surface, Zeng *et al.* (2009) defined the lower boundary conditions as free drainage, while the upper boundary condition was described by the surface energy balance. For heat the lower boundary condition was set to a gradient of zero and the soil surface temperature was defined as upper boundary condition. The initial conditions for the model nodes were determined by interpolation of the soil water content and soil temperature measurements of the first day. Daily meteorological data from a meteorological station was used by Saito *et al.* (2006) consisting of air temperature, relative humidity, precipitation rate, solar radiation and wind speed. These data were used to calculate continuous meteorological values to define the upper boundary condition in terms of hourly records (Simunek *et al.*, 2008). The upper boundary conditions for liquid water and water vapour were calculated from the water balance equations and for the heat conservation equation from the surface energy balance equations. The bottom boundary had a temperature gradient of zero, and free drainage was assumed because of deep groundwater tables. As initial condition Saito *et al.* (2006) used the average soil water content measured on the first day and average soil temperatures were calculated from the measured values at three depths on the first day.
Novak (2010) used the same lower boundary conditions in his study; matric potential gradients and temperature gradients are zero. The upper boundary conditions were the soil heat flux for the heat mass balance and the evaporation rate at the soil surface for the mass balance of water. The first measurements of soil water contents and soil temperatures were taken as initial conditions. All the energy balance terms were measured on a half-hour basis. The latent and sensible heat fluxes were determined by the Bowen ratio technique using psychrometers (Novak, 2010). Deb *et al.* (2011) used the first measurements of soil temperatures and soil water contents at depths of 5 and 50 cm as respectively lower and upper initial conditions. Linear soil water content and soil temperature profiles were assumed for the initial conditions to give every node in the model an initial value. Deb *et al.* (2011) used the meteorological data to compute the soil heat flux and defined this value as the upper boundary condition for the heat mass balance. A temperature gradient of zero was taken as lower

boundary condition. The transfer of heat across the lower boundary was assumed to occur only by convection of liquid water and water vapour (Deb *et al.*, 2011). For the mass conservation equations for water the evaporation at the surface was taken as upper boundary condition, and free drainage as lower boundary condition was assumed because of the deep groundwater tables. The top and bottom boundary conditions used for the mass balance and heat conservation equation are important information for model studies. This helps in this report for subsequent chapters about modeling coupled heat and water transport.

3.2.3 Parameters

For the calculation of the water vapour and liquid water fluxes the vapour and liquid diffusivity coefficients are required (Parlange *et al.*, 1998). In their paper measured soil water contents and the soil temperatures were used for these calculations. Changes in the gaseous pore space and temperatures over time were used to calculate a soil air velocity. The velocity of the soil air is the central variable for the convective vapour transport. Bittelli *et al.* (2008) installed soil heat flux sensors 2 and 7 cm below the soil surface. The determination of the soil heat flux was important for the calculation of the evaporation from the energy balance. The radiation was measured at a meteorological station nearby so only the sensible heat flux had to be measured to calculate the latent heat flux and the evaporation rate. The sensible heat flux is calculated using high frequency temperature measurements above the soil surface. The aerodynamic resistance, used in the study by Bittelli *et al.* (2008), is calculated from wind speed measurements. In the study by Zeng *et al.* (2009) the precipitation was measured using a tipping bucket gauge with a precision of 0.01 mm. Also other meteorological variables like the relative humidity, net radiation, air temperature and the wind velocity at 2 meter were measured. Soil samples were taken by Zeng *et al.* (2009) at depths of 10, 20, 30, 40 and 50 cm to determine the soil hydraulic properties. Only samples from the top layer were taken because that is the most active layer for coupled heat and water flow (Zeng *et al.*, 2009). At 50 cm depth hysteresis occurred, which makes it hard to determine the Van Genuchten parameters by the inverse method. Instead of the inverse method, a pressure extraction chamber was used to determine the parameters. Zeng *et al.* (2009) note the importance of hysteresis and the necessity to understand this process because of the impact on the water fluxes in the soil. Novak (2010) had to do one parameter calibration; the saturated hydraulic conductivity, which was determined by iteration so that measured and simulated latent heat fluxes agree sufficiently. Measurements from the first day were used for the calibration. Deb *et al.* (2011) used measurements of a meteorological station, which was 100 meters away from the experimental site. Precipitation, solar radiation, air and soil surface temperatures, wind speed and relative humidity were measured on a hourly time scale. The parameters soil emissivity and soil surface albedo were estimated.

3.3 Discussion experiments

From the sections above a difference can be noticed between laboratory and field experiments. Laboratory experiments focus on parameters such as the enhancement factor and the saturated hydraulic conductivity. The convective vapour flux is also thoroughly investigated in a laboratory. The field experiments focus more on the evaporation rate at the soil surface. The surface energy balance is also an important component in field experiments. Many times the surface energy balance is used as the upper boundary condition (Saito *et al.*, 2006; Zeng *et al.*, 2009; Deb *et al.*, 2011) for the calculation of which meteorological data is necessary. In the laboratory the upper boundary conditions is most of the time controlled by a constant high temperature. This has the result that diurnal effects of coupled heat and water movement are more investigated in the field than in the laboratory. The lower boundary conditions for heat and water balances in the laboratory are often prescribed state variables, of a Dirichlet type. A constant water table is used with a fixed temperature as lower boundary conditions.

While in the field frequently flux conditions, Von Neumann types of boundary conditions, are chosen with zero gradient.
The same kind of measurement devices are used in the field as in the laboratory. Soil water content is measured gravimetrically or by TDR probes. Dielectric soil moisture ECH_2O sensors were used by Bittelli *et al.* (2008) and Smits *et al.* (2011). Soil pressure head is in the field measured with tensiometers or pF-meters; in the laboratory researches next to these devices also pressure chambers, Tempe cells and suctions cells are used. In the field and in the laboratory temperature profiles are measured with many different devices as EC-5 sensors, profile sensors. Most of the time however thermocouples are used, especially the copper constantan thermocouple.
In almost all the papers the accuracy of the experiments is not presented due to difficulty to quantify the accuracy. Further the measurement error depends often on many factors, like MPS-1 sensors become less accurate if the soil water pressure decreases to -25000 cm. According to Smits *et al.* (2011) the difference between the computations from a model and the results from field experiments under transient conditions makes it very difficult to draw conclusions about the accuracy about the experiment or the model.

4 Fieldwork in Trabadillo

4.1 Field situation

Area

The measurement profiles are situated in the La Mata catchment which is a subcatchment of the Sardon catchment. The La Mata catchment has a size of circa 4.5 km^2 and inside the La Mata catchment there is a small village, Trabadillo. All are located in the Salamanca district, see figure 1. The topography of the La Mata catchment is hilly and it is situated on a plateau at 600 meters above see level. The catchment is used for the grazing of cows, sheep and pigs. On the top of the hills shallow soils are found with a depth of around 30 cm on a weathered granite layer. Closer to the valley deeper soils are found with a maximum depth of circa 2.5 meters on weathered granite again. The soils on the top of the hills consist primarily of sand, while the soils closer to the valley consist in majority of silty material. The measurement profiles are located on a slope. In the wet season the wadies are filled with water and a high amount of surface water flow occurs. In September, the end of the dry season, the wadies are already dried up and the groundwater levels have dropped to al least 3 meters beneath the surface in the (fractured) granite on the hills, because the piezometer is not able to measure the groundwater table.

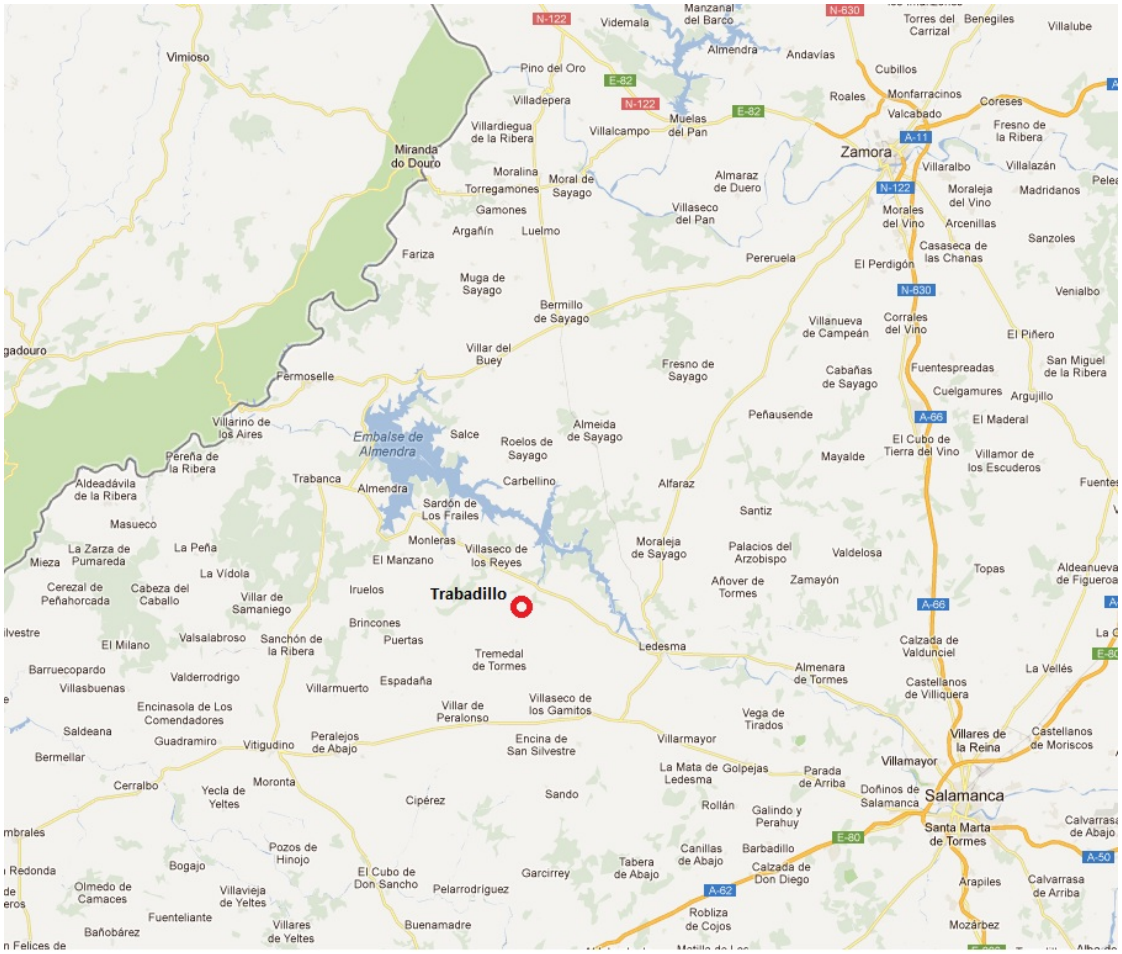

Figure 1: Map of the district of Salamanca where Trabadillo is located.

4.2 Measurement method

Profiles

In two locations measurement profiles are installed to measure soil water content, soil temperature and matric potential. One location is near a tree and has three measurement profiles; (1) close to the tree, (2) beneath the canopy and (3) five meters away from the stem, not influenced by the canopy shadow. The other location is roughly 50 meters downhill near a weather station. One measurement profile (4) is in the bare soil, the other profile (5) is placed in a plastic tank with a depth of one meter and a diameter of around 50 cm. A large diameter is chosen to avoid unwanted wall effects. The soil depth of measurement profile 4 is at its maximum circa 300 cm deep with a (fractured) granite layer beneath it. The plastic tank is installed by digging a hole in layers of 5 cm which were carefully kept apart. The plastic tank is placed in the hole and the layers were put back in the same order as they were present and the layers were slightly compressed. In this way the soil inside the tank is assumed to have a similar soil textural build up as the original soil around the tank. Finally the sensors were installed. A soil description based on soil texture divided the soil profile in four different layers. The division is based on visual soil texture analysis. In a laboratory the soil hydraulic properties are determined for these four layers and are assumed to be constant for a particular soil layer. The tank is made from plastic to create an one dimensional heat flow inside the tank; the heat conductivity of the plastic is very low compared to the heat conductivity of the soil. After the installation one hydrological cycle, one year, is waited before the measurements can start due to the time needed for the soil to equilibrate to the surrounding area with respect to heat and water conditions. Profile 4 was installed to compare with profile 3 and is assumed to have similar conditions. In profile 4 the total evaporation from the unsaturated zone and saturated zone can be computed while in profile 5 only the evaporation from the unsaturated zone can be computed, because profile 5 is enclosed at the bottom of the tank. The difference between those two profiles shows the evaporation from the groundwater and thus in this way the evaporation from the unsaturated soil and the groundwater can be partitioned.

Devices

The measurement devices are installed in the same way in almost every soil profile. At the same depths hydraprobes (Hydra Probe II soil sensor from Stevens) and MPS-1 sensors (MPS-1 Dielectric water potential sensor from Decagon) are installed. Only profile 2 has no MPS-1 sensors. At depths of 25, 50, 75 and around the 100 cm (close to weathered granite) hydraprobes are placed to measure the soil moisture content and the soil temperature. MPS-1 sensors were installed at depths of 25 and 75 cm to measure the matric potential. A schematic view of the experimental set-up can be seen in figure 2. Although the MPS-1 sensor can measure up to -25000 cm the matric potential, the accuracy decreases closer to -25000 cm and so the top soil is too dry to measure accurately the matric potential. On the basis of this low measurement accuracy there were no MPS-1 sensors installed in the top soil. The MPS-1 sensor consist of a ceramic cone which in the soil will come to equilibrium with the surrounding with respect to soil water content. The sensors uses a dielectric technique to measure the soil water content. Because the ceramic never changes and the relation between soil moisture and matric potential is known, the matric potential can be determined from a soil water content measurement. The hydraprobe has four needles of which the centre needle sends an electrical pulse and the other three needles measure the strength of the signal. The strength of the signal is related to the soil water content with a simple formula with calibrated coefficients. The centre needle also measures the soil temperature. The hydraprobes are calibrated on the soil moisture data for the site-specific soil at Trabadillo. This is only needed for soil water content measurements. All the sensors and probes are connected to a data logger, a Campbell CR1000 (from Campbell Scientific, Inc.). Additionally, profiles 4 and 5 both have a POT sensor at the depth of 15 cm to measure the matric potential and the soil temperature. This sensor should be able to measure in the very dry

conditions of the top soil. The POT sensor is a polymer tensiometer which has a ceramic cone with a very small volume of polymer solution inside the tensiometer (Van der Ploeg *et al.*, 2010). The cone shape results in a larger contact area with the soil. The small volume of the POT sensor gives acceptable response time for laboratory and field experiments. The POT sensor has an internal data logger. The error of the measurements for all installed devices is estimated to be 10% at maximum, in which an increase in soil water content will result in more accurate measurements with smaller errors. Except for the POT sensor which becomes more accurate in drier conditions.

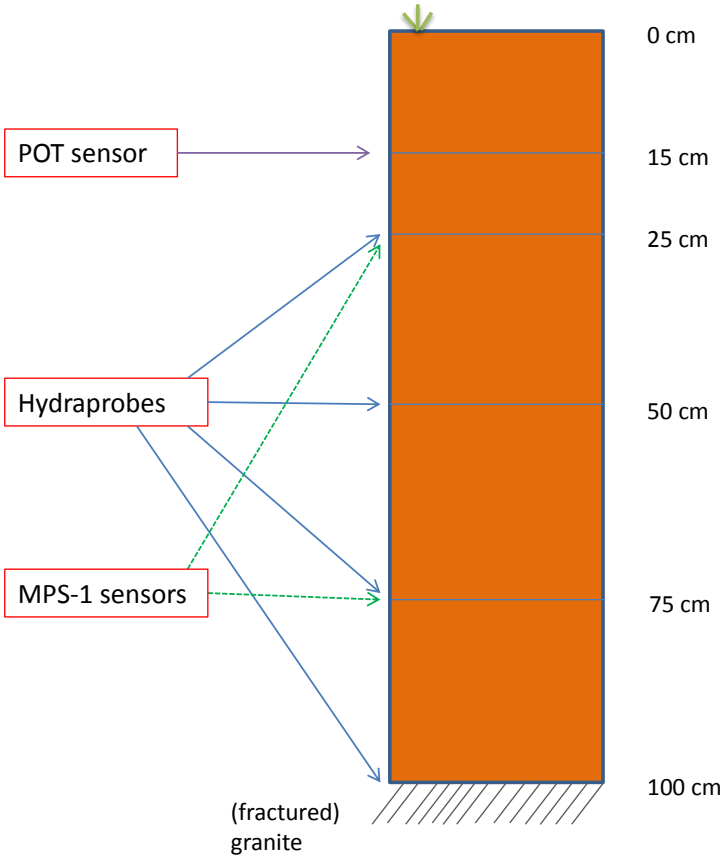

Figure 2: Schematic view of the experimental set up of the installed devices.

Boundary conditions

Circa five meters from profile 4 a piezometer is located which measures the groundwater level automatically by using a diver with a pressure transducer installed inside the piezometer. There is also a piezometer with a diver with pressure transducer installed in the plastic tank to measure the height of the water table inside the tank. In the wet season water can accumulate at the enclosed bottom and the plastic tank can become saturated. For profiles 4 and 5 the soil surface temperature is measured with an infra-red meter (SI-111 Precision Infrared Radiometer from Campbell Scientific, Inc.). In the weather station observations of the atmospheric conditions are taken. Relative humidity and air temperature are measured at the heights of two and six meters. Wind speed is only measured at six meters above the surface, the device at two meters above the surface is broken. Short and long in- and outgoing radiation is measured two meters above the surface. In the weather station two rain gauges

are placed; one with a diameter of 10 cm and the other with a diameter of 30 cm. Inside both rain gauges a tipping bucket counts the amount of precipitation during a rainfall event. The hydraprobes installed 100 cm beneath the soil surface measure both the soil water content as the soil temperature. These soil temperature at that particular depth will serve as bottom boundary condition for the heat balance equations. The measured soil water content will be used as initial condition for the water balance equations.

Interval

The measurements of the variables in the soil, the atmosphere and the piezometers are all logged on a hourly time basis. The measurement period is from the 2nd of May till 28th of September 2011, which are 149 days. The rain gauges record the tip and the hour of the tip. This can easily be summed per hour to get the hourly time basis. Data recording on a hourly time basis should be sufficient for analysing the daily behaviour of a coupled heat and water transport model. Note that in the field experiments of Steenpass *et al.* (2010), Novak (2010) and Deb *et al.* (2011) measurements are taken every 30 minutes for a shorter period of time, because their interest is more detailed. Hourly records of the time-variable boundary conditions will be provided to the models used in this thesis.

Infiltration/evaporation experiment

On Tuesday 20th of September an infiltration experiment was performed with a piston flow inside the plastic tank of profile 5. From this experiment the soil hydraulic properties can be calculated and these can be compared to the soil hydraulic properties determined in the laboratory. A metal circular ring was placed around the plastic tank. A sealing construction was used to avoid leakage, thus the actual input of water can be determined. The sealed construction consisted of by plastic bags taped around the metal ring. Water was inserted into the metal ring and the time was recorded to measure the infiltration rate. Leakage occurred and the experiment for the determination of the infiltration rate was a failure. Without the leakage ponding water inside the metal circular form justifies the assumption of an one dimensional downward water flow. In the end the soil inside the plastic tank was fully saturated with water. From that moment the soil will have potential evaporation rate. After one week the data is downloaded from the CR1000 data logger and from the POT internal data logger.

4.3 Measured data

Soil hydraulic properties

The soil hydraulic properties are determined by the ITC students Abubeker (2010), Agbakpe (2010) and Salinas Revollo (2010). In table 1 the measured values are shown. They used two different methods to determine the parameters and it's not clear which method is used for which layer or sample. What is known is that the choice of the method depended on the type of measurement. When a sample was taken from the field, texture analysis was done and the soil hydraulic parameters were retrieved from the SPAW software or by the Rosetta software. Both programs focus on the relative contribution of the different soil textures in the total soil. Pedotransfer functions calculate from the relative distributions of the different soil components the soil hydraulic properties of that particular soil. When the students took ring samples they determine the parameters separately. The saturated hydraulic conductivity is determined by an infiltrometer produced by Eijkelkamp. The bulk density and the porosity were gravimetrically determined. The WP4 (WP4 Dewpoint Potentiameter from Decagon) is used to find the soil moisture characteristics. Finally the textures of the ring samples were analysed. The measurement parameters are described in a data set, with no information regarding the confidence intervals of those parameters. The determination is done for four different depths, at 25, 50 ,75 and 100 cm. There is little variability in the parameters θ_r, α and n between the four depths.

For two parameters θ_s and K_s a larger variability is found between depths. So it is better to use four different layers instead of one layer in the model study with a specific parameter set of soil hydraulic properties for each layer. The empirical shape parameter l was not determined by the ITC students, but fixed at a value of 0.5. Fixing the value of l is more often done in research (Mualem, 1976; D'Urso, 1997).

Table 1: Soil hydraulic properties determined in laboratory by Abubeker (2010), Agbakpe (2010) and Salinas Revollo (2010).

Layer (beneath soil surface (cm))	$\theta_r(cm^3/cm^3)$	$\theta_s(cm^3/cm^3)$	$\alpha(1/cm)$	$n(-)$	$K_s(cm/d)$	$l(-)$
1 (0-37.5)	0.02350	0.39890	0.060300	1.758400	612.15524	0.5
2 (37.5-62.5)	0.02473	0.29880	0.037786	1.460343	364.96359	0.5
3 (62.5-87.5)	0.02510	0.23580	0.023300	1.352800	44.77700	0.5
4 (87.5-100)	0.02510	0.24820	0.023300	1.352800	0.86659	0.5

Meteorological data

A data set is available with measurements of several meteorological variables starting from the first of May 2011 till the 28th of September 2011. The meteorological variables consist of the air temperature and relative humidity measurements from a height of 2 and 6 meters above the surface. The wind speed is only measured at a height of 6 meters above the surface. The soil heat flux is measured at 10 cm beneath the surface and the short wave in- and out-going radiation is measured at 2 meters height. The rain is measured with rain gauges with tipping buckets inside the gauge. All of these data will be used to compute the potential evaporation during time which defines the upper boundary conditions for the mass conservation equation for water. For these calculations the SWAP model will be used (Kroes *et al.*, 2008).

Profile data

From the 25th of August 2010 measurements are done in the soil profiles. Because of the possible influence of the tree in profiles 1, 2 and 3, these profiles can not be used for in this thesis. Profile 4 and 5 are situated in the bare soil and will further be called as respectively the open and the closed profile. For the open profile measurements of the soil water pressure, soil temperature and soil water content are available in the set up as described in section 4.2 and as can be seen in figure 2. The POT sensor has measured since the 26th of April 2011. In the closed profile some unknown problems occurred. The POT sensors stopped on the 17th of May 2011 for an unknown reason. Next to that the hydraprobes measured strange soil moisture contents and soil temperatures, while in the period before April 2011 the measurements were good. However these measurements are taken from the wet season and not useful in this thesis. So the closed profile can't be used for the simulations because of the lack of reliable data. The cause(s) for the failures of the measurement devices is still unknown. This stresses the necessity to include replicate measurements in multiple soil profiles. Only the data from profile 4, the 'open' profile, is available and will be used for the model simulations. The soil surface temperature measured with an infra-red meter is available on a hourly time scale.

5 Calibration

5.1 Calibration method

The soil hydraulic parameters are very important properties for the modelling of coupled heat and water movement. The seven parameters which represent the soil hydraulic properties are θ_s, θ_r, α, n, m, K_s and l. The soil hydraulic parameter m is excluded from the calibration by assuming that $m = 1 - 1/n$. The accuracy of the modeling results depends on the accuracy of these parameters. The soil hydraulic properties determined by the ITC students are doubtful, that's the reason an additional calibration will be performed on the parameters. The profile is divided into four layers with the sections 0-37.5 cm, 37.5-62.5 cm, 62.5-87.5 cm and 87.5-100 cm. These sections are chosen because the soil samples and measurements for determining the soil hydraulic properties are done on depths of 25 cm, 50 cm, 75 cm and 100 cm, which is in the middle of a section. The upper two layers show the most variability in the parameters, so the calibration can be performed for the four layers or only for the upper two layers. Further will only the parameters α, n, K_s be calibrated. The parameter l will at first be fixed at 0.5 which is frequently done in research (Mualem, 1976; D'Urso, 1997; Saito *et al.*, 2006; Sakai *et al.*, 2009). The parameters θ_s and θ_r are easy to measure in the laboratory and the confidence in the values of both parameters is high. The parameters α, n, K_s will be calibrated for the upper two layers and for all the four layers by inverse parameter estimation method which is included in Hydrus-1D. Hourly data from a period of one month will be selected for the calibration. The 2nd of May until the 31st of May is selected because in this month the change in soil water content is the largest. Thus the largest part of the soil water retention curve is described by this data selection, which is essential for a good estimation of the soil hydraulic properties. The results of the inverse parameter estimation will consist of an estimation of the parameter, a standard error and a 95% confidence interval. The first inverse parameter estimations show an unacceptable large standard error for the saturated hydraulic conductivity, K_s. The decision is taken to use the K_s measured in the laboratory and to calibrate the parameter l which has also effect on the calculation of the unsaturated hydraulic conductivity as can be seen in eq 2.8. Further the parameters b_1, b_2 and b_3 from equation 2.27 need to be calibrated to represent the observation profile. Inverse parameter optimization of these parameters is not implemented in Hydrus, so this will be in another explicit way. By manually adjusting the parameters the modelled soil temperatures will be fitted to the measured soil temperatures for four depths till the difference between the measured and computed soil temperatures is sufficiently small.

5.2 Input data

Data from the open profile will be used for the calibration of the soil hydraulic properties. Soil moisture measurements at depths of 25, 50, 75 and 100 cm beneath the soil surface and soil water pressure head measurements on depths of 25 and 75 cm will be used as input data. The data will be related to time and to each other for the inverse modeling. Next to that the measurements over time from the POT sensor will be applied in the inverse parameter estimation. The POT sensor measured the soil water pressure 15 cm beneath the soil surface. With the program SWAP the potential evaporation for the specified month is computed on a hourly time base. SWAP uses Penman-Monteith to calculated the potential evaporation and as input data for that calculation the incoming shortwave radiation, the air temperature and relative humidity at 2 meters above the surface, the wind speed at 6 meters above the surface and the amount of rain are provided(Monteith, 1965). The inverse parameter estimation in Hydrus is executed by using the potential evaporation as upper boundary condition for the mass balance of water. Next to that free drainage is taken as bottom boundary condition. For the heat conservation equation the surface temperatures measured with the infra-red sensor are used as time-variable top boundary condition and the soil temperature measured with the hydraprobe at 100 cm below the soil surface is taken as the lower boundary condition.

For the determination of the parameters b_1, b_2 and b_3 of equation 2.27 the modelled soil temperatures at depths of 25, 50, 75 and 100 cm will be compared to the measured soil temperatures measured at those depths with the hydraprobes.

5.3 Calibration results

The results of the inverse parameter estimation will be an estimation of the parameter, a standard error and a 95% confidence interval. These results can be seen in appendix A. Next to that a correlation matrix is produced by Hydrus which gives the correlation between the parameters, given in appendix B. A high correlation between parameters means that a parameter contains less unique information. And thus will have a higher uncertainty. In table 2 the soil hydraulic properties are given for the four layers with the mean calibrated values for the parameters α, n and l. Because the parameters are doubtful, simulation with the calibrated parameters doesn't match the observations. Especially the differences between the calculated soil water pressures in Hydrus and the measurements of the POT sensor are unacceptable large as can be seen in appendix C. The abrupt change in soil water pressure head for the POT measurements at day 112 is due to a rain event. This rain event is unnoticeable in the computed results because probably the input of rain is evaporated quickly. This can be due to (1) the POT hasn't measured accurately, (2) the weight factor for the POT sensor has to be lower than for the other data for the inverse parameter estimation procedure, (3) the POT data can't be fitted by the parameters l and K_s, and (4) the Mualem-Van Genuchten curve is not able to fit the POT data because only data from the dry range is available (Van Genuchten, 1980). In table 3 the fitted parameters b_1, b_2 and b_3 can be found for the four layers. These will be used in the model simulations.

Table 2: Calibrated soil hydraulic properties.

Layer (beneath soil surface (cm))	$\theta_r(cm^3/cm^3)$	$\theta_s(cm^3/cm^3)$	$\alpha(1/cm)$	$n(-)$	$K_s(cm/d)$	$l(-)$
1 (0-37.5)	0.02350	0.39890	0.02748	1.53790	612.15524	0.00004
2 (37.5-62.5)	0.02473	0.29880	0.03625	1.44140	364.96359	1.98110
3 (62.5-87.5)	0.02510	0.23580	0.03431	1.48830	44.77700	0.04064
4 (87.5-100)	0.02510	0.24820	0.01920	1.62800	0.86659	1.03120

Table 3: Soil thermal parameters.

Layer (beneath soil surface (cm))	$b_1(W \cdot m^{-1} \cdot K^{-1})$	$b_2(W \cdot m^{-1} \cdot K^{-1})$	$b_3(W \cdot m^{-1} \cdot K^{-1})$
1 (0-37.5)	-28.65	-44.5	196.5
2 (37.5-62.5)	-28.75	-45	197
3 (62.5-87.5)	-29	-50	200
4 (87.5-100)	-29	-50	200

Figures 3 and 4 show the result of the fitted soil thermal parameters. The measured temperatures at depths of 25 cm and 75 cm are plotted against the modelled temperatures at 25 cm and 75 cm. In total 3576 points are plotted, which are all the hourly measured and computed soil temperatures for the total 149 days of the data set. Further a one-by-one line is plotted inside the graphs. At both depths the modelled soil temperatures fit the measurements quite reasonable. Only for low soil temperatures, $285 - 290$ Kelvin, the measurements are somewhat higher than the modelled temperatures. The largest difference between the model and the measurements is 5 Kelvin and can be found for the depth of 25 cm. Although this is only for one point, so further is assumed that the Hydrus can model the soil temperatures with a sufficient accuracy.

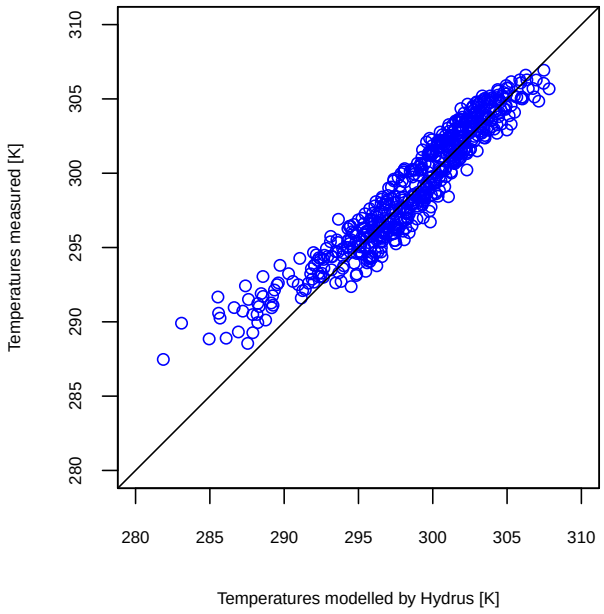

Figure 3: Graph of measured soil temperatures (K) plotted against modelled soil temperatures (K) for the depth of 25 cm.

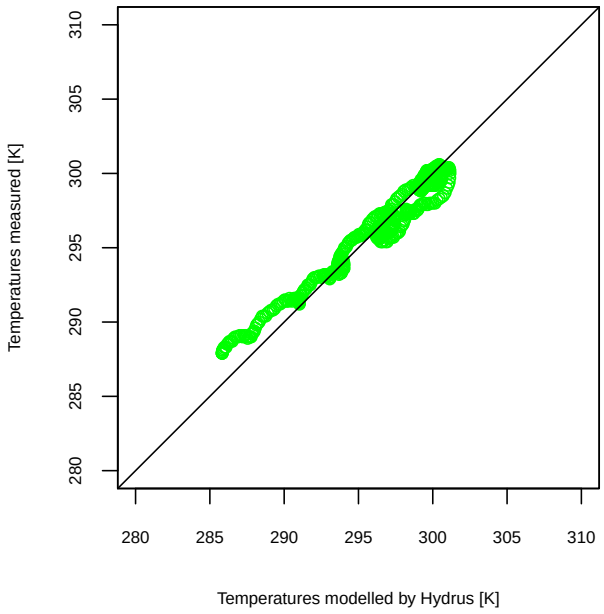

Figure 4: Graph of measured soil temperatures (K) plotted against modelled soil temperatures (K) for the depth of 75 cm.

6 Modeling the fluxes

6.1 Objective

The contribution of water vapour movement in addition to the transport of liquid water on the perspective of a daily time scale is the main research question of this thesis. The programs Hydrus and SWAP will be used to investigate the different fluxes. Hydrus will be used to calculate the liquid water-, isothermal water vapour- and thermal water vapour fluxes, while the latest SWAP version will compute only the liquid water flux. The liquid water flux is in the output of Hydrus unfortunately not subdivided into a thermal and an isothermal part. Nevertheless, As noted earlier, according to Milly (1984) and Jassal *et al.* (2003) the thermal liquid flux has no effect on the total liquid water flux. It's undesirable to draw a conclusion about the contribution of the different fluxes to the total water movement in the soil by using uncertain soil hydraulic parameters. A solution to overcome this uncertainty in the parameters is doing Monte Carlo simulations. More specifically, a large amount of samples of parameter sets will be taken from correlated (log)normal distributions and for every parameter set the different fluxes will be computed. The soil hydraulic parameter α is assumed to be log-normal distributed. The parameter n is assumed to be distributed as log-normal-1 (n can not become lower than 1) and l is regard to be normal distributed. Equations 6.1 and 6.2 describe the transformation between the mean and the standard deviation of a normal distribution, respectively μ and σ, and the mean and standard deviation of a log-normal distribution, respectively M and S.

$$M = exp(\mu + \frac{\sigma^2}{2}) \tag{6.1}$$

$$S^2 = exp(2 \times \mu + \sigma^2)[exp(\sigma^2) - 1] \tag{6.2}$$

Different kind of simulations will be executed: one set of simulation runs will focus on the different fluxes from Hydrus, i.e. the partitioning of the isothermal water vapour flux, thermal water vapour flux and the liquid water flux. The other simulations will focus on the differences between Hydrus and SWAP. For the partitioning of the fluxes simulated by Hydrus multiple runs will be performed and the fluxes will be presented in box plots to analyse them. In total three runs will be done each consisting of 100 parameter sets of soil hydraulic properties. The three runs will be compared with each other to find out if the runs are significantly different. Welch's t-tests will be performed on the runs to investigate if 100 parameter sets are enough to overcome the uncertainty of the soil hydraulic properties. The level of significance is set at 5%. In case the three runs are not significantly different from each other, conclusions can be drawn about the significance of the different fluxes and a decision can be taken about which flux will be implemented in addition to the liquid water flux in the SWAP model. Notice that the output from Hydrus only provides instantaneous fluxes for selected moments in time for the partitioned different fluxes, although for this research the daily time scale is of interest. To be able to decide about the significance of the difference between the fluxes, box plots will be made for midnight and for 12 o'clock. It's not possible in Hydrus to calculate cumulative water vapour fluxes over one day, only instantaneous fluxes are given in the output. Integrating the instantaneous fluxes over one day is impossible due to the error in the flux of the upper node. This will be discussed in more detail in section 6.3.1. The simulation for the difference between Hydrus and SWAP will result in three daily cumulative outputs. These will include the results from the SWAP model with only liquid water flow, the Hydrus model with only liquid water flow and the coupled Hydrus model with liquid water and water vapour flow. In this way Hydrus and SWAP can be compared when both are modeling the same processes. Additionally the contribution of movement of water vapour in the soil can be assessed. This method will be used to investigate the significance of the fluxes and a decision can be made if an additional flux must be implemented in SWAP which currently contains only an isothermal liquid water flux.

6.2 Modeling settings SWAP and Hydrus

To make a justifiable comparison between the output fluxes from the SWAP and Hydrus model it is essential to use similar input conditions for both models. The units days and centimetres are chosen for the time and spatial scales. As lower boundary condition for the mass balance of water free drainage is taken for both models. As upper boundary condition both models have also the same conditions. The precipitation is measured in the field and the potential evaporation is calculated in SWAP using detailed data about rainfall, radiation, relative humidity and wind speed on a hourly time base. These calculated potential evaporation rates over time are used as input for Hydrus, so both have the same top boundary conditions for the mass balance of water. For the conservation of heat the measured soil surface temperatures are used as upper boundary conditions in Hydrus and the soil temperatures measured by the hydraprobe at 100 cm below the soil surface is used as lower boundary condition. For the SWAP model (only liquid water transport) the temperature is less important because only isothermal liquid water flow is considered. As upper boundary condition the air temperature at 2 meter is used and a logarithmic velocity profile is assumed (Kroes *et al.*, 2008). Zero heat flux is implemented as lower boundary condition.
In Hydrus the soil column of 1 meter is discretisized in 101 nodes, which result in an inter-nodal distance of 1.0 cm. This is a rather coarse discretization, but large mass balance errors forced this coarse discretization to achieve minimum mass balance errors. According to Simunek *et al.* (2008) the nodal spacing of 1 cm should be small enough to compute reliable values. Deb *et al.* (2011) faced the same problems and noticed smaller nodal distances, so a finer discretization most of the time results in better simulations, but also causes the model not to converge. The mass balance errors are all based on the total flux. The SWAP model doesn't have an equally distributed discretization. The upper 10 cm has an inter-nodal distance of 0.4 cm and the rest of the profile has an inter-nodal discretization of 0.5 cm, which results in 205 nodes in total. In SWAP the option is selected to calculate the actual evaporation rate according to Darcy's law. This method has a tendency to overestimate the amount of evaporation, because of the soil hydraulic properties of the upper layer, which are often invalid for the top few centimetres. The alternative methods by Black (1969) or Boesten & Stroosnijder (1986) were not selected to avoid a more complex comparison between the models by adding an additional degree of freedom. The initial conditions for the mass balance equation consist of the soil water contents 0.1 $cm^3 \cdot cm^{-3}$ at the top and 0.135 $cm^3 \cdot cm^{-3}$ at the bottom. For the heat conservation equation the top boundary has an initial value of 8 °C and the initial bottom boundary condition is 14.4 °C. The soil water content and soil temperature profiles are assumed to be linear initially, similar to the study by Deb *et al.* (2011). The soil thermal apparent conductivity, $\lambda(\theta)$, is a coefficient for computing the amount of heat transported through the porous media without the transport by liquid water or water vapour flow. In Hydrus equations 2.26 and 2.27 are used to calculated $\lambda(\theta)$. SWAP uses a more physical approach to calculate the soil apparent thermal conductivity. In this approach the soil apparent thermal conductivity is calculated by weighted averages of the thermal conductivities of the different soil components, like clay, silt, sand, organic matter, water and air (De Vries, 1975).

6.3 Modeling results

6.3.1 General

In figure 5 the soil water pressure heads are plotted against the soil water contents for the measurements and calculations from the Hydrus and SWAP model. The upper graph shows the results for 25 cm below the soil surface and the lower graph for the depth of 75 cm. Because the period is from 2nd of May till the end of September only dry conditions are obtained. And less than half of the soil water retention curve is plotted. First of all the results from Hydrus and SWAP are similar for both depths. It has to be noticed that the models should correspond because both consist of the same soil hydraulic parameters, thus the soil water retention curve is plotted in figure 5. At the depth of 25 cm the results

from the Hydrus and SWAP model seem to describe the soil water conditions in the soil well, because the differences with the measurements are quite small. The models perform worse for the depth of 75 cm, drier results are computed compared to the measurements. This phenomenon could be due to the soil hydraulic parameter θ_r, the residual soil water content being too small. As can be seen in table 2, a value of 0.02510 is used. This value is measured in the laboratory, but according to figure 5 a value of about 0.07 $cm^3 \cdot cm^{-3}$ seems to be more plausible. But on the other side the measurements are also doubtful, especially in the dry range where a small change in θ results in a large change in soil water pressure head, h, large measurement errors are often unavoidable. Thus the subquestion if the Hydrus-1D model is able to simulate the field data can partly be answered by figure 5. At the depth of 25 cm the models correspond satisfactory to the measurements, while at 75 cm beneath the soil surface there is a discrepancy.

A point of discussion are the upper nodes in the discretized soil columns of the Hydrus and SWAP model. The upper one or two nodes behave different compared with the lower nodes. This happens in both Hydrus and SWAP. The flux calculated in SWAP at 0.2 cm beneath the soil surface is very small, in the order of 10^{-8} meter per second, compared to the nodes beneath it for almost every time step. In Hydrus the same magnitude of the flux can be observed or the flux can even have an opposite direction with respect to the flux of the nodes exactly below the top node. This leads to the question whether the flux at the upper nodes is really the flux at the soil surface or whether the models have difficulties calculating the flux at the soil surface because of the boundary conditions. The discretization is assumed to be small enough which should not be the issue. An investigation of the flux in the upper node (van Dam, pers. comm.) led to the conclusion that there's a large influence of the atmospheric conditions. Due to the very small flux, the water balance errors deeper in the profile cause the behaviour of the upper node. The flux of the third node, at 1 cm below the surface, is used for analysis in both Hydrus and SWAP to avoid the problem mentioned above. This flux gives a good representation of the fluxes in the upper part of the soil, as the error of the water balance is dampened. The flux of the third node will be assumed to be the in- or out-going flux over the top boundary.
As noted earlier the variance between the runs of a simulation will show the effect of the uncertainty in the soil hydraulic properties and soil thermal parameters. Three runs will be done in both Hydrus and SWAP, each consisting of 100 parameter sets of soil hydraulic properties. The soil hydraulic parameter sets are taken from normal and log-normal distributions as described earlier in section 5.1. Welch's t-tests are executed on the runs and the probability values (p-values) are assessed against a level of significance of 5%. The results are given in appendices D and F in which the italic values are below the level of significance. So the italic values represent for a specific instantaneous flux the runs which are significantly different from each other. There are some non-significant differences between the runs in Hydrus, especially in the dry period. At first glance it seems that a Monte Carlo simulation with 100 parameter sets is insufficient to overcome the uncertainty in the calibrated soil hydraulic properties. However when the figure 7 and appendix E are compared to each other the runs look quite similar. The insignificance can be explained by the small variance of these fluxes. When in the next run somewhat higher or lower soil hydraulic properties are used and the size of the flux is just a little bit higher or lower, it can result in a probability of being equal or lower than 5%. In absolute sense there's hardly no discrepancy between those two calculated fluxes. For taking away all the uncertainty it would be advisable to do runs with 200 or even more parameter sets of soil hydraulic properties, which will cost much more computation time. However it is still possible to draw conclusions about the box plots and the significance of the fluxes, because the behaviour of the fluxes in time remains the same. The difference in the magnitude of the fluxes is very small. And also the cumulative flux won't have a large standard deviation as can be seen later. Thus simulations with 100 parameter sets is sufficient to overcome the uncertainty in the calibrated soil hydraulic properties.

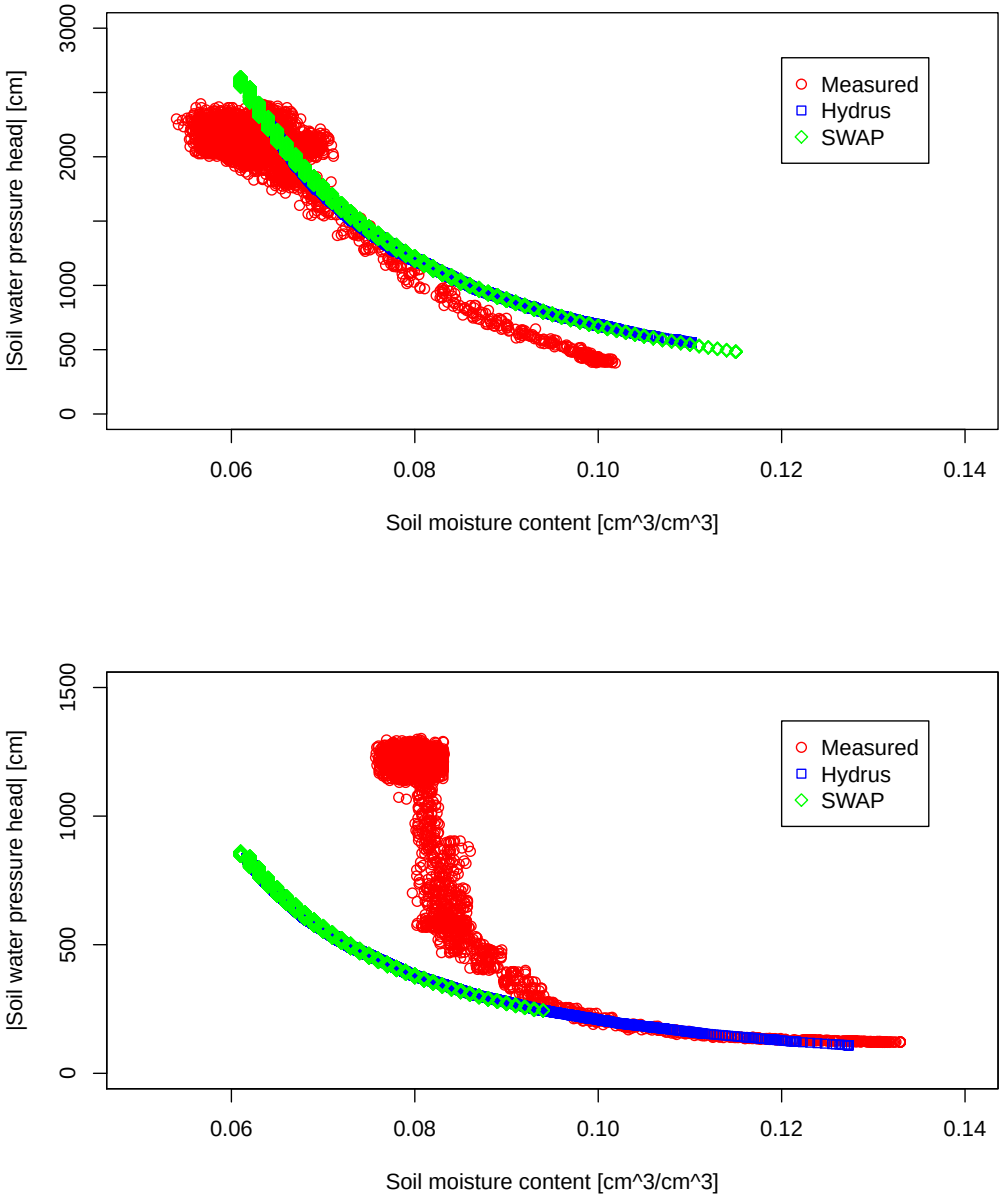

Figure 5: Figures of soil water conditions for depths of 25 cm (top) and 75 cm (bottom).

6.3.2 Isothermal water vapour flux

The isothermal water vapour flux can be seen in figure 7. This is an instantaneous flux at several specific moments in time. It is clearly visible that this flux is very small in comparison to the liquid water and thermal water vapour flux. This holds for both times of the day; midnight and at 12 o'clock. Only at 12 o'clock during the 2nd day an isothermal water vapour flux is visible with a mean still very close to zero. Appendix E shows a similar size of this isothermal water vapour flux for that particular moment in time. The other two fluxes have both larger variances and this spreading gives a small isothermal water vapour flux. The cause for the somewhat larger variances in the liquid water and thermal water vapour flux at this specific moment in time is unknown. It is interesting to find the explanation for this low isothermal water vapour flux. The cause of the negligible contribution to the total water transport can be understood from the equation for the isothermal water vapour flux, equation 2.4. The isothermal water vapour flux depends on a gradient and a conductivity factor. In figure 6 the pF (logarithm of soil water pressure head) and vapour density at different levels are plotted. Using equation 2.19 the vapour densities in the soil are derived from the measured and modelled soil water pressure heads. The Hydrus model corresponds closely to the field measurements for vapour density, meanwhile the similarities between measured and modelled soil water pressure heads are significantly different from each other (p-value<0.0001). Figure 6 shows a difference in head between the levels, so a gradient is present in the soil profile. However the hydraulic conductivity described in equation 2.13 is very low because the coefficient of the diffusivity of water vapour in air, D_a, is very low and this causes a very low isothermal water vapour flux.

6.3.3 Thermal water vapour flux

The thermal water vapour flux is shown in figure 7 and appendix E, which are graphs of two different runs with 100 parameters sets of soil hydraulic properties. In contrast to the isothermal water vapour flux this flux fluctuates in time. Although these fluxes are also instantaneous fluxes, the fluxes at midnight and at 12 o'clock give a clear view about the daily behaviour of the thermal water vapour flux. In the dry season, from 62nd day, the thermal water vapour flux is negative during the day (day 62.5, 100.5 and 148.5), the flux is directed inwards into the soil; during night (62nd, 100th and 148th day), the flux is positive directed out of the soil. The fluctuations of this flux are due to the diurnal temperature change; during the day the soil surface warms up faster than the soil at e.g. a depth of 50 cm due to the incoming radiation by the sun and a temperature gradient develops directed into the soil. During the night the opposite occurs: the soil surface cools down faster than the soil at 50 cm below the soil surface and a inverse temperature gradient develops directed out of the soil. During the night the thermal water vapour flux is the dominant flux, especially in the dry period from 62nd day. On the 2nd day the thermal vapour flux is positive during the night, probably because of the initial soil temperature profile with 8 °C on the surface and 14.4 °C at the bottom. This will result in an outgoing thermal vapour flux. Note that the thermal water vapour flux is based on the temperature gradient at midnight and at 12 o'clock. This temperature gradient can grow in magnitude during other moments of the day, which can result in even larger thermal water vapour fluxes.

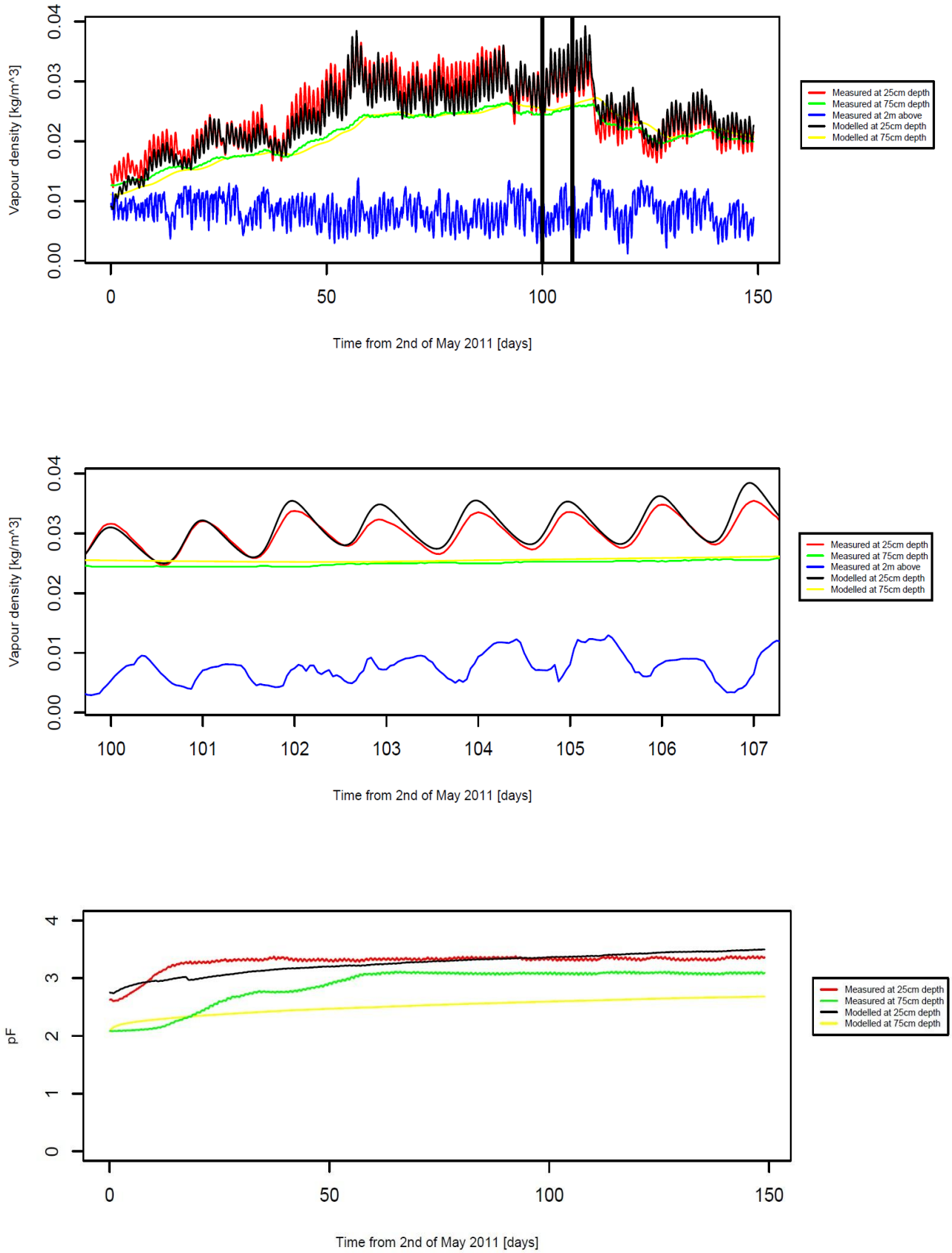

Figure 6: Top and center: Vapour densities ($kg \cdot m^{-3}$) for different levels in time. Bottom: pF at different levels in time.

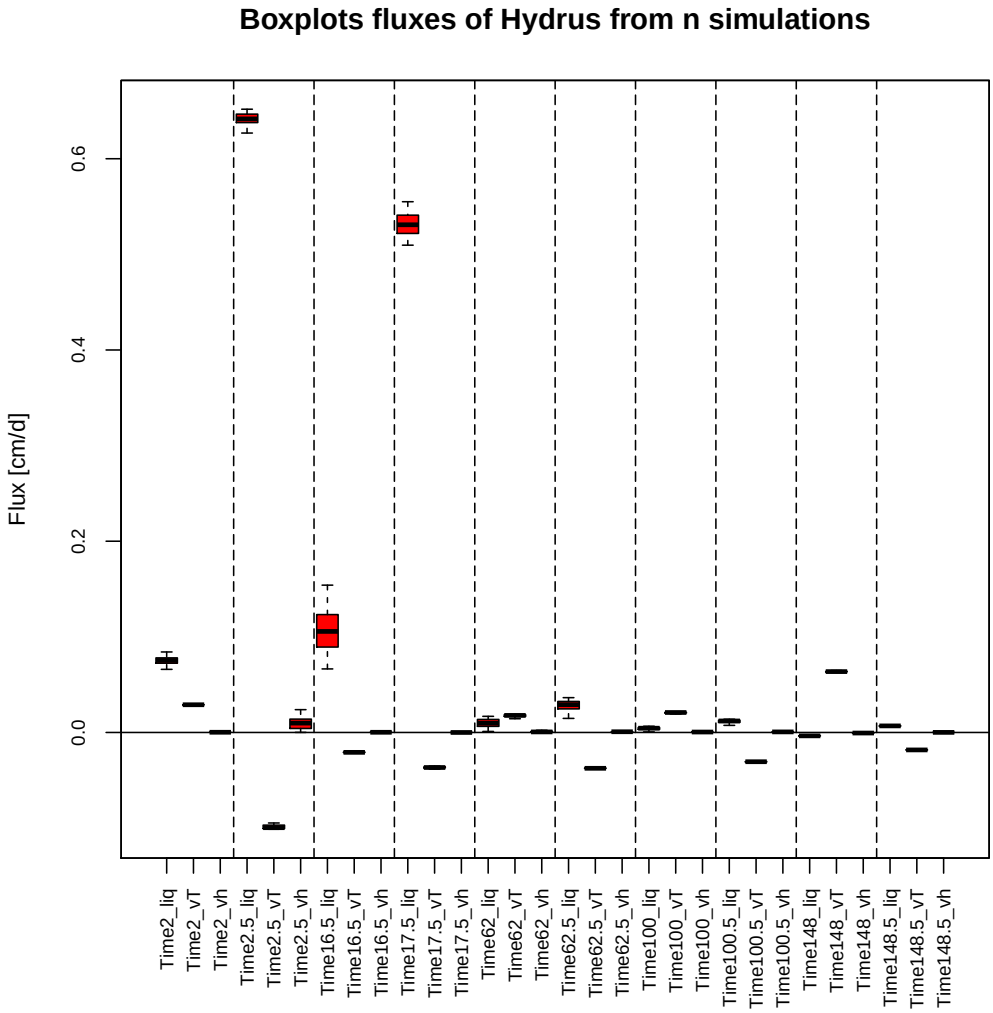

Figure 7: Box plots of the instantaneous fluxes from SWAP for different moments in time.

Abrevation	Explanation
Time2	2nd day, midnight
Time2.5	3rd day, noon
_liq	liquid water flux
_vT	Thermal water vapour flux
_vh	Isothermal water vapour flux

6.3.4 Liquid water flux

In addition to the isothermal and thermal water vapour fluxes the liquid water flux is also presented in figure 7 and appendix E. Again these are instantaneous fluxes shown at several moments in time. In SWAP the liquid water flux is calculated at the same moments in time and are shown in figure 8. During the dry season the soil dries out, as figure 6 shows. The soil water pressure head becomes more negative in time, this is presented by a higher pF-value in the bottom graph of figure 6. The hydraulic conductivity becomes lower at smaller soil water contents, as can be seen in equation 2.8. This results in a lower upward liquid water flux, and both Hydrus and SWAP models show a liquid water flux decreasing in time. At day 17 there was a large rain event which clarifies the large liquid flux at day 17.5. After a rain event the unsaturated hydraulic conductivity coefficient increases as can be analysed from equation 2.8, and a larger flux occurs in the soil. In the SWAP model the liquid water flux declines during time to almost zero and also the liquid water flux in Hydrus becomes very low upwards during day (day 62.5, 100.5 and 148.5) and eventually a very small downwards flux during night (day 148). In the dry period from day 62.5 (12 o'clock), the outgoing liquid water flux is a little bit higher in Hydrus than in SWAP. But in Hydrus the additional thermal water vapour flux is directed inwards during day. Thus the incoming water vapour condensates at a certain depth and will be transported as liquid water to the soil surface where it evaporates into the atmosphere. Note this is an additional input of water which is computed assuming thermodynamic equilibrium exists at the boundary condition. This equilibrium between water vapour and liquid water might not exist depending on the dynamic vapour transport conditions above and below the soil surface.
Comparing the sum of the fluxes in Hydrus with the liquid water flux in SWAP for the first days till day 17.5, the total flux of Hydrus seems to be higher than the liquid water flux of the SWAP model. While in section 6.2 it was noted that the SWAP model tends to overestimate the evaporation. Remark that the box plots show instantaneous fluxes whereas in section 6.3.5 the cumulative net fluxes will be compared between the SWAP and the Hydrus model, which will give a much better view of the difference regarding the two models.

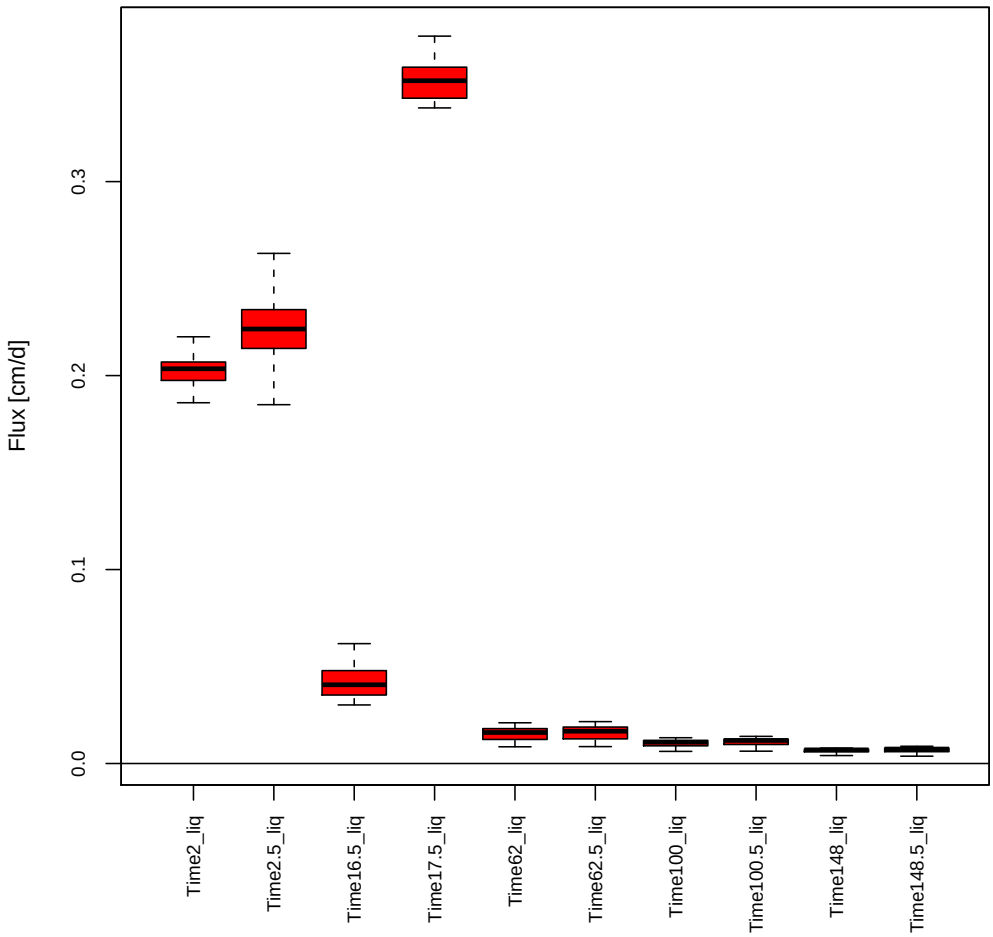

Figure 8: Box plots of the instantaneous fluxes from 100 runs in Hydrus for different moments in time.

Abrevation	Explanation
Time2	2nd day, midnight
Time2.5	3rd day, noon
_liq	liquid water flux
_vT	Thermal water vapour flux
_vh	Isothermal water vapour flux

6.3.5 Daily cumulative net flux

In the sections above the fluxes are presented as instantaneous fluxes because of the earlier mentioned limitations of Hydrus in section 6.1. Although it is interesting to explore the behaviour of the different fluxes during a day, the cumulative daily fluxes are used for the comparison between Hydrus and SWAP because the research question is based on the fluxes on a daily time scale. Cumulative fluxes can be calculated in Hydrus, but the cumulative amount of the different fluxes are not given in the output, no distinction is made between the fluxes. Thus only the total net flux is given as output in the Hydrus model. To compare the models Hydrus and SWAP, another simulation in Hydrus will be performed with exactly the same processes and input data as SWAP uses. Thus a simulation in Hydrus with only liquid water flow and no temperature dependency. In addition a coupled Hydrus simulation will be done with water vapour flow and temperature processes.
In figures 10 and 11 the results of the simulations are presented. In which positive fluxes are directed out of the soil; the negative fluxes are pointed into the soil. Figure 11 includes the measured rain in Trabadillo and in figure 10 the rain is excluded from the input data and a kind of recession curve can be seen. Figure 10, which is the simulation without the input of rain, shows a decline in net upward flux in time. The evaporative flux in the SWAP model and in the Hydrus model with only liquid water flux are both approaching to zero during the summer. But the coupled Hydrus model which has vapour flow included, remains just above the two liquid transport models and shows some fluctuations. These fluctuations are due to diurnal heating with the resulting changing soil temperature profiles and the combination of liquid water and water vapour transport. Figure 11 shows the net fluxes when rain is included as input for the models. When rain events occur a clear negative downward flux is visible in the figure for all the three models (SWAP, Hydryus coupled and Hydrus liquid flow). Due to the temporary increase in moisture an increase in upward net flux occurs for a short period of time till drier conditions are reached again. Please note that in the simulation with the input of rain the flux from the coupled Hydrus model is fluctuating just above the fluxes from the liquid transport models as can be seen in figure 11.
For the comparison of both models one-by-one plots are made as can be seen in figure 9. Those are three plots in which the net fluxes of one model are plotted against the net fluxes of another model. In case both models simulate equal results, the points would lay on the linear lines also plotted in the graphs. In the graphs of figure 9 can be seen that the Hydrus coupled model, the model with vapour flow, simulates somewhat higher net fluxes than the Hydrus liquid model. But the difference is very small between the models. The SWAP model has higher net fluxes, but the coupled Hydrus model has somewhat higher fluxes in the situation that the net fluxes are lower, so in drier conditions. The two liquid transport models, Hydrus Liquid and SWAP Liquid, do not take vapour flow and soil temperatures into account. In the lower graph of figure 9 the SWAP model seems to have higher net fluxes than the Hydrus Liquid model. For both models the processes and the input data are identical. Please remark that the differences are not so clear between the models in all the three graphs of figure 9, all points are very close to the x=y line (identity), in the other words the one-by-one line.
Figure 9 gives a good view over the differences and similarities between the models, but no statistical proof regarding the significance of the difference between the model. So Welch's t-tests are performed on the 100 runs between the three models at a significance level of 0.05, The difference between the three models are not proven to be significantly different. This holds for all four simulations for the three models. which all consist of 100 different parameter sets of soil hydraulic properties. The four simulations consist of three simulations with rain as input data and one simulation without the rain input. Given these simulations and their variation currently the uncertainty in the soil hydraulic parameters masks the difference between the coupled- and non-coupled models. This is confirmed by the statistical tests. Further the absence of a significant difference between the liquid Hydrus model and the liquid SWAP model implies that the two models are giving similar results. The Welch's t-tests confirm the one-by-one graphs of figure 9 were all the circles are along the one-by-one line.

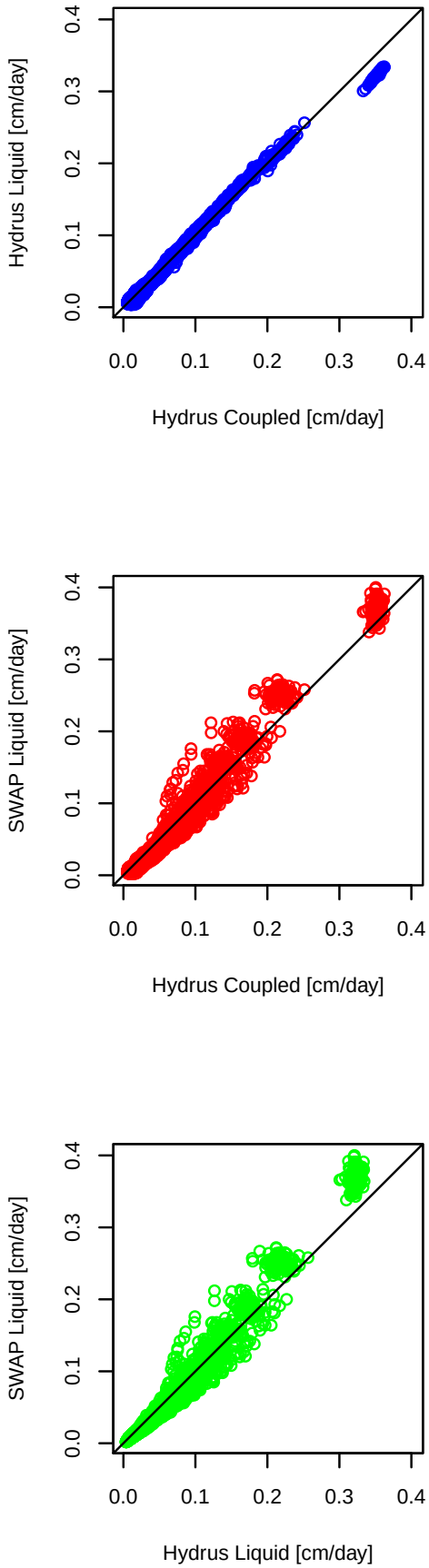

Figure 9: Comparison fluxes calculated with Hydrus and SWAP in one-by-one plot.

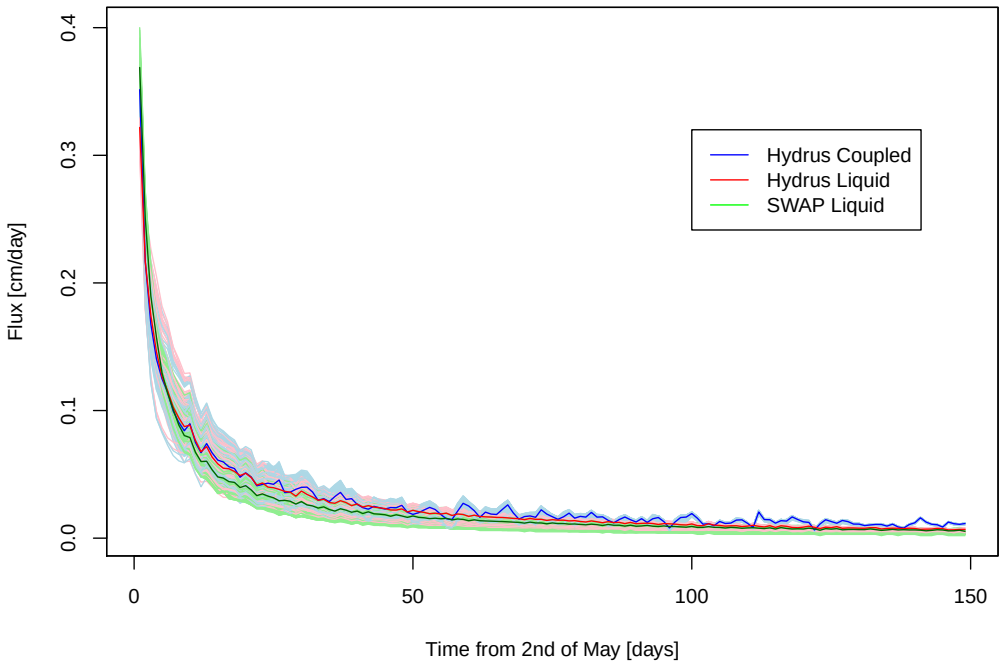

Figure 10: Comparison fluxes calculated with Hydrus and SWAP in a simulation without rain

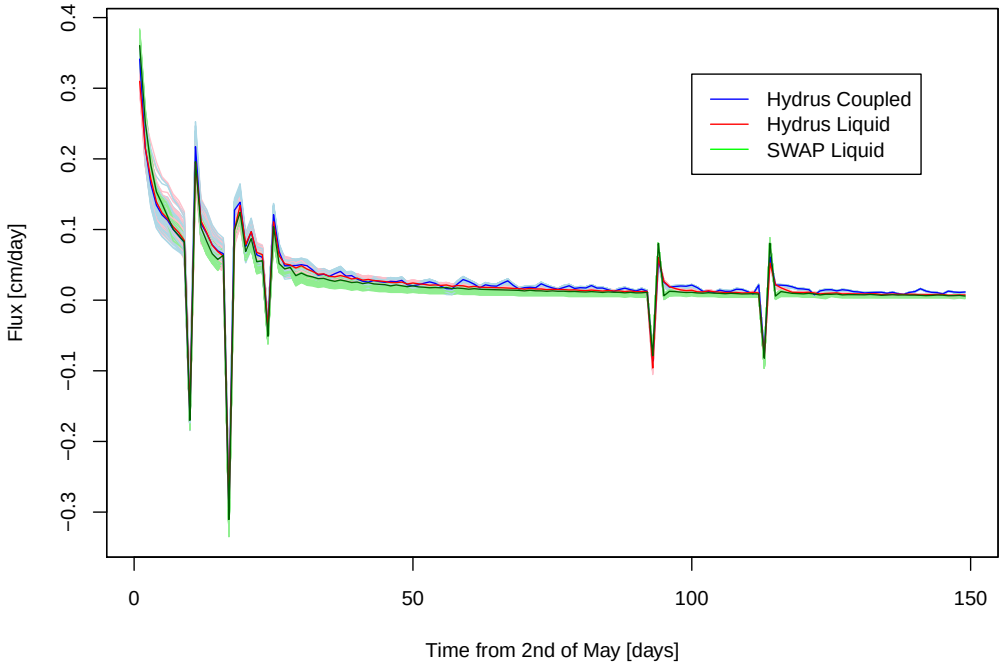

Figure 11: Comparison fluxes calculated with Hydrus and SWAP in a simulation with rain

6.4 Discussion of the fluxes

The Hydrus model is used to simulate the different fluxes for a couple of moments in time. On the basis of these simulations it can be concluded that the size of the isothermal water vapour flow is insignificant and can be neglected. The liquid water and thermal vapour flow show significant fluxes during night and during day, which is shown in figure 7. Three simulations are performed in addition to these simulations, each consisting of 100 different parameter sets of soil hydraulic properties, and the cumulative daily net flux is assessed. The three different simulations are executed with the SWAP model with only liquid water flow, the Hydrus model with only liquid water flow and the Hydrus model with liquid water and water vapour flow. So only the latter includes a dependency on temperature. Figure 9, 10 and 11 show that water vapour flow has an influence on the daily cumulative net flux. The coupled Hydrus model fluctuates just above the values of the two liquid water models. The model comparison plots (figure 9) show that the difference between the coupled Hydrus model and the two liquid transport models are small. In the one-by-one plots the coupled Hydrus model has in drier soil water conditions somewhat higher fluxes than the models with only liquid water flow because the data points are situated more on the side of the coupled model. This is just a tendency, as the differences between the models were not significant. After a rain event in figure 11 the models are similar to each others. The isothermal liquid water flux is dominant after such an event. In the drying period the situation becomes drier and the fluxes of the models without water vapour flow go to zero and the coupled Hydrus model still shows some fluctuations, although not significantly different from the other models.

6.5 Implementation vapour flow in SWAP

In section 6.4 is discussed that the thermal water vapour flux is dominant in the dry period. The thermal water vapour flux will be implemented in SWAP in addition to the isothermal liquid water flux. The SWAP model is already able to compute the soil temperature. In SWAP the calculation of soil temperature is different from that in Hydrus. More specifically the thermal conductivity, λ, is calculated in a different way in both models. This coefficient is in Hydrus based on three soil thermal parameters, whereas in SWAP it is based on the composition of the soil. The thermal liquid water flux will be neglected which is assumed in several studies (Milly, 1984; Saito *et al.*, 2006; Smits *et al.*, 2011) of coupled heat and water transport. Some additional processes have to be implemented in the existing SWAP model to include the thermal vapour flow. The model starts from equation 2.1, which is the mass balance of water. In which the total liquid water flux only consists of the isothermal liquid water flux:

$$q_l = q_{lh} = -K_{lh}(\frac{\partial h}{\partial z} + 1) \tag{6.3}$$

The total water vapour flux only consist of the thermal water vapour flux:

$$q_v = q_{vT} = -K_{vT}\frac{\partial T}{\partial z} \tag{6.4}$$

The combination of equations 2.1, 6.3 and 6.4 results in the mass balance equation 6.5.

$$\frac{\partial \theta}{\partial t} = \frac{\partial}{\partial z}[K_{lh}\frac{\partial h}{\partial z} + K_{lh} + K_{vT}\frac{\partial T}{\partial z}] \tag{6.5}$$

In equation 6.5 two hydraulic conductivity coefficients are presented; K_{lh} and K_{vT}. These two parameters are defined in equations 2.8 and 2.14. All the parameters in these two equations are all extensively described in section 2.2.2.

We chose to implement water vapour flow explicitly in SWAP. The water vapour flux is regarded as an additional in- and/or outgoing flux, just as root water extraction is commonly described in the Richards equation (Van Dam & Feddes, 2000). The soil water vapour content, θ_v, is neglected because the change in soil water vapour content over time is usually very small and this gradient would be used in the numerical code to solve the extended Richards equation 6.5. And thus the soil moisture content, θ, only consists of the soil liquid water content, θ_l, as can be seen in equation 6.6.

$$\theta = \theta_l \qquad \frac{\partial \theta_v}{\partial t} = 0 \tag{6.6}$$

Currently the thermal heat flux implemented in SWAP depends on the temperature gradient and the thermal conductivity of the soil as can be seen in equation 6.7. In Hydrus extra terms are included to compute the soil heat flux, see equation 6.8. The soil heat flux depends in addition to the sensible heat conduction by the porous media also on the convection of sensible heat by liquid water and water vapour, and the latent heat by vapour flow as defined by De Vries (1987). The assumption is draw that the convection of sensible heat by liquid water and water vapour and the latent heat by vapour flow can be neglected, because of the low magnitude of the liquid water and water vapour flux in the dry period. Bear *et al.* (1991) also neglected the convection of sensible heat by liquid water flow because of the small contribution to the total energy transfer. In the simplest case only the conductive sensible heat flux through the soil will have an effect on the temperature distribution in the soil. This flux is calculated as:

$$q_h = -\lambda(\theta)\frac{\partial T}{\partial z} \tag{6.7}$$

$$q_h = -\lambda(\theta)\frac{\partial T}{\partial z} + C_w T q_l + C_v T q_v + L_0 q_v \tag{6.8}$$

in which λ is described in a different way than in Hydrus-1D. The thermal conductivity lambda can be calculated on the basis of an empirical approach, as in Hydrus, or on the basis of a composition weighted contribution of individual components, as in SWAP. More specifically in the SWAP model the thermal conductivity, λ, is computed by considering the soil as a continuous phase of liquid or gas, in which soil particles and respectively gas or liquid particles are dispersed (Kroes *et al.*, 2008). The thermal conductivity for a wet soil, $\theta \geq 0.05$, is described by equation 6.9 based on the assumption that liquid water is the continuous phase.

$$\lambda = \frac{x_{sand-water} f_{sand} \lambda_{sand} + x_{clay-water} f_{clay} \lambda_{clay} + x_{organic-water} f_{organic} \lambda_{organic} + x_{water-water} \theta \lambda_{water} + x_{air-water} f_{air} \lambda_{air}}{x_{sand-water} f_{sand} + x_{clay-water} f_{clay} + x_{organic-water} f_{organic} + x_{water-water} \theta + x_{air-water} f_{air}} \tag{6.9}$$

The volumetric fraction of the different components, sand, clay, organic material, water and air, are defined as f ($cm^3 \cdot cm^{-3}$). The thermal conductivities, λ, are given for the different individual components ($J \cdot cm^{-3}\,^{\circ}\mathrm{C}^{-1} \cdot d^{-1}$). The values for x are weighting factors for the particles of a component in the continuous phase which depend on the ratio of the thermal conductivity of the component of the particles and the liquid phase and the particle shape in the temperature gradient direction. For the assumption of spheroid particles and randomly directions of the axes the following equation from Ten Berge (1986) can be used:

$$x_{part-phase} = \frac{2}{3 + 3g_{part}(\frac{\lambda_{part}}{\lambda_{phase}} - 1)} + \frac{1}{3(1 + (\frac{\lambda_{part}}{\lambda_{phase}} - 1)(1 - 2g_{part}))} \tag{6.10}$$

Subscript *part* in the equation above stands for the component of the particles and the parameter g_{part} is the shape factor of a component. If the soil moisture content is very low, $\theta \leq 0.02$, air will be regarded as the continuous phase and equation 6.11 must be used to calculate the thermal conductivity.

This equation is similar equation 6.9 but in this case air as phase component and with an additional empirical correction factor.

$$\lambda = 1.25 \frac{x_{sand-air} f_{sand} \lambda_{sand} + x_{clay-air} f_{clay} \lambda_{clay} + x_{organic-air} f_{organic} \lambda_{organic} + x_{water-air} \theta \lambda_{water} + x_{air-air} f_{air} \lambda_{air}}{x_{air-water} f_{sand} + x_{clay-air} f_{clay} + x_{organic-air} f_{organic} + x_{water-air} \theta + x_{air-air} f_{air}} \quad (6.11)$$

In the situation the soil moisture content is neither wet nor dry, $0.02 < \theta < 0.05$, the thermal conductivity will be interpolated between the λ_{dry} and λ_{wet}. The following equation has to be used:

$$\lambda(\theta) = \lambda(\theta_{dry}) + \frac{\lambda(\theta_{wet}) - \lambda(\theta_{dry})}{\theta_{wet} - \theta_{dry}} (\theta - \theta_{dry}) \quad (6.12)$$

6.6 Simulation vapour flow in SWAP for Trabadillo

The simulations in section 6.3.5 will be repeated for the version of SWAP in which water vapour transport has been incorporated for the purpose of comparison. The coupled SWAP model with implemented water vapour transport will now be used to simulate the fluxes in a similar way as done in section 6.3.5 with the Hydrus coupled and liquid model and the SWAP model with only liquid water transport. Again simulations are performed with 100 parameter sets of soil hydraulic properties. The atmospheric data from the field work in Trabadillo is used again as time-variable top boundary condition. For one simulation the rain records are removed again from the atmospheric input data. In figures 12 and 13 the result of this simulation is shown. In both figures the net flux is plotted in time, in which positive values represent the flux out of the soil. The negative peaks in figure 13 are rain events. After a rain event the net flux is higher, so a larger amount of evaporation, which can occur because at that moment more water is available in the soil to evaporate. Although the rain is removed as input in figure 12 still some disturbances result from a rain event, for example at day 115. The reason for these disturbances can be found in the atmospheric input. The input of rain is removed but variables as soil surface temperature carry also some information about the rain. During the day soil surface temperatures will be lower when a rain event occurs.
Figures 12 and 13 allow to compare the different model versions Hydrus and SWAP on the contribution of water vapour transport. There is a difference between the coupled and the non-coupled Hydrus model, whereas for the two SWAP versions there is no effect of the added water vapour flow. The mean net flux of the coupled SWAP model fluctuates around the mean of the models with only liquid water transport. The coupled Hydrus model produces output with a mean slightly higher than that of the other 3 models. Especially in the dry periods without rain the coupled Hydrus model shows higher net fluxes than the models with only liquid water transport and the coupled SWAP model. Figure 12 shows the recession of the evaporation. Whereas the fluxes of models with only liquid water flow and the coupled SWAP model are becoming very small, the coupled Hydrus model still has a net flux, probably driven by temperature. Thus if water vapour transport is not taken into account in the Hydrus model the evaporation rate is lower than in the case vapour flow is taken into account.
The difference between the models is not only due to the different kind of processes involved in the models. Mass balance errors required a careful discretization, especially for the coupled Hydrus model. The cumulative mass balance error after the 149th day is used to determine the reliability of the model itself. The SWAP version with liquid water transport only has a cumulative mass balance error of 0.00 cm, and the coupled SWAP model has an error of -0.03 cm over the period of 149 days. Over a total cumulative net flux of around the 4 cm these mass balance errors are negligible. The Hydrus model with only liquid water transport has a cumulative mass balance error of -0.01 cm, which can also be neglected. These mass balance errors are similar for the simulations with and without the input of rain data. As mentioned before the coupled Hydrus model may generate results with large mass balance errors. Notice that in the study by Deb *et al.* (2011) the same problems occurred with

the Hydrus model in that Hydrus did not always converge to a stable solution. The simulation with the rain data as input resulted in a cumulative mass balance error of 0.09 cm over a total cumulative net flux of 4.6 cm, see table 5. For the simulation without the input of rain data the cumulative mass balance error is larger, 0.11 cm over 149 days. These errors are in the order of 1%, thus sufficiently low. The larger mass balance error in the simulation without the input of rain data explains probably the small difference in the cumulative net fluxes of the Hydrus coupled model between tables 4 and 5. While the other three models show a logical increase of net outgoing flux for the simulation with the input of rain data. In this case more water is available for evaporation.

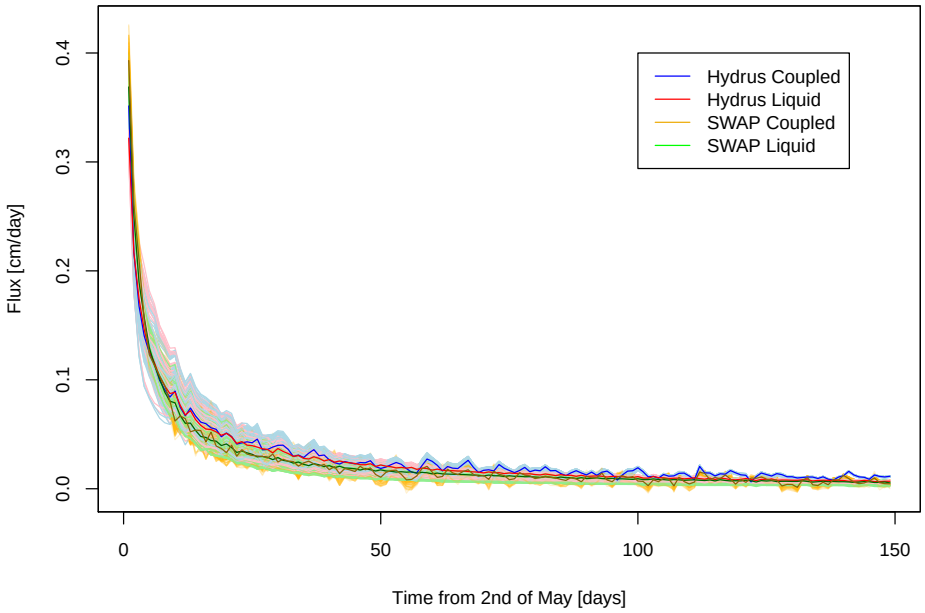

Figure 12: Comparison fluxes calculated with Hydrus Coupled and Liquid and SWAP Coupled and Liquid in a simulation without rain.

Figure 14 shows a model intercomparison whereas on the left side the Hydrus Liquid, SWAP Liquid and the SWAP Coupled model are plotted against the Hydrus Coupled model. In case of identical model output, the relation between the models is defined by x=y. In this figure can be seen that all plots do not show a clear picture about which model consistently predicts higher fluxes. Further the Hydrus Coupled and the Hydrus Liquid models have all the points more or less on one line, so the net fluxes are almost the same for both models. The same holds for the two SWAP models, the SWAP Coupled and the SWAP Liquid model have also all the points among the one-by-one line. So the two kind of models, Hydrus and SWAP, seem to calculate similar fluxes for the model with only liquid water transport and the model with the additional water vapour transport. The SWAP-coupled model simulates fluxes which are higher than both SWAP liquid, and Hydrus-liquid as shown in figure 14. Moreover this figure also indicates a difference between the Hydrus and the SWAP models. SWAP calculates higher fluxes in absolute sense, which occurs in wetter soil conditions, whereas Hydrus calculates higher fluxes in dry situations. An explanation can be found in appendices H and I in which the cumulative fluxes are plotted against the time. During the first days the soil is relatively wet and the SWAP results are larger than the Hydrus results, but after 25 days Hydrus simulates larger values than SWAP. So in the drier period the Hydrus models have a higher flux compared to the SWAP models, although in an absolute sense the fluxes are small. The

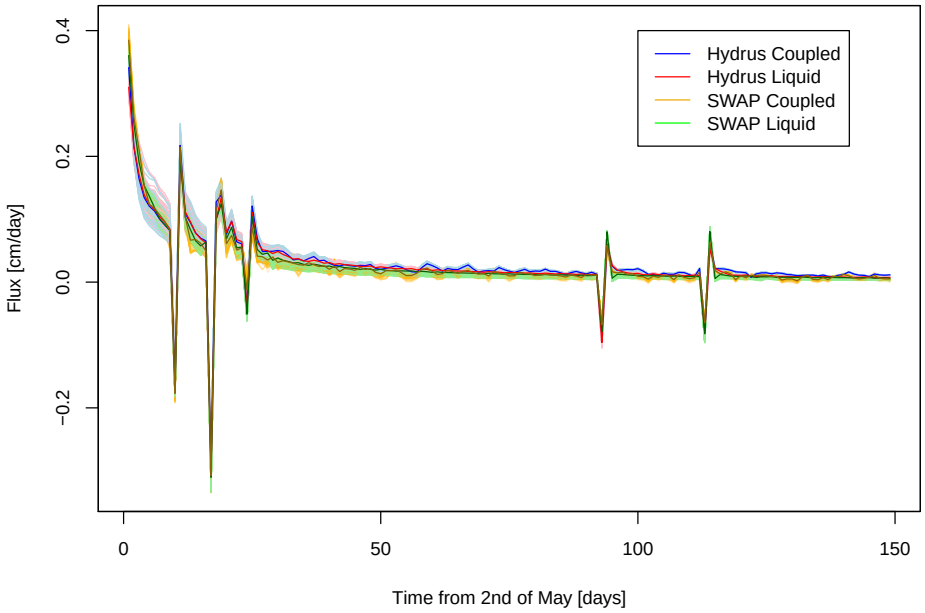

Figure 13: Comparison fluxes calculated with Hydrus Coupled and Liquid and SWAP Coupled and Liquid in a simulation with rain.

SWAP results are falling on top of each other, because of the almost perfect correspondence between fluxes over time. The downward peaks in appendix I are caused by rain events, which give a flux going into the profile. Figure 14 allows a qualitative assessment of the model behaviour, but does not allow testing statistical significance. In case a model is significantly different from another than a justified conclusion can be drawn about water vapour transport. As done before in section 6.3.5, the significance of differences between the means of the cumulative model output was tested using a t-test at 0.05 significance level. The results are presented in appendix G. The t-tests allow to concludes that the models do not differ significantly. The t-tests between the two SWAP models computed very high values, which emphasizes that these two models are very similar. Despite the non-significant difference between the models tables 4 and 5 suggest that there is a difference between the models. The difference between the Hydrus Coupled model and the other three models is much larger than the mass balance error, so another process, a flux, could be responsible for this insignificant difference, like for example the thermal liquid water flux. The simulated soil temperatures over time at depths of circa 1 cm and 10 cm beneath the soil surface are remarkable as table 6 shows. The soil temperatures calculated with the coupled Hydrus model have larger extremes, minimum and maximum, than the soil temperatures calculated with the coupled SWAP model. The amplitude of the soil temperature at those depths is larger in Hydrus than in SWAP. Even more important is the larger difference in soil temperatures between 1 cm and 10 cm beneath the soil surface for the coupled Hydrus model. This difference will result in a larger temperature gradient in the top layer. A larger temperature gradient can result in a larger thermal vapour flux. This difference in soil temperatures explains the difference between the coupled Hydrus and coupled SWAP model.

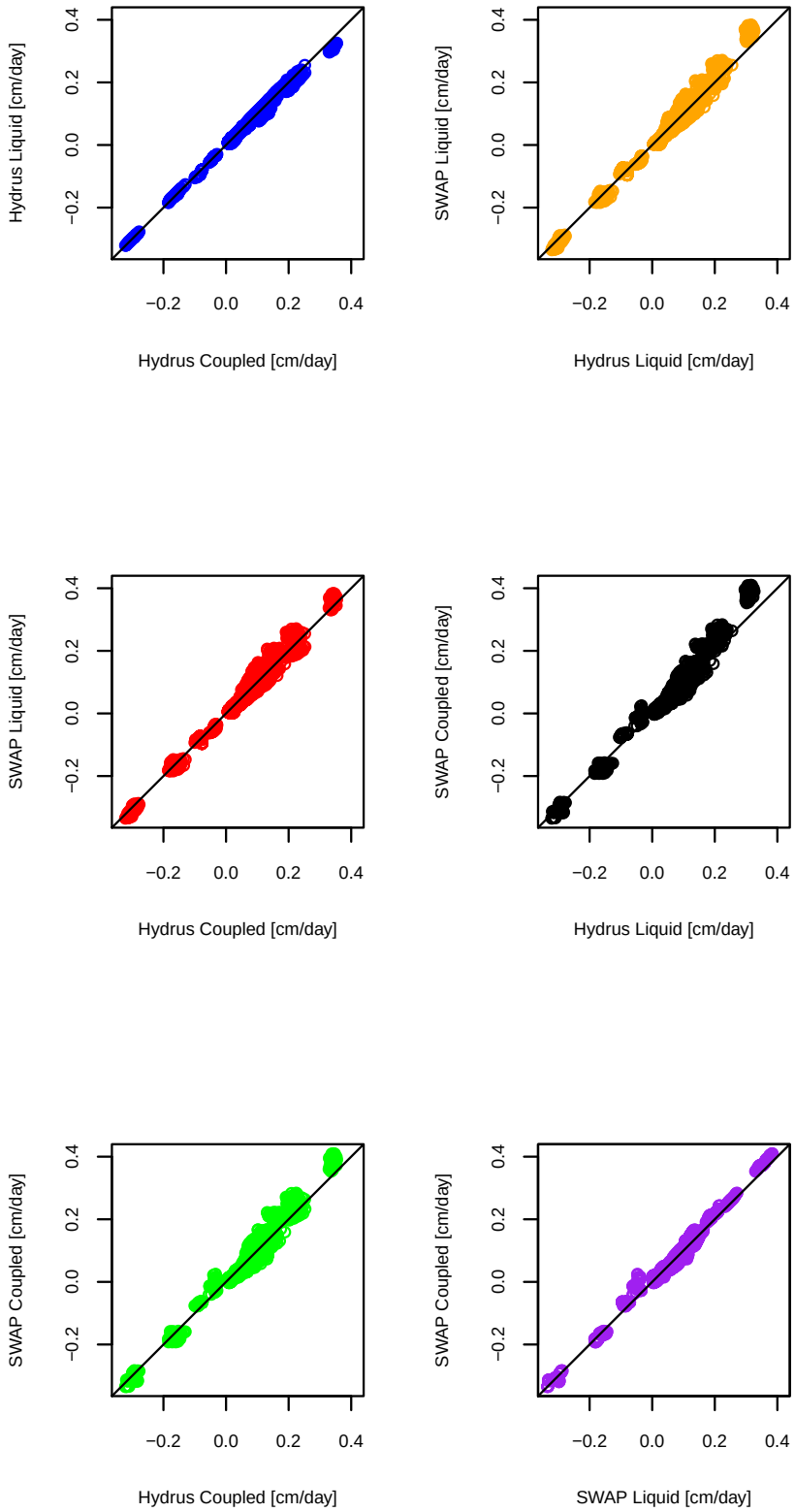

Figure 14: Comparison fluxes calculated with Hydrus Coupled and Liquid and SWAP Coupled and Liquid in one-by-one plot.

Table 4: General statistics from the cumulative net flux (cm) at 27th of September in simulation without rain.

	Hydrus Coupled	Hydrus Liquid	SWAP Liquid	SWAP Coupled
mean	4.53	4.13	3.73	3.75
standard deviation	0.51	0.56	0.59	0.60

Table 5: General statistics from the cumulative net flux (cm) at 27th of September in simulation with rain.

	Hydrus Coupled	Hydrus Liquid	SWAP Liquid	SWAP Coupled
mean	4.58	4.20	3.87	3.90
standard deviation	0.45	0.48	0.55	0.56

Table 6: Statistics soil temperature (°C) from the Hydrus and SWAP models and measured.

	Hydrus		SWAP		Measured	
Soil temperature (°C)	1 cm	10 cm	1.2 cm	10.2 cm	top	bottom
Minimum	4.00	7.70	8.30	10.03	2.65	14.40
Maximum	37.65	31.21	29.95	26.97	55.67	26.20
Average	21.13	21.76	18.94	18.92	24.67	22.31

6.7 Vapour transport in other soil types

In the previous section the contribution of water vapour flow to the total water flux is discussed. Several simulations were executed to investigate the water vapour and liquid water fluxes. These simulations were executed using one specific soil determined from the Trabadillo site. The unsaturated hydraulic conductivity and the soil water retention curve have an undeniably large effect on the liquid water and water vapour transport. Next to that the calibrated soil hydraulic parameters give an uncertainty in the cumulative net fluxes as can be seen in appendix I and H. This uncertainty has influence on the intercomparison between the models and thus the ability to draw conclusions about the contribution of water vapour transport. So to be able to give a more general answer on the main research question a sensitivity analysis will be performed with other soil types; the contribution of vapour flow in other types of soil will be investigated. The soils from the HYPRESS database are selected for these simulations (Wosten *et al.*, 1999). These soils are based on a very large database created of soil properties from 5521 soil descriptions out of twelve countries in Europe. The HYPRESS project defined eleven soils in total, based on the six textural defined soil classes by the FAO, five mineral and one organic soil and two pedological classes; topsoil and subsoil. For the organic soils there is no distinction between the topsoil and the subsoil, that is why the total amount of soil types is eleven and not twelve. For the HYPRESS project pedotransfer functions are developed to calculate soil hydraulic properties from soil parameters, acquired during a standard soil survey. Table 7 shows the eleven soils presented in the HYPRESS project. Notice that organic soils are not found in (semi-)arid regions because the soils can not exist in regions with dry soil water conditions and high temperatures. Maybe a greenhouse situation can be sketched for an organic soil type in semi-arid conditions.

The soil hydraulic properties from table 7 are used as input for the four models; the coupled Hydrus model, the coupled SWAP model, and the Hydrus and SWAP model with only liquid water flow. For the thermal properties which need to be defined for the two coupled models, the Hydrus model gets the values associated to the soil type, from one of the three standard soil thermal properties

Table 7: The eleven soil standards derived in the HYPRESS projects (Wosten *et al.*, 1999).

		$\theta_r(cm^3/cm^3)$	$\theta_s(cm^3/cm^3)$	$\alpha(1/cm)$	$n(-)$	$m(-)$	$l(-)$	$K_s(cm/d)$
Topsoils	Coarse (1)	0.025	0.403	0.0383	1.3774	0.274	1.25	60
	Medium (2)	0.01	0.439	0.0314	1.1804	0.1528	-2.3421	12.061
	Medium-fine (3)	0.01	0.43	0.0083	1.2539	0.2025	-0.5884	2.272
	Fine (4)	0.01	0.52	0.0367	1.1012	0.0919	-1.9772	24.8
	Very Fine (5)	0.01	0.614	0.0265	1.1033	0.0936	2.5	15
Subsoils	Coarse (6)	0.025	0.366	0.043	1.5206	0.3424	1.25	70
	Medium (7)	0.01	0.392	0.0249	1.1689	0.1445	-0.7437	10.755
	Medium-fine (8)	0.01	0.412	0.0082	1.2179	0.1789	0.5	4
	Fine (9)	0.01	0.481	0.0198	1.0861	0.0793	-3.7124	8.5
	Very Fine (10)	0.01	0.538	0.0168	1.073	0.068	0.0001	8.235
	Organic (11)	0.01	0.766	0.013	1.2039	0.1694	0.4	8

in Hydrus; sand, loam or clay. For the coupled SWAP model the distributions of the soil components are derived from the paper by Wosten *et al.* (1999) and used as input. The atmospheric weather data from Trabadillo is used because this data represents semi-arid conditions under which water vapour flow is likely to contribute significantly to the total water transport in the soil. After the simulation the cumulative net fluxes are summed over the entire period of 149 days and the cumulative values for each soil type are compared with the other models. In all models the soil profile is assumed to be homogeneous with a depth of 1 meter. The Hydrus solution did not converge in some cases. Adapting the spatial and time discretization and exploring the best possible time steps resulted in computations with minimal water balance errors. For the spatial discretization a grid size of 5 cm was required to achieve an acceptable mass balance error of around the 1%. A nodal space of 5 cm is according to the Hydrus manual way too large to compute the fluxes (Simunek *et al.*, 2008). Advisable is a maximum nodal space of 1 cm. The coupled Hydrus model with the coarse grid size of 5 cm still did not converge for the fine and very fine soils (soils 4, 5, 9 and 10). The two soils 1 and 6 are most similar to the top layer of the determined soil in Trabadillo, as can be seen in table 2. In table 8 the cumulative net fluxes are presented for the eleven soils. The abbreviations in the heading are listed in appendix G. The models which did not converged, get the value NaN (Not a Number). The absolute water balance errors of the Hydrus models are included in table 8. The water balance errors are related to the total flux and indicate the reliability of the simulation. The water balance errors of the SWAP models were checked and all of them are negligible small and thus the errors are not shown in table 8. Using the coupled Hydrus model the simulations for soils 4,5,9 and 10 did not converge to a stable solution. For the Hydrus-liquid model the simulation results for these soils show a large water balance error. The coupled Hydrus model has a sufficient low water balance error for the coarse soils 1 and 6, the medium soils 2 and 7 and the medium-fine soils 3 and 8. The water balance errors of the Hydrus Liquid model are sufficiently low for soils 1, 2, 3, 6, 7 and 8.

There is a large difference in cumulative net fluxes between the two types of models; Hydrus and SWAP. For the two versions of a model the simulations are quite similar. The calculated cumulative net fluxes from the Hydrus model are somewhat questionable given the large nodal space of 5 cm required, the convergence problems and the mass balance errors. Conclusions are therefore formulated on the basis of the SWAP simulations only.

The cumulative fluxes for the two SWAP models are very similar to each other for every type of soil. For every soil type the coupled SWAP model computes a slightly higher cumulative flux than the SWAP model with only liquid water transport. The largest difference exists for soil type 1, which is around the 4.6% of contribution of water vapour flow to the total flux. The results for both SWAP models assign a clear pattern for the subsoil and the topsoil. The cumulative net fluxes are the highest

Table 8: Cumulative net fluxes (cm), water balance errors (cm) and relative difference (%) for the eleven HYPRESS soils.

soil	HC	HL	SC	SL	Water bal. error HC	Water bal. error HL	Rel. dif. SC-SL
1	0.473	0.553	0.737	0.703	0.000	0.000	4.613
2	0.011	0.110	3.811	3.727	0.001	0.000	2.204
3	0.194	0.267	5.070	5.001	0.000	0.000	1.361
4	NaN	-0.402	2.168	2.123	NaN	0.933	2.076
5	NaN	-0.420	0.937	0.916	NaN	1.220	2.241
6	1.194	1.076	0.186	0.184	0.000	-0.006	1.075
7	-0.064	0.007	2.277	2.200	0.000	0.000	3.382
8	0.015	0.081	4.445	4.355	0.000	0.000	2.025
9	NaN	-0.461	2.575	2.566	NaN	1.371	0.350
10	NaN	0.427	1.346	1.336	NaN	5.187	0.743
11	-0.092	-0.141	4.666	4.535	0.656	0.169	2.808

for the medium-fine soils, soils 3 and 8 for both SWAP models. The finer or coarser in particle size the soils are with respect to these medium-fine soils, the lower cumulative net flux will be. The loamy soils 3 and 8 have both the best soil hydraulic properties for the transport of water and will also have the largest amount of capillary rise. Nevertheless the coarse textured soil 1 has the highest relative contribution of water vapour flow to the total water flux.

7 Designing a laboratory experimental setup

7.1 Objective

This section includes a detailed description for a laboratory experiment with the aim to optimally investigate vapour movement. The usefulness of the theory of Philip and de Vries to simulate liquid water and water vapour transport is mentioned in a paper by De Vries (1987), moreover De Vries emphasises the uncertainties; limitations of the theory, and the uncertainty about the experiments. To decrease the uncertainty in the experiment is the intention of this laboratory experiment design. More specific the objective of this description is to give a ideal and feasible plan for doing measurements which are intended for a coupled liquid water and water vapour model. The measurements are necessary for the investigation of importance of the water vapour flux and the calibration and validation of a coupled model.
This experiment will take into account the diurnal changes in the fluxes by imposing a 12-hour interval of heating up and cooling down the soil surface. The implementation of a temperature cycle is highly recommended by Parlange *et al.* (1998). According to them the discrepancy between model computations and laboratory measurements are due to the commonly imposed steady state boundary conditions. In this design time-variable boundary conditions are described. A model study will be performed to explore the optimal installation of the measurement devices. This model study will focus on the amount, the depth and the type of measurements and the resulting quality of the inverse parameter estimation. Further some practical details about building a column experiment will be given according to the paper by Lewis & Sjostrom (2010).

7.2 Soil column experiment

7.2.1 Soil column

For the model it is essential to force an one dimensional water and heat flow with minimal wall effects. A circular soil column is common for this kind of experiments. The size of the diameter influences the effective contribution of the wall on the flow patterns. Smits *et al.* (2011) and Sakai *et al.* (2009) use a diameter of around the 10 cm, while Gowing *et al.* (2006) uses a diameter of 20 cm. Columns with a large diameter have the disadvantage that the increase in weight make the columns impracticable. Enrico Balugani, one of my supervisors, uses for his laboratory experiment two columns with diameters of 28 and 23 cm. Based on the paper by Lewis & Sjostrom (2010) a column with a diameter to length ratio of 1:4 should be sufficient enough to have minimal wall effects. Also the length of the column influences the measurements. Sakai *et al.* (2009) use a soil column with a length of 10 cm, Gowing *et al.* (2006) uses lengths of 45 and 70 cm and Smits *et al.* (2011) a soil column with a length of 120 cm. So there's a large variety of the lengths chosen in earlier research. Note that also the soil type has influence on the choice of the length, because soil types have differences in capillary rise, soil thermal conductivity and available pore space for vapour movement. Smits *et al.* (2011) took an uniform silica sand consisting for almost 100% of quartz, Sakai *et al.* (2009) took Hamaoka dune sand and Gowing *et al.* (2006) a sandy loam soil. A sandy soil is the most suitable soil type, because as noted in section 6.7 the relative contribution of vapour flow is the highest for a coarse textured soil. Next to that the advantage of sand is the faster transport processes, so the drying out will occur in a shorter period of time. And the Hydrus model has the least convergence problems and smallest mass balance errors for sandy soils and so an acceptable spatial discretization can be maintained.
The field measurements taken in Trabadillo show a diurnal temperature effect in the soil at depths of 25, 50 and 75 cm. At 100 cm depth the diurnal temperature change has effectively disappeared, and only a seasonal temperature change is visible. The capillary rise for a soil with a loamy soil texture is up to around the 80 cm (Lewis & Sjostrom, 2010), for coarse sand it will be up to a shallower

depth. A soil column with a length of around the 100 cm is recommended, to avoid capillary rise till the surface and to create a stationary soil temperature at the bottom. A column with a length of 100 cm and a diameter of 25 cm will meet the requirements as formulated above. The setup of the laboratory experiment can be done in two types of construction methods; packed and monolithic (Lewis & Sjostrom, 2010). Monolithic columns are extracted from the field, kept intact and put into a column. These undisturbed soils have the advantage of owning a better representation of the field conditions and have the disadvantage to be worse in (1) the reproducibility, (2) not sure if your column is actually the representation of your study area and (3) it's practically difficult to obtain an undisturbed monolithic soil column. The disadvantage of packed soil columns are that (1) the macropores are not present anymore, (2) heterogeneities are less, due to mixing and (3) disturbed soils do not exactly represent the field conditions The advantage of the packed soil columns is their reproducibility. The choice for either one or the other will influence the experimental results (Lewis & Sjostrom, 2010). Because this research is not restricted to a specific site, a column construction with the packed soil column is the most practical option. Three kind of materials are commonly used as shell for the soil column; acrylic, glass and stainless steel. For this research acrylic is the best option because glass is more expensive and heavier and stainless steel is not suitable because of its high thermal conductivity. The sides of the column must be isolated with insulation material which has a very low heat conductivity, because the insulation of the column will ensure an one-dimensional heat flow through the column. Smits *et al.* (2011) conclude a layer of 5 cm thick fibreglass is sufficient as insulation. The method of dry packing will be used for packing the soil column, in which small increments of circa 1 cm must be put into the column and have to be compacted by hand or by using a metal pestle. The entire soil column can be put on a balance; the loss in weight over time is equal to the amount of evaporation over time (assuming no irrigation).

7.2.2 Soil thermal and soil hydraulic properties

The soil thermal properties are required to compute the soil heat flux through the soil. The distribution of the different components (e.g. clay, silt, sand, water, air), the conductivity coefficients and the soil water content are all combined into one parameter, the thermal conductivity coefficient λ. As mentioned in subsection 6.3.1, the soil thermal properties have a large influence on the model output. In Hydrus the parameters b_1, b_2 and b_3 are important for calculating the λ. These parameters are empirical and only general values for sand, loam and clay values are available. So calibrating those parameters for a specific soil using measured soil temperatures and soil water contents, can give an enormous improvement. The thermal conductivity λ is defined differently in SWAP. The parameter is based on the contribution of the different components like clay, sand, organic matter, water and air. It's necessary to define the contribution of every component of the soil in the column experiment. Relative to each other the contribution of the components can change every time step because of a change in soil moisture content and/or air content.
The soil hydraulic properties are the most important parameters for the water movement in the soil. The seven parameters θ_r, θ_s, α, n, K_s, l and m describe the soil water retention curve. Notice that m can easily be calculated from n mentioned in the description of equation 2.10. The soil profile from the field work in Trabadillo is schematized in four different layers with six parameters for each layer. Determining all parameters will result in 24 parameters which need to be estimated. For a laboratory experiment it is common to use an uniform soil, thus six parameters need to be determined. Reducing the number of parameters for the inverse parameter estimation ensures better convergence, and sometimes more accurate estimates. Two of the six parameters can be determined in rather simple laboratory experiments; the saturated hydraulic conductivity and the saturated soil water content. (De Vries, 1987) urges the determination of these soil hydraulic parameters by experiments. The saturated hydraulic conductivity can be determined on the basis of a number of methods. Deb *et al.* (2011) use the constant head method and Sakai *et al.* (2009) use the falling head method. The saturated hy-

draulic conductivity from the field site at Trabadillo was measured by the ITC students (Abubeker, 2010; Agbakpe, 2010; Salinas Revollo, 2010) using an infiltrometer. The saturated water content, θ_s, can be determined gravimetrically. Than only the four parameters, θ_r, α, n and l, are left for the inverse parameter estimation method. In addition the soil thermal parameters b_1, b_2 and b_3 have to be calibrated which results totally in seven parameters for the inverse parameter estimation method.

7.2.3 Soil temperature, soil water content and soil pressure head

Soil temperature measurements are necessary for the calibration and validation of the soil thermal parameters. The soil temperature has its maximum variation at the soil surface and the lowest at the bottom of the soil profile in the perspective of one-dimensional heat flow. For this reason it seems common sense to install more temperature measurement devices at the top of the profile than at the bottom. Several soil water content measurement devices can also measure the soil temperature, so it is a good idea to combine those two measurements. This will decrease the amount of devices installed in the soil column, which also reduces the amount of disturbances in the soil column. Thermocouples are often used in scientific research for measuring soil temperatures (Saito *et al.*, 2006; Bittelli *et al.*, 2008; Sakai *et al.*, 2009; Novak, 2010; Steenpass *et al.*, 2010). EC-T temperature probes were used by Smits *et al.* (2011). Because of the uniform soil in the column, the dampening of the soil temperatures will largely depend on the depth and to a lesser extent on soil water content. The proposition would be to install mostly measurement devices which combine measurements.
A small model study will be done to explore the "ideal" amount and depths for installing the devices. A measurement interval of one hour should be sufficient to model the soil temperatures in a laboratory experiment. For a field experiment with more fluctuations an interval of 30 minutes can be considered (Novak, 2010; Steenpass *et al.*, 2010; Deb *et al.*, 2011).
Soil water pressure heads are more sensitive to changes than soil water contents. This can be an advantage because small effects can be noticed in changes in soil water pressure heads while the soil water contents remain constant. However this can also be a disadvantage especially as in dry situations the measurement error of devices for soil water pressure measurements, becomes larger. De Vries (1987) remarks that for a coupled heat and water model accurate measurements of soil water content and soil temperature are essential, as the gradients of those two variables need to be known. The measurements of soil water pressure head and the unsaturated hydraulic conductivity, both depending on soil water content, are less easy to obtain and more time consuming. Two kind of measurement devices are commonly used for measuring soil water content; the ECH_2O probe by Bittelli *et al.* (2008); Smits *et al.* (2011) and the TDR probe by Parlange *et al.* (1998); Saito *et al.* (2006); Sakai *et al.* (2009); Steenpass *et al.* (2010); Deb *et al.* (2011). Both measurement devices have types which can simultaneously measure the soil temperature. Soil water pressure is often measured with tensiometers (Sakai *et al.*, 2009). Soil water pressure is, however, measured less often in research experiments than soil water content. The POT sensor should be very suitable for the measurements of the soil water pressure, especially for this experiment in which dry conditions will be imposed (Van der Ploeg *et al.*, 2010). As was seen in section 5.1, there were some problems with the calibration of the soil hydraulic properties using the measurements from the POT sensor executed in the field.
Just as soil temperature also soil water content and soil water pressure have maximum variations in the upper part of the profile. So it's evident to install more measurement devices in this part of the profile. In a model study both the optimal combination of measurement devices, their optimal number, and their optimal depth will be explored.

7.2.4 Initial and boundary conditions

Before the experiment starts the soil column must already be placed in the experiment room long enough until the column has reached one uniform soil temperature equal to the room temperature. When the experiments starts a temperature gradient from the top to the bottom will arise by the imposed top boundary condition. The development of the soil temperature profile over time is needed for the estimation of the soil thermal parameters. The column can be filled with water until the soil is saturated. The soil is assumed to be at or near saturation initially. A net upward flux will occur due to heating from above and the soil water content in the profile will decrease. After some time the soil reaches very dry conditions. The entire soil water retention curve can be described because measurements are taken from the soil in a saturated state till very dry soil water conditions. And the soil hydraulic properties could be estimated accurately by using the measurements over the entire range of soil water content.
The contribution of vapour flow to the total water movement in the soil is especially important when the soil is dry. This implies deep groundwater levels. So free drainage is assumed as bottom boundary conditions for the mass conservation of water. As upper boundary condition high evaporative conditions are desired and little or no rain. This is typical for (semi-)arid conditions. For the heat conservation equation the bottom boundary condition will assumed to be a zero gradient condition in the model. By using a soil column of 100 cm high the soil doesn't have diurnal fluctuations in temperature at the depth of 100 cm. For a model with a daily time scale this assumption is justifiable. As top boundary condition for heat it is desirable to have a diurnal effect, given that the thermal vapour flux discussed in section 6.3.3 shows a diurnal movement and moreover it is recommended by Parlange *et al.* (1998). An infrared heating element has to be installed above the soil column. A diurnal heating effect can be created in different ways. The infrared heating element can be switched on and off every 12 hours, the element can be lifted and dropped in a 24-hours cycle or by using more advanced infrared heating elements the amount of radiation can regulated over time. In addition an infrared sensor can be installed to regulate and measure the temperature at the soil surface of the column. These measurements will serve as the top boundary condition for the model. During the experiment the temperature of the room is assumed to remain at a constant temperature of 15 °C. In the model study for this laboratory experiment the upper boundary conditions are 40 °C and 15 °C each for 12 hours. As bottom boundary condition a constant soil temperature of 15 °C is chosen. The potential evaporation during the warm 12-hour is defined as 10 mm/day.

7.3 Model study

7.3.1 Objective of the model study

A model study will be performed to investigate the ideal set-up of measurements devices in the soil column experiment. This model study focusses on the amount of measurement devices, the depth and the variables to measure. Three types of measurable variables are interesting in this study; soil water pressure head, soil water content and soil temperature. The method for finding the ideal set-up consists of multiple steps which are schematically shown in figure 15. First a direct simulation will be executed with chosen soil hydraulic properties and soil thermal properties. From the Staring-series the O5 soil is chosen, which is a coarse grained, sandy soil (Wosten *et al.*, 2001). The soil hydraulic properties of this soil type will be used as input for the direct simulation. In addition the soil thermal properties of sand from the Hydrus standards will be taken as input. Values of the soil water content, soil water pressure head and soil temperature from several depths will be selected from the results of this direct simulation. This data will serve as input data for the inverse parameter estimation and will be treated as measurements from a laboratory experiment. An amount of noise will be added to the data, which represents the measurement error. The chosen parameters will be estimated with an inverse parameter estimation method using different kind of selections of the data acquired during the

direct simulation. The estimated parameter sets need to compared to the direct simulation with the parameters from the 05 soil type. The estimated parameters sets with associated standard deviations and correlation matrices will then be used as input for a direct simulation. For every data selection 50 samples of parameter sets will be drawn from the (log)normal distributions and feed into the direct simulation to compute the daily net flux at the top of the profile. This flux will be compared to the "real" configuration; the net flux computed with the soil hydraulic parameters from the 05 soil type. A criterion will be used for the comparison. The lowest criterion will give the "ideal" setup of measurement devices in the soil column. In figure 15 a schematic picture is presented with all the steps to be followed.

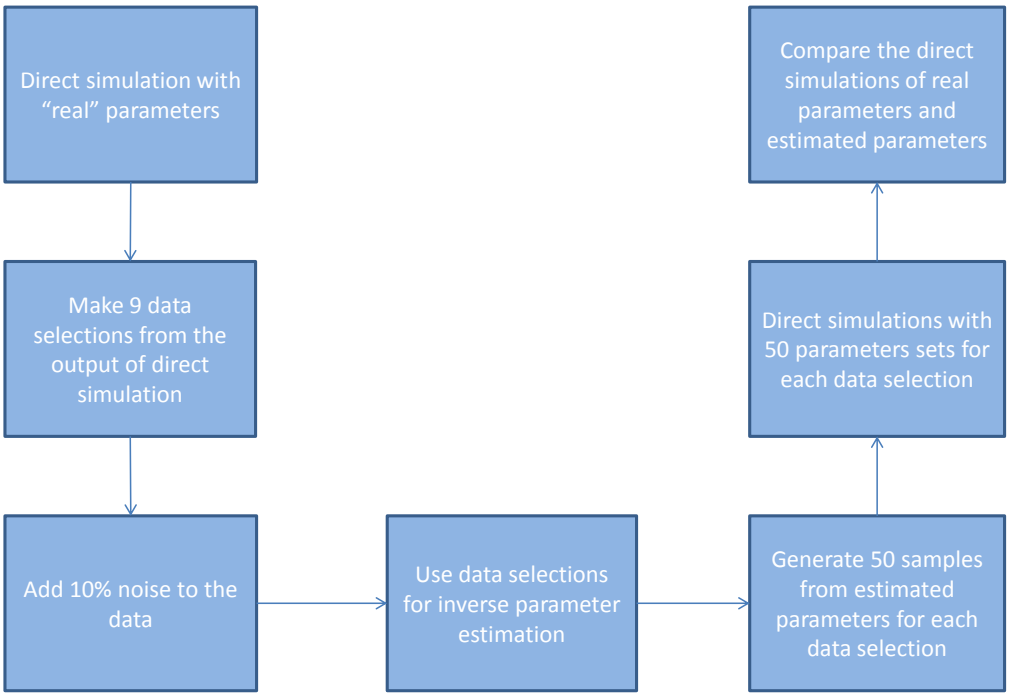

Figure 15: Method for investigating the ideal set-up.

7.3.2 Boundary and initial conditions of the model

The boundary conditions are kept simple. The bottom boundary condition for heat transport will be kept constant at 15 °C. The top boundary condition is 40 °C and 15 °C representing respectively day and night, both 12 hours. The boundary conditions of the mass balance of water consist of a zero flux boundary as bottom boundary condition and a potential evaporation rate of 10 mm/day during "day" and 0 mm/day during "night" as top boundary condition. As initial condition the soil water content is set at 0.27 $cm^3 cm^{-3}$, which is not at full saturation. This is required to keep the duration of the experiment acceptable. This initial condition should however be still wet enough to have soil evaporation over the full range of liquid and vapour fluxes. The dry soil water conditions must be reached because measurements in these conditions are important for the discussion on the significance of the water vapour fluxes. The initial temperature is 15 °C uniform within the soil column.

7.3.3 Data for inverse parameter estimation

It would be great to explore all depth(s) for different measurement devices for the column experiment at every 1 cm over the entire range from 0 to 100 cm deep. Unfortunately this is not possible because this will cost too much computation time. So eight depths are selected as possible measurement locations. As noted in section 7.2.3 the upper zone is more dynamic than the lower part of the column, thus it is better to measure in more detail in this upper zone. Observation nodes are placed in the Hydrus model on eight different depths; 1, 5, 10, 15, 25, 50, 75 and 100 cm deep with respect to the soil surface. At these depths hourly values are recorded of the soil water pressure head, the soil water content and the soil temperature. This is done for a period of 28 days. The total data set consists of 16128 records (8 depths $\times$ 3 variables $\times$ 28 days $\times$ 24 hours). For the inverse parameter estimation different kind of combinations of data can be used, e.g. time versus soil water pressure head, time versus soil water content, soil water pressure head versus soil water content and time versus soil temperature). Table 9 shows the nine data selections for the inverse parameter estimation. The data selections represent experimental setups. Selection 1 is to examine the case if only soil water contents and soil temperatures are measured in time at all eight depths. Selection 2 is the situation in which soil water pressure heads and soil temperatures are measured in time at all depths. The other seven selections combines data of all the three variables from different depths. Data selection 9 is similar to the data acquired from the fieldwork in Trabadillo with measurements of soil water content, soil water pressure head and soil temperature at depths of 25, 50, 75 and 100 cm beneath the soil surface. Every possible input combination from a data selection is used for the inverse parameter estimation. In first trial runs however the input type soil water pressure head versus soil water content did not result in converged solutions of the model. Thus only time series of soil water content and soil water pressure head are used as input for the inverse parameter estimation.

Table 9: Data selections (experimental setups) for the inverse parameters estimation; depths of measurements.

Data selection	θ	h	T
1	-	1,5,10,15,25,50,75,100	1,5,10,15,25,50,75,100
2	1,5,10,15,25,50,75,100	-	1,5,10,15,25,50,75,100
3	1,5,10,15,25,50,75,100	1,5,10,15,25,50,75,100	5,25
4	5,10,15,25	5,10,15,25	5,10,15,25
5	5,25,50	5,25,50	5,25,50
6	1,100	1,100	1,100
7	5,25	5,25	5,25
8	50	50	50
9	25,50,75,100	25,50,75,100	25,50,75,100

7.3.4 Inverse parameter estimation

The inverse parameter estimation is executed with nine selections of data from the total amount of data acquired with the direct simulation. Noise is added to the data to make the inverse parameter estimation correspond more to a real laboratory experiment in which measurement errors are unavoidable. Measurement errors can especially become large in the situation that the soil moisture content is very low. So a random noise with a maximum deviation of 10% is added to the data. The nine selections of data represent nine possible measurement set-ups; these are presented in table 9. The input of the selection for the inverse parameter estimation are time series of soil water content, soil water pressure head and soil temperature. The Hydrus model does not always converge to a stable solution and the parameters can not be estimated using a selection from table 9. The output of the inverse

parameter estimation consists of the estimated parameters, the standard deviations and a correlation matrix in case the model converge to a stable solution. Only the data selections which converged in the inverse parameter estimation can be used in the following direct simulation. The diverged ones will be marked NA (Not Available).

Table 10: Soil hydraulic properties.

	$\theta_r(cm^3/cm^3)$	$\theta_s(cm^3/cm^3)$	$\alpha(1/cm)$	$n(-)$	$K_s(cm/d)$	$l(-)$
Initial estimate (Simulation 1)	0.030	0.32	0.0301	2.01	25	0.0100
Initial estimate (Simulation 5)	0.015	0.32	0.0500	2.20	25	0.0005
O5 soil type	0.009	0.32	0.0560	2.267	25	0.0001

Table 11: Thermal parameters.

	$b_1(W \cdot m^{-1} \cdot K^{-1})$	$b_2(W \cdot m^{-1} \cdot K^{-1})$	$b_3(W \cdot m^{-1} \cdot K^{-1})$
Initial estimate (Simulation 1)	0.2301E+17	-0.2098E+18	0.3217E+18
Initial estimate (Simulation 5)	0.2301E+17	-0.2098E+18	0.3217E+18
Sand	0.1471E+17	-0.1552E+18	0.3166E+18

Additional simulations will be carried out to investigate the convergence problems and the influence on the results. One simulation will be done in which less noise is added to the input data; 1% of noise is added to the data instead of 10% of noise. Reducing the measurement error will provide some information as to the effect of errors on model convergence and the uncertainty in the parameter estimated. In another simulation only one soil thermal parameter is estimated, i.e. b_3. The other two soil thermal parameters are fixed. The standard simulation shows in the correlation matrix values close to 1 or -1 between the soil thermal parameters (appendix B). A high correlation between parameters implies a very small amount of information, in other words a large uncertainty in the estimated parameters. If only one soil thermal parameter is estimated, this one is probably estimated with a smaller standard deviation. Although you can argue if the other two fixed parameters have proper values.
In another simulation the model is executed on a time scale of seconds instead of on a daily time scale. A more detailed execution of the model may prevent the non-convergence of the model. The last simulation uses a different initial estimate of the soil hydraulic properties for the estimation of the parameters. In table 10 the second initial estimate belongs to the additional simulation 5 with initial soil hydraulic properties closer to the real values. The initial values of the soil thermal properties are kept the same, because to assess those parameters in the field or in the lab is less convenient. A closer initial estimate of the soil hydraulic properties will probably reduce the convergence problems. The nine data selections are used as input for the inverse parameter estimation for all the five simulations. In table 12 all the simulations are listed.

Table 12: Different simulations for evaluating the model performance.

	Simulations
1	Standard
2	1% of noise
3	Estimate one soil thermal parameter
4	Model time step in seconds
5	Better initial estimate of soil hydraulic properties

7.3.5 Direct simulation

The output of the inverse parameter estimation is used as input for the direct simulation of the model. From the direct simulation the cumulative net flux over de top boundary will be compared to the cumulative flux calculated in advance with the "real" soil thermal and soil hydraulic parameters. The estimated parameters have standard deviations and are correlated to some extent. This uncertainty in the parameters implies that it is not possible to accurately compute the net flux in a single direct simulation. Therefore Monte Carlo simulations will be applied again. Samples of parameter sets are drawn from (log)normal distributions and with these parameter sets direct simulation runs are performed multiple times. Every time 50 samples of parameter sets are taken from each selection of data for all of the five simulations. The parameters θ_r, n, α are assumed to have lognormal distributions and the parameters l, b_1, b_2, b_3 are assumed to be normal distributed. In figure 16 the result of the

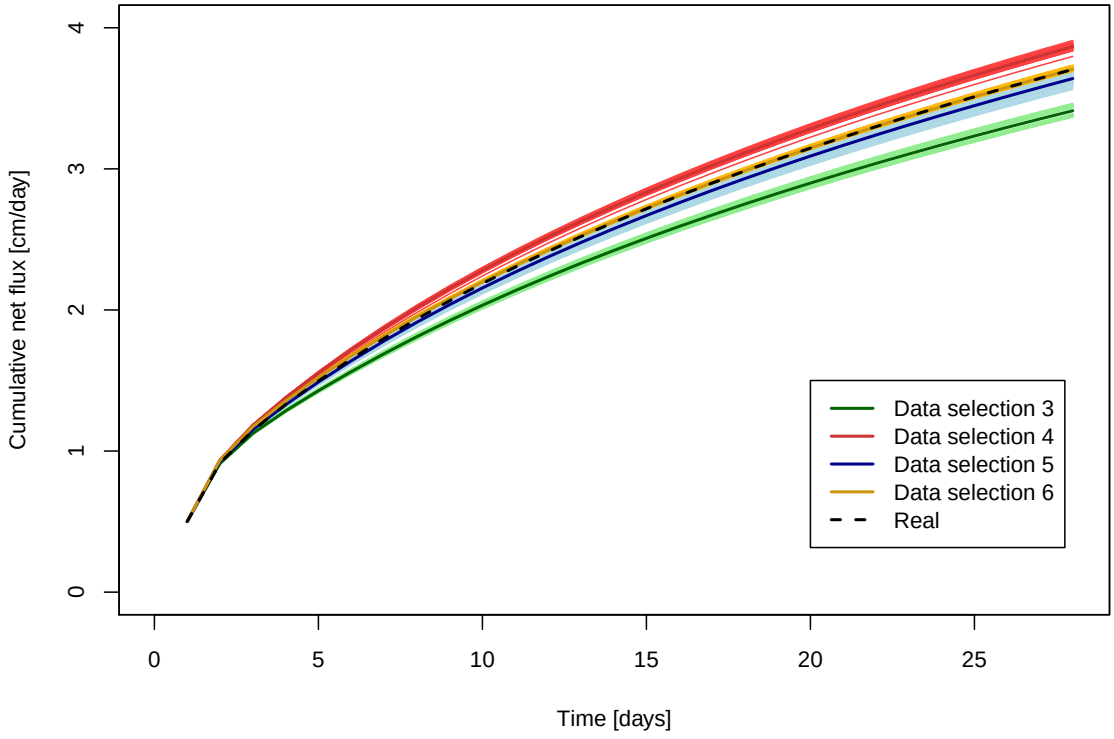

Figure 16: Cumulative net fluxes of direct simulation 1, the standard simulation. Black line is the flux with the real parameters, the other lines depict the fluxes from a data selection from table 9.

standard simulation is presented. Cumulative net fluxes over time are shown in which the black line is the flux computed with the real parameters. The other lines depict a data selection from table 9 which is used for the inverse parameter estimation. The cumulative net flux is chosen for the comparison, because a better distinction is expected from the comparison between cumulative fluxes. From every data selection a sample of 50 parameter vectors is generated from the estimated parameter distribution and the cumulative net flux is computed 50 times. The thin lines show every individual cumulative net flux calculated with a sampled parameter set and the thick line represents the ensemble of the cumulative net fluxes of the 50 samples. Most of the simulations do not show all nine data selections, because sometimes the parameters can't be estimated from these data selections due to convergence problems in the inverse parameter estimation. The results from the other simulations from table 12

can be seen in appendices J, K, L and M. In the standard simulation only four of the nine data selections converged, so only for those four a direct simulation is performed as can be seen in figure 16. Reducing measurement error form 10 to 1% does not improve the performance of the parameter estimation procedure, see appendix J. Some data selections are converging for this simulation while others converge in the standard simulation. Only data selection 5 hasn't problems in both simulations. The simulation in which only one soil thermal parameter is estimated, shows better results. Results are presented in appendix K. The model converged for seven out of nine data selections, while for the standard simulation only four data selections reached a stable solution. Experimental setups 4 and 5 converge in both simulations.
When the model is running on a time scale of seconds instead of on a daily time scale the convergence problems are even larger; only three out of nine data selections come to a stable solution. For this simulation the cumulative net fluxes are all higher than the real cumulative net flux. Again data selections 4 and 5 converged in both simulations.
The simulation with an initial estimate of the soil hydraulic properties closer to the real soil hydraulic properties gives much better results; all data selections converged to a stable solution. The comparison between runs based on the 50 sampled parameter vectors and the original run is made on the basis of a criterion using the cumulative net flux at day 28. This criterion is calculated from the mean and standard deviation of the cumulative flux over the 50 runs compared to the cumulative net flux of the original simulation. A smaller criterion implies a more suitable experimental setup. The criterion is calculated according to equation 7.1:

$$criterion = \sqrt{(real - mean\ data\ selection)^2 + standard\ deviation\ data\ selection^2} \qquad (7.1)$$

Table 13 presents the criteria calculated with equation 7.1 for all the data selections. The simulations are listed in table 15. NA is used for data selections which did not converge. For the standard simulation data selections 6 and 5 are the best and second-best experimental setup. In simulation 2 less noise is added to the data; 1% instead of 10%. The criteria are the lowest for data selections 5 and 2. If only one soil thermal parameter is estimated the criteria are the lowest for data selections 4 and 7 as can be seen for simulation 3. Changing the time scale of the model to seconds (simulation 4) results in only worse criteria in which data selection 5 has the lowest criterion. Simulation 5 has a better initial estimate of the soil hydraulic parameters, and consists of criteria values for all data selections. Data selections 3, 4 and 5 have the lowest criteria. Data selection 8 has by far the highest criterion and this data selection uses only input data from a depth of 50 cm as shown table 9.

Table 13: Comparison of the real cumulative net flux and the data selections from the five simulations.

	Simulation 1	Simulation 2	Simulation 3	Simulation 4	Simulation 5
Data selection 1	NA	NA	0.0283	NA	0.0816
Data selection 2	NA	0.0290	0.0379	NA	0.0480
Data selection 3	0.2947	NA	NA	NA	0.0337
Data selection 4	0.1632	NA	0.0130	0.1220	0.0341
Data selection 5	0.0742	0.0206	0.0298	0.0862	0.0378
Data selection 6	0.0115	NA	NA	NA	0.0717
Data selection 7	NA	0.0614	0.0160	0.1342	0.0570
Data selection 8	NA	0.1210	0.0696	NA	0.1420
Data selection 9	NA	0.1219	0.0788	NA	0.0564

7.3.6 Discussion

The objective of this model study is to find the ideal experimental set-up for a column experiment trying to determine the amount of measurements, the measurement depth(s) and the variables to measure. Eight depths in total were selected as possible measurement depths; 1, 5, 10, 15, 25, 50, 75 and 100 cm deep with respect to the soil surface. Measuring at a depth of 1 cm beneath the soil surface is complicated, because the installation of the sensor will break the surface layer which influences the evaporation from the soil surface. For this model study however it is useful to include this depth because it provides information about the effect of measuring as close to the surface as possible. The model study consists of several simulations as listed in table 15, to investigate the convergence problems. It was a good choice to avoid the estimation of all the soil hydraulic properties, because often the estimation of more parameters will presumably yield more uncertainty in the parameters. The parameters θ_s and K_s can be determined accurately in a separate laboratory experiment. The convergence problems are tedious and influence the method to find the best set-up for the measurement devices. Nevertheless the data selections from table 14 are compared using equation 7.1.

Table 14: Data selections (experimental setups) for the inverse parameters estimation; depths of measurements (recurrence of table 9).

Data selection	θ	h	T
1	-	1,5,10,15,25,50,75,100	1,5,10,15,25,50,75,100
2	1,5,10,15,25,50,75,100	-	1,5,10,15,25,50,75,100
3	1,5,10,15,25,50,75,100	1,5,10,15,25,50,75,100	5,25
4	5,10,15,25	5,10,15,25	5,10,15,25
5	5,25,50	5,25,50	5,25,50
6	1,100	1,100	1,100
7	5,25	5,25	5,25
8	50	50	50
9	25,50,75,100	25,50,75,100	25,50,75,100

All the data selections for simulation 4 are slightly above the real flux as can be seen in appendix L. The cumulative net flux is computed on a daily time scale. The upper boundary condition for the mass equation of water is variable in time. In both models hourly data is used as input data for the time variable boundary condition. So the model on a time scale of days has relatively more detailed input data. This can be the cause of the discrepancy between the simulation in a time scale of seconds and the real flux computed on a time scale of days.
Simulations 1, 2, 4 and 5 which estimated all three soil thermal parameters, have all high correlations between the soil thermal parameters. These highly correlated parameters contain less information about the precise value of that particular parameter and thus have a higher uncertainty. For every data selection 50 parameters sets are drawn from the estimated parameters, the standard deviation and the correlation matrix. It is assumed that a sample size of 50 is sufficient to characterize the effect of parameter uncertainty. In contrast to section 6.3.5 no Welch's t-test are performed. So it is questionable whether 50 samples of parameter sets are sufficient.
As can be seen in table 13 the optimal data selection, which has the lowest criterion, is dependent on many factors. In simulation 1 becomes clear that more measurements do not result in lower criteria, which is contracting. Data selection 3 consist of much more measurement than data selection 6, but has a higher criterion. Probably the measurement error of 10% on a larger amount of data is the cause of the higher criterion. Simulation 2 has some higher and some lower criteria. More accurate measurements do not result in a better description of the measured data. Simulation 3 shows that the estimation of only one soil thermal parameter result in a better description of the measured data,

because the three soil thermal parameters are highly correlated. The criteria for this simulation are low. Simulation 4 with the time scale in seconds has large convergence problems and the three data selections for which parameter estimates converged, show high criteria. So running the Hydrus model in time steps of seconds does not improve the inverse parameter estimation. What does improve the inverse parameter estimation is using an initial estimate of the parameters which is closer to the real values. It is recommended to do an extensive experimental analysis of the soil material to provide a better initial parameter estimate. Another option is to execute a Monte Carlo simulation. Generate many parameter sets and run the model for every set as new initial estimate. Using several initial estimates is a way to reach close to the real parameters, which are usually unknown.
The five simulations from table 15 do not agree convincingly about the optimal data selection. Simulation 5 shows the lowest criterion for data selection 3, which consist of the largest amount of measurements of soil water pressure head and soil water content, and soil temperature at only two depths. The highest criterion in simulation 5 is for data selection 8, which contains of data from one depth; 50 cm below the soil surface. Based on table 13 data selection 5 would be recommended for the model study. Overall the best experimental setup for this column experiment will contain measurement devices for soil water content, soil water pressure head and soil temperature at depths of 5, 25 and 50 cm beneath the soil surface. In this model study data selection 5 is also the only one without

Table 15: Different simulations for evaluating the model performance (recurrence of table 12).

	Simulations
1	Standard
2	1% of noise
3	Estimate one soil thermal parameter
4	Model in seconds time scale
5	Better initial estimate of soil hydraulic properties

convergence problems. The convergence problems are especially coming from the soil hydraulic and soil thermal parameters. If the initial estimate is not close to the real value the parameters can diverge which results in unstable solutions. This is also the reason simulations 3 and 5 from table 15 have less problems or even no convergence problems. It is remarkable that for the inverse parameter estimation the input type soil water pressure head versus soil water content leads to divergence of the model. This input type describes the soil water retention curve and intuitively this would result in a better estimation of the parameters. The cause for these problems is probably related to the inverse parameter estimation method used in Hydrus. Hydrus simulates a coupled heat and water flow experiment to estimate the parameters. The coupled processes with vapour flow are probably too complex with many degrees of freedom. Instead of a flow simulation, the measurements of soil water pressure head and soil water content can be used in software like Rosetta to estimate the parameters only based on the soil water retention curve. Further it is also a possibility to take flux variables as input type for the inverse parameter estimation instead of state variables as is done in this model study. It's naturally to use flux variables as input if the variables of interest are of the same type.
Free drainage is assumed for the mass balance equation for water. It's more convenient to use a free flow boundary condition. Free drainage indicates water flow by gravitation only, which is in this experiment almost zero. While free flow states water will flow if the soil pressure head becomes positive, which will never occur during this experiment. So in this experiment it does not matter which one of the two boundary conditions is used. It is however more convenient to use free flow as bottom boundary condition in laboratory experiments.

8 Conclusion and discussion

8.1 Conclusion

The sections above showed that coupled water and heat transport is very challenging given the large number of processes involved, and their associated uncertainties. The uncertainties are about the processes involved, the contribution of the fluxes, the soil hydraulic properties, the data, the numerical models and about the theory of Philip and de Vries itself. In this thesis the contribution of water vapour movement with respect to the total water transport on a daily time scale is investigated. After the calibration of the model the different fluxes are computed for multiple moments in time. The isothermal liquid water flux, the thermal water vapour flux and the isothermal water vapour flux are calculated in Hydrus and instantaneous fluxes are plotted in box plots, see 7. The isothermal water vapour flux can be neglected during day and night.
The thermal water vapour flux has a clear daily pattern. During night the flux is directed out of the soil, because the soil is warmer than the air above the soil surface. During daytime the opposite process occurs. The air above the soil surface is warmer than the soil itself, the temperature gradient will be directed into the soil. And thus during daytime an inwards directed thermal water vapour flux will occur.
The isothermal liquid water flux is simulated in Hydrus and in the standard SWAP model with only liquid water flow. The box plots in figures 7 and 8 show clearly that the isothermal liquid water flux declines during time. The soil water conditions will become drier and this will decrease the unsaturated hydraulic conductivity coefficient and so this flux decreases. In the SWAP model this flux approaches zero in time. In Hydrus a small isothermal liquid water flux remains, fluctuating in a daily cycle. This small daily pattern of the isothermal liquid water flux is caused by the thermal water vapour flux which during day transports water into the soil. The water vapour condensates at a certain depth and that amount of water can be transported as liquid water upwards due to a soil water pressure gradient. So the instantaneous thermal water vapour flux does significantly contribute to the total flux at 12 o'clock and at midnight.
Thermal water vapour movement is additionally implemented explicitly in the SWAP model, so the model becomes a coupled heat and water transport model. Simulations are performed with four models; the Hydrus Coupled model, SWAP Coupled model, the Hydrus Liquid model and the SWAP Liquid model. The mean cumulative net fluxes in table 5 are the results of the simulations with 100 samples of parameter sets for each simulation. The coupled Hydrus model seems to compute a higher cumulative net flux than the other models. However Welch's t-tests showed that all of four models do not differ significantly from each other, as shown in appendix G. The soil hydraulic and soil thermal parameters determined of the soil at Trabadillo are used as input for all of these simulations. The main research question if water vapour does contribute to total water transport on a daily time scale, can be answered more generally if the models are simulated using parameters for several types of soils. The soil hydraulic properties from the HYPRESS project by Wosten *et al.* (1999) are taken to explore the contribution of water vapour transport on the total water flux more thoroughly. Again the four different models are used for the simulations. Numerical problems forced to assign a too large discretisation which is the cause for the strange results from the two Hydrus models as shown in table 8. The SWAP model does not have problems with mass balance errors and converged to a stable solution with a spatial discretization of 1 cm. The difference between the coupled SWAP model and the SWAP model with only liquid water transport is negligibly small. The cumulative net flux is the highest for medium-fine textured soils, both coarser as finer textured soils evaporate a smaller amount of water during the same period. While the coarse soil has relatively the highest contribution of water vapour to the total water flow.

Finally a proposal for a laboratory experiment related to coupled heat and water transport is presented. A model study is executed to find the optimal types of measurements and measurement depths for a study to water vapour and liquid water transport in (semi-)arid conditions. The results of the model study suggest that the best solution may be to install measurement devices for soil water content, soil water pressure head and soil temperature at depths of 5, 25 and 50 cm beneath the soil surface. The recommended soil column height is 100 cm with a diameter of 25 cm. Time-variable top boundary conditions are imposed as urgently suggested Parlange *et al.* (1998). Notice that multiple simulations with different adjustments were necessary to overcome the numerical problems in Hydrus and thus to be able to draw a conclusion on the optimal measurement set-up.

The final conclusion states that although the box plots show a significant thermal water vapour flux during day and during night, the cumulative net fluxes for models with only liquid water flow and coupled water and heat transport are not significantly different. And so water vapour transport does not contribute significantly in coupled heat and water transport models for bare soil in semi-arid regions on a daily time scale.

8.2 Discussion

The conclusion drawn about the contribution of water vapour flow is supported by the paper of Milly (1984). He notes that due to the diurnal heating effect the thermal vapour flux can be neglected for evaporation calculations on a daily time scale. The process of convective water vapour flow however isn't taken into account in the Hydrus model and this process can have an effect on the water vapour transport according to Rose (1968b); Bear *et al.* (1991); Nassar & Horton (1997); Parlange *et al.* (1998). Expansion and contraction of soil air due to diurnal warming of the land surface will result in a convective movement of water vapour in the soil. Convective water vapour movement can also occur due to changes in barometric pressure, temperature gradients or wind at the land surface according to Nassar & Horton (1997). A convective flux of water vapour will change the concentration gradients within the soil which have an influence on the other fluxes. Bittelli *et al.* (2008) argued that the water vapour flux is especially important close the soil surface. The three causes for this are; (a) near the soil and atmosphere interface higher vapour concentration gradients exist, (b) larger thermal gradients near the soil surface will result in larger thermal fluxes and (c) a lower soil water content results in a higher air-filled porosity which is available space for vapour.
These arguments emphasize the importance of a reliable model with a fine discretization of the grid close to the top. Novak (2010) used a very fine grid near the top of the profile to be able to determine all the variables of interest very accurately. At the top the grid size was $10^{-5}m$ increasing to $0.4m$ at the bottom of the profile. In the study presented here serious problems occurred when using the Hydrus model; large mass balance errors and convergence problems required the use of a coarser spatial discretization of 1 cm. Smaller time steps didn't solve the numerical issues and only an unwanted larger nodal space avoided these issues. For the soil hydraulic properties from the HYPRESS database (Wosten *et al.*, 1999), the Hydrus model was often not able to converge to a stable solution. Deb *et al.* (2011) were confronted with the same kind of problems in Hydrus and they remark that a finer grid most of the time generates better simulation results, but can also cause convergence problems. The numerical problems were probably not caused by the boundary conditions. Evaporation rates as time-variable top boundary conditions and free drainage as bottom boundary conditions were also used by Saito *et al.* (2006) and Deb *et al.* (2011) for the mass balance of water, who both also used the Hydrus model. The bottom boundary condition for the heat conservation equation were defined in both papers as zero gradient and as upper boundary condition the soil heat flux at the top was used. The soil heat flux is calculated from a surface energy balance. In this thesis state variables were taken as boundary conditions, respectively the soil surface temperature and the soil temperature at the bottom of the profile. Importing Neumann boundary conditions in the Hydrus model to calculate

fluxes can result in better computations. Despite of the numerical issues in Hydrus the conclusions based on the results of the Hydrus model are still justified. The mass balance errors are checked for every simulation and are sufficiently small (around the 1%). Most of the convergence problems are solved by modifying the numerical model parameters, maintaining an acceptable nodal spacing of 1 cm. In addition the soil temperatures are checked with measurements and the output results from the Hydrus model are critically analysed. The explicit implementation of thermal water vapour flow in SWAP is supported by justified assumptions. Saito *et al.* (2006) note that the amount of sensible heat transferred by isothermal liquid water flow is significant and this process is included in Hydrus. While Bear *et al.* (1991) argued that this kind of energy transfer is negligible due to the presence of the thermal liquid water flux and the main contribution of energy transfer by the porous media itself. For this thesis the explicit approach for water vapour transport as done in SWAP, is more suitable than the implicit numerical solution in Hydrus. The instability of Hydrus can possible be attributed to a not balanced solution of the coupled system of equations. Nevertheless it would be good to execute test simulations with the two coupled models and compared both models with measurements of evaporation rates as proposed in the designed plan for a laboratory experiment in section 7.
The assumption about instantaneous vaporization is put into question by Smits *et al.* (2011). Experiments in numerous studies have shown that it takes a lot of time before equilibrium is reached between liquid water and water vapour (Benet *et al.*, 2009; Chammari *et al.*, 2008). Especially near the soil surface this assumption have a large effect; unrealistic low soil water pressure heads at the soil surface were computed Smits *et al.* (2011). The larger soil water pressure gradient will result in an overestimation of the evaporation rate. Smits *et al.* (2011) calculated an overestimation of 35% due to the assumption of thermodynamic equilibrium. In the studies by Saito *et al.* (2006) and Bittelli *et al.* (2008) which used equilibrium models, the overestimation of the evaporation rate was corrected by using a soil surface resistance. Avoiding the assumption about instantaneous vaporization will imply to use an additional mass balance for the total gas phase. An additional coupling between water, energy and the total gas phase will make the model more complex in many aspects.
In addition Deb *et al.* (2011) mentioned a significant thermal liquid water flux can be noticed after an input of water. While most of the papers neglected the contribution of thermal liquid water flow because of the dominant isothermal liquid water flux (Milly, 1984; Saito *et al.*, 2006; Smits *et al.*, 2011). The rain events in the meteorological input data used in this thesis overcome the uncertainty about this phenomenon of a significant thermal liquid water flux after an input of water. Unfortunately the thermal liquid water flux can not be assessed specifically in the Hydrus model.
The theory of Philip and de Vries is popular for coupled heat and water transport but two main doubts are arising many times in the literature; (a) the limitations of the theory, which processes need to be taken into account or can be neglected, and (b) uncertainty about the field and laboratory experiments (De Vries, 1987). Many times the computed results from coupled heat and water models don't correspond to the field measurements. According to Parlange *et al.* (1998) there are two explanations; (a) only a few field experiments are performed to test the theory and (b) most observations result from laboratory experiments with steady state boundary conditions. In this thesis field data is used from one soil profile, while initially more soil profiles were available with installed with measurement equipment. Unfortunately the other soil profile is not measured correctly for soil water content and soil pressure head for unknown reasons. At first the plan was to use the data from one soil profile for the calibration and the data from the other soil profile for the validation of the Hydrus model, but this was not possible.

In addition a plan for a laboratory experiment is proposed specifically focussed on a coupled heat and water transport model, in which measurement of evaporation rates can be compared with model computations. Time-variable boundary conditions are imposed as top boundary conditions as urgently remarked by Parlange *et al.* (1998). The ideal measurement set-up for the laboratory experiment is determined by a model study. This set-up is probably in some way influenced by the numerical problems in Hydrus. Nevertheless the execution of this experiment would be very interesting with installed measurement devices for soil water content, soil water pressure head and soil temperature at depths of 5, 25 and 50 cm.

8.3 Recommendations

Data from more than one soil profile is highly recommendable to study coupled heat and water transport. Before installing the measurement devices it is advisable to perform a model study. This information prior to the experiment helps to determine the measurement depths and the variables to measure. Nowadays too often the installation set-up is based on the availability of measurement devices. Especially near the soil surface the use of POT-sensor is recommended to be able to measure the very low soil water pressures. In addition it would be interesting to model in Hydrus with flux boundary conditions in stead of state boundary conditions for the heat conservation equation. It is more natural to use fluxes as boundary conditions to calculate the fluxes in between these conditions. Next to that it would be great to simulate the coupled heat and water transport model for 10.000 parameters set of soil hydraulic parameters and associated soil thermal properties, thus investigating water vapour flow for many types of soils. Also more extreme climates can be created for the input of the models. Related to climate change it is interesting to investigate if water vapour flow is more likely to contribute in the future when higher temperature gradients will occur. In addition the contribution of water vapour flow on a daily scale can be investigated using models including one or more of the following processes; convective water vapour flow, a third mass balance for air flow and a non-equilibrium approach between water vapour and liquid water.

References

Abubeker, A.M. 2010. *Hydro - geophysical assessment of sub surface to improve groundwater models : Sardon case study, Spain.* Master thesis report. Enschede, University of Twente Faculty of Geo-Information and Earth Observation ITC.

Agbakpe, B.A. 2010. *Estimating tree groundwater transpiration in La Mata catchment, Spain.* Master thesis report. Enschede, University of Twente Faculty of Geo-Information and Earth Observation ITC.

Bear, J., Bensabat, J., & Nir, A. 1991. Heat and mass transfer in unsaturated porous media at a hot boundary: I. One-dimensional analytical model. *Transport in Porous Media*, **6**(3), 281–298.

Benet, J.C., Lozano, A.L., Cherblanc, F., & Cousin, B. 2009. Phase change of water in a hygroscopic porous medium: Phenomenological relation and experimental analysis for water in soil. *Journal of Non-Equilibrium Thermodynamics*, **34**, 133–153.

Bittelli, M., Ventura, F., Campbell, G.S., Snyder, R.L., Gallegati, F., & Pisa, P.R. 2008. Coupling of heat, water vapor, and liquid water fluxes to compute evaporation in bare soils. *Journal of Hydrology*, **362**(3-4), 191–205.

Black, T.A., Gardner W.R. Thurtell G.W. 1969. The prediction of evaporation, drainage, and soil water storage for a bare soil. *Soil Science Society America Journal*, **33**, 655–660.

Boesten, J.J.T.I., & Stroosnijder, L. 1986. Simple model for daily evaporation from fallow tilled soil under spring conditions in a temperate climate. *Netherlands Journal of Agricultural Science*, **34**, 75–90.

Bouyoucos, G.T. 1915. Effect of temperature on the movement of water vapor and capillary moisture in soils. *J. Agr.Res.*, **5**, 141–172.

Camillo, P.J., & Gurney, R.J. 1986. A resistance parameter for baresoil evaporation models. *Soil Science*, **141**, 95–105.

Campbell, G.S. 1985. *Soil physics with BASIC: Transport models for soil plant systems*. Elsevier, New York.

Cass, A., Campbell, G.S., & Jones, T.L. 1984. Enhancement of thermal water vapor diffusion in soil. *Soil Science Society America Journal*, **48**, 25–32.

Chammari, A., Naon, B., Cherblanc, F., Cousin, B., & BÃl'net, J.C. 2008. Interpreting the drying kinetics of a soil using a macroscopic thermodynamic nonequilibrium of water between the liquid and vapor phase. *Drying Technology*, **26**, 836–843.

Currie, J.A. 1960. Gaseous diffusion in porous media Part 1. - A non-steady state method. *British Journal of Applied Physics*, **11**(8), 314–317.

De Vries, D.A. 1975. Heat transfer in soils. *Semin on Heat and Mass Transfer in the Environ of Veg, Heat and Mass Transfer in the Biosphere*, 5–28.

De Vries, D.A. 1987. The theory of heat and moisture transfer in porous media revisited. *International Journal of Heat and Mass Transfer*, **30**(7), 1343–1350.

Deb, S.K., Shukla, M.K., Sharma, P., & Mexal, J.G. 2011. Coupled liquid water, water vapor, and heat transport simulations in an unsaturated zone of a sandy loam field. *Soil Science*.

D'Urso, G. Basile, A. 1997. Physico-empirical approach for mapping soil hydraulic behaviour. *Hydrology and Earth System Sciences*, **4**, 915–923.

Fares, A., & Polyakov, V. 2006. Advances in Crop Water Management Using Capacitive Water Sensors. *Advances in Agronomy*, **90**, 43–77.

Gowing, J.W., Konukcu, F., & Rose, D.A. 2006. Evaporative flux from a shallow watertable: The influence of a vapour- liquid phase transition. *Journal of Hydrology*, **321**(1-4), 77–89.

Heitman, J.L., Xiao, X., Horton, R., & Sauer, T.J. 2008a. Sensible heat measurements indicating depth and magnitude of subsurface soil water evaporation. *Water Resources Research*, **44**.

Heitman, J.L., Horton, R., Sauer, T.J., & DeSutter, T.M. 2008b. Sensible heat observations reveal soil-water evaporation dynamics. *Journal of Hydrometeorology*, **9**, 165–171.

Idso, S.B. 1981. A set of equations for full spectrum and 8- to 14-mm and 10.5- to 12.5-mm thermal radiation from cloudless skies. *Water Resources Research*, **17**(2), 295–304.

Jackson, R.D., Kimball, B.A., Reginato, R.J., & Nakayama, F.S. 1973. Diurnal soil-water evaporation: time-depth-flux patterns. *Soil Sci Soc Am Proc*, **37**(4), 505–509.

Jackson, R.D., Reginato, R.J., Kimball, B.A., & Nakayama, F.S. 1974. Diurnal soil-water evaporation: comparison of measured and calculated soil-water fluxes. *Proc Soil Sci Soc Am*, **38**(6), 861–866.

Jassal, R.S., Novak, M.D., & Black, T.A. 2003. Effect of surface layer thickness on simultaneous transport of heat and water in a bare soil and its implications for land surface schemes. *Atmosphere - Ocean*, **41**(4), 259–272.

Kroes, J.G., van Dam, J.C., Groenendijk, P., Hendriks, R.F.A., & Jacobs, C.M.J. 2008. *SWAP version 3.2. Theory description and user manual*. Alterra-report 1649. Alterra, Research Institute, Wageningen, The Netherlands.

Lewis, J., & Sjostrom, J. 2010. Optimizing the experimental design of soil columns in saturated and unsaturated transport experiments. *Journal of Contaminant Hydrology*, **115**(1-4), 1–13.

Milly, P.C.D. 1984. A simulation analysis of thermal effects on evaporation from soil. *Water Resources Research*, **20**(8), 1087–1098.

Monteith, J.L. 1965. Evaporation and environment. *Symposia of the Society for Experimental Biology*, **19**, 205–234.

Monteith, J.L., & Unsworth, M.H. 1990. *Principles of environmental physics*. 2nd edition Edward Arnold, London.

Mualem, Y. 1976. A new model for predicting the hydraulic conductivity of unsaturated porous media. *Water Resources Research*, **12**(3), 513–522.

Nassar, I. N., & Horton, R. 1989. Water transport in unsaterated nonisothermal salty soil: II. Theoretical development. *Soil Science Society America Journal*, **53**, 1330–1337.

Nassar, I. N., & Horton, R. 1992. Simultaneous transfer of heat, water, and solute in porous media: I. Theoretical development. *Soil Science Society America Journal*, **56**, 1350–1356.

Nassar, I. N., & Horton, R. 1997. Heat, Water, and Solution Transfer in Unsaturated Porous Media: I – Theory Development and Transport Coefficient Evaluation. *Transport in Porous Media*, **27**, 17–38.

Nimmo, J.R., & Miller, E.E. 1986. The temperature dependence of isothermal moisture vs. potential characteristics of soils. *Soil Science Society of America Journal*, **50**(5), 1105–1113.

Novak, M.D. 2010. Dynamics of the near-surface evaporation zone and corresponding effects on the surface energy balance of a drying bare soil. *Agricultural and Forest Meteorology*, **150**(10), 1358–1365.

Parlange, M.B., Cahill, A.T., Nielsen, D.R., Hopmans, J.W., & Wendroth, O. 1998. Review of heat and water movement in field soils. *Soil and Tillage Research*, **47**(1-2), 5–10.

Philip, J.R., & de Vries, D.A. 1957. Moisture movement in porous materials under temperature gradients. *Trans. American Geophysical Union*, 222–232.

Rose, C.W. 1968a. Water transport in soil with a daily temperature wave. I. Theory and experiment. *Australian Journal of Soil Research*, **6**(1), 31–44.

Rose, C.W. 1968b. Water transport in soil with a daily temperature wave. II. Analysis. *Australian Journal of Soil Research*, **6**(1), 45–57.

Rose, D.A. 1963. Water movement in porous materials: Part 2 - The separation of the components of water movement. *British Journal of Applied Physics*, **14**(8), 491–496.

Saito, H., Simunek, J., & Mohanty, B.P. 2006. Numerical analysis of coupled water, vapor, and heat transport in the vadose zone. *Vadose Zone Journal*, **5**(2), 784–800.

Sakai, M., Toride, N., & Simunek, J. 2009. Water and vapor movement with condensation and evaporation in a sandy column. *Soil Science Society of America Journal*, **73**(3), 707–717.

Salinas Revollo, A.I. 2010. *A study case on the upscaling of tree transpiration in water limited environments.* Master thesis report. Enschede, University of Twente Faculty of Geo-Information and Earth Observation ITC.

Shokri, N., Lehmann, P., & Or, D. 2009. Critical evaluation of enhancement factors for vapor transport through unsaturated porous media. *Water Resources Research*, **45**(10).

Simunek, J., Sejna, M., Saito, H., Sakai, M., & Van Genuchten, M.Th. 2008. *The HYDRUS-1D software package for simulating the movement of heat, water, and multiple solutes in variably saturated media, Version 4.08.* HYDRUS Software Series 3. Departement of Environmental Sciences, University of California.

Smits, K.M., Cihan, A., Sakaki, T., & Illangasekare, T.H. 2011. Evaporation from soils under thermal boundary conditions:Experimental and modeling investigation to compare equilibriumand nonequilibrium-based approaches. *Water Resources Research*, **47**(5).

Steenpass, C., Vanderborght, J., Herbst, M., ÅăimÅŕnek, J., & Vereecken, H. 2010. Estimating soil hydraulic properties from infrared measurements of soil surface temperatures and TDR data. *Vadose Zone Journal*, **9**(4), 910–924.

Ten Berge, H.F.M. 1986. *Heat and water transfer at the bare soil surface: aspects affecting thermal images*. PhD thesis. Wageningen Agricultural University, Wageningen, The Netherlands.

Van Bavel, C.H.M., & Hillel, D.I. 1976. Calculating potential and actual evaporation from a bare soil surface by simulation of concurrent flow of water and heat. *Agriculture and Forest Meteorology*, **17**(6), 453–476.

Van Dam, J.C., & Feddes, R.A. 2000. Numerical simulation of infiltration, evaporation and shallow groundwater levels with the Richards equation. *Journal of Hydrology*, **233**(1-4), 72–85.

Van der Ploeg, M.J., Gooren, H.P.A., Bakker, G., Hoogendam, C.W., Huiskes, C., Koopal, L.K., Kruidhof, H., & De Rooij, G.H. 2010. Polymer tensiometers with ceramic cones : Direct observations of matric pressures in drying soils. *Hydrology and Earth System Sciences*, **14**(10), 1787–1799.

Van Genuchten, M.Th. 1980. Closed-form equation for predicting the hydraulic conductivity of unsaturated soils. *Soil Science Society of America Journal*, **44**(5), 892–898.

Webb, S.W., & Ho, C.K. 1998. *Review of enhanced vapor diffusion in porous media*. Report SAND98-1819C. Sandia National Laboratories, Albuquerque, New Mexico.

Wosten, J.H.M., Lilly, A., Nemes, A., & Le Bas, C. 1999. Development and use of a database of hydraulic properties of European soils. *Geoderma*, **90**(3-4), 169–185.

Wosten, J.H.M., Veerman, G.J., de Groot, W.J.M., & Stolte, J. 2001. *Waterretentie- en doorlatendheidskarakteristieken van boven- en ondergronden in Nederland: de Staringreeks. Vernieuwde uitgave*. Alterra-report 153. Alterra, Research Institute, Wageningen, The Netherlands.

Zeng, Y., Su, Z., Wan, L., Yang, Z., Zhang, T., Tian, H., Shi, X., Wang, X., & Cao, W. 2009. Diurnal pattern of the drying front in desert and its application for determining the effective infiltration. *Hydrology and Earth System Sciences*, **13**(6), 703–714.

Zeng, Y., Su, Z., Wan, L., & Wen, J. 2011. Numerical analysis of air-water-heat flow in unsaturated soil: Is it necessary to consider airflow in land surface models? *Journal of Geophysical Research D: Atmospheres*, **116**(20).

Appendices

A Calibrated soil hydraulic properties

Table 16: Calibrated soil hydraulic parameters α, n and l for four layers with information about the uncertainty.

			95% Confidence limits	
Variable (Layer)	Value	S.E.Coeff.	Lower	Upper
α (1)	0.027	0.00060	0.026	0.029
n (1)	1.538	0.00457	1.529	1.547
l (1)	0.000	0.00351	-0.007	0.007
α (2)	0.036	0.01008	0.016	0.056
n (2)	1.441	0.05518	1.333	1.550
l (2)	1.981	0.59075	0.823	3.139
α (3)	0.034	0.00256	0.029	0.039
n (3)	1.488	0.01881	1.452	1.525
l (3)	0.041	0.03208	-0.022	0.104
α (4)	0.019	0.00329	0.013	0.026
n (4)	1.628	0.07363	1.484	1.772
l (4)	1.031	0.44667	0.156	1.907

B Correlation matrix soil hydraulic parameters

Table 17: Correlation matrix for the soil hydraulic parameters α, n and l for four layers.

	α 1	n 1	l 1	α 2	n 2	l 2	α 3	n 3	l 3	α 4	n 4	l 4
α 1	1	-0.8591	-0.5666	0.0551	-0.0452	0.0016	0.1444	-0.1516	-0.3537	0.1832	-0.3019	-0.477
n 1	-0.8591	1	0.4539	-0.0419	0.0337	-0.0048	-0.1099	0.1156	0.2847	-0.1547	0.2494	0.388
l 1	-0.5666	0.4539	1	0.139	-0.1453	-0.1786	-0.1071	0.1101	0.0586	-0.4346	0.4546	0.353
α 2	0.0551	-0.0419	0.139	1	-0.992	-0.9927	0.0485	-0.0439	0.1538	-0.1464	0.1205	0.018
n 2	-0.0452	0.0337	-0.1453	-0.992	1	0.994	-0.122	0.1265	-0.1475	0.1578	-0.1284	-0.0257
l 2	0.0016	-0.0048	-0.1786	-0.9927	0.994	1	-0.0903	0.0921	-0.1551	0.1655	-0.1432	-0.0469
α 3	0.1444	-0.1099	-0.1071	0.0485	-0.122	-0.0903	1	-0.9791	-0.2028	-0.0054	0.0196	-0.0493
n 3	-0.1516	0.1156	0.1101	-0.0439	0.1265	0.0921	-0.9791	1	0.199	0.0109	-0.0115	0.045
l 3	-0.3537	0.2847	0.0586	0.1538	-0.1475	-0.1551	-0.2028	0.199	1	-0.1366	0.1312	0.0479
α 4	0.1832	-0.1547	-0.4346	-0.1464	0.1578	0.1655	-0.0054	0.0109	-0.1366	1	-0.9674	-0.7097
n 4	-0.3019	0.2494	0.4546	0.1205	-0.1284	-0.1432	0.0196	-0.0115	0.1312	-0.9674	1	0.8184
l 4	-0.477	0.388	0.353	0.018	-0.0257	-0.0469	-0.0493	0.045	0.0479	-0.7097	0.8184	1

C POT sensor data

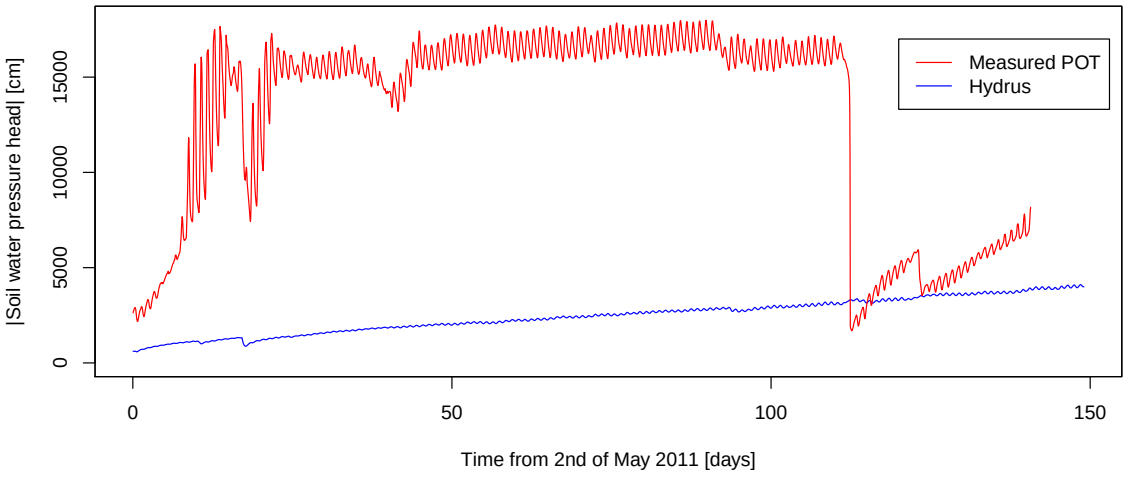

Figure 17: Graph of soil water pressure head (cm) measured with the POT sensor compared with Hydrus model results at the depth of 15 cm.

D P-values of instantaneous fluxes Hydrus

Table 18: P-values between runs of simulation in Hydrus of instantaneous fluxes.

Flux	"1-2"	"1-3"	"2-3"
Time2_liq	0.133990219	0.114182881	0.879934117
Time2_vT	0.121481712	0.53404705	0.423845325
Time2_vh	0.480937232	0.133712176	0.426761459
Time2.5_liq	0.339443259	0.171572756	0.681176073
Time2.5_vT	0.633372482	0.147391543	0.328191016
Time2.5_vh	0.749523968	0.759839614	0.549898678
Time16.5_liq	0.102038336	*0.019254318*	0.456338616
Time16.5_vT	0.097757098	*0.049061505*	0.71558937
Time16.5_vh	*0.01803501*	*0.032613359*	0.90359103
Time17.5_liq	0.169722564	*0.021152885*	0.367745535
Time17.5_vT	0.072198566	*0.007464535*	0.348345047
Time17.5_vh	*0.028921619*	*0.027084278*	0.875923306
Time62_liq	0.412115005	0.762197928	0.594025574
Time62_vT	0.186927084	*0.010156354*	0.198205773
Time62_vh	0.587775491	0.104823299	0.272810618
Time62.5_liq	0.065549512	*0.014891017*	0.52652728
Time62.5_vT	0.16561879	0.883198933	0.111868741
Time62.5_vh	0.088134791	0.055836861	0.807488417
Time100_liq	0.077361963	*0.007687586*	0.352867652
Time100_vT	0.412313713	*0.040032445*	0.227469459
Time100_vh	0.152583036	*0.027751497*	0.468648086
Time100.5_liq	0.118487927	*0.018516557*	0.41038836
Time100.5_vT	0.062891521	0.145415141	0.744762486
Time100.5_vh	*0.002469999*	*0.004300637*	0.834041185
Time148_liq	0.377277962	0.463385237	0.114775194
Time148_vT	0.894275203	0.145980353	0.159061456
Time148_vh	0.122830555	0.074220983	0.747443469
Time148.5_liq	0.873962466	0.143444512	0.161504464
Time148.5_vT	0.123147202	*0.04137852*	0.587249429
Time148.5_vh	0.419192916	0.071083996	0.302352113

E Box plots of the instantaneous fluxes in Hydrus

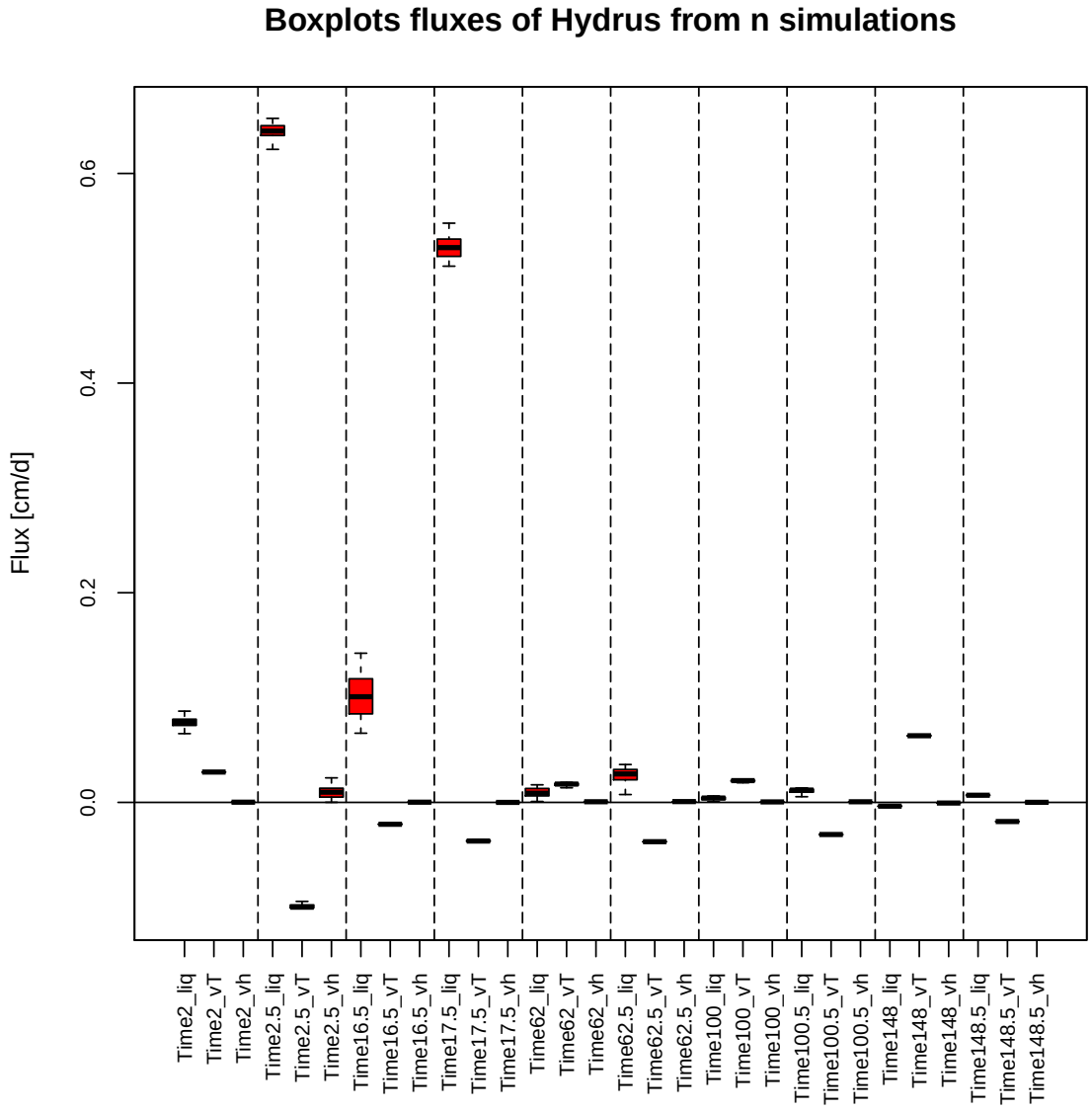

Figure 18: Box plots of the instantaneous fluxes in Hydrus for different moments in time for another set of 100 soil hydraulic parameters with respect to figure 7.

F P-values of instantaneous fluxes SWAP

Table 19: P-values between runs of simulation in SWAP of instantaneous fluxes.

Flux	"1-2"	"1-3"	"2-3"
Time2_liq	0.59611468	0.1172205	0.299614086
Time2.5_liq	0.542510819	0.106810838	0.315837269
Time16.5_liq	0.430363763	0.47421497	0.129187965
Time17.5_liq	0.79179368	0.410904768	0.558604507
Time62_liq	0.919272977	0.280461086	0.320706687
Time62.5_liq	0.940486584	0.285996472	0.314435201
Time100_liq	0.783847457	0.17124642	0.273135327
Time100.5_liq	0.852692178	0.170930179	0.245729919
Time148_liq	0.668708015	0.107690828	0.246773737
Time148.5_liq	0.713008498	0.133507606	0.260575164

G P-values between the four models

Table 20: Abbreviations of the models.

Model	Abbreviation
Hydrus Coupled	HC
Hydrus Liquid	HL
SWAP Liquid	SL
SWAP Coupled	SC

Table 21: P-values between the four models for 100 parameter sets.

HC-HL	HC-SL	HC-SC	HL-SL	HL-SC	SL-SC
0.722	0.499	0.515	0.743	0.757	0.989
0.701	0.991	0.968	0.706	0.691	0.978
0.719	0.359	0.371	0.570	0.585	0.987
0.726	0.323	0.342	0.518	0.541	0.979
0.696	0.353	0.368	0.581	0.598	0.986
0.681	0.336	0.345	0.571	0.581	0.991
0.728	0.509	0.525	0.752	0.768	0.986
0.705	0.341	0.358	0.555	0.574	0.983
0.547	0.529	0.533	0.953	0.953	0.999
0.720	0.530	0.549	0.785	0.802	0.986
0.700	0.980	0.997	0.730	0.718	0.983
0.698	0.949	0.969	0.766	0.749	0.981
0.716	0.656	0.683	0.926	0.952	0.975
0.671	0.349	0.362	0.597	0.614	0.981
0.644	0.526	0.539	0.844	0.859	0.986
0.691	0.674	0.691	0.965	0.981	0.985
0.716	0.619	0.647	0.883	0.910	0.975
0.671	0.267	0.277	0.486	0.497	0.992
0.699	0.505	0.531	0.766	0.793	0.976
0.711	0.445	0.461	0.679	0.696	0.986
0.721	0.460	0.482	0.691	0.716	0.976
0.668	0.529	0.543	0.822	0.836	0.988
0.724	0.419	0.443	0.644	0.669	0.979
0.695	0.356	0.371	0.580	0.597	0.986
0.682	0.489	0.512	0.762	0.788	0.976
0.707	0.625	0.652	0.898	0.924	0.976
0.701	0.573	0.592	0.841	0.860	0.983
0.693	0.331	0.346	0.550	0.568	0.985
0.657	0.515	0.528	0.815	0.829	0.988
0.672	0.306	0.315	0.539	0.550	0.989
0.715	0.733	0.762	0.987	0.960	0.974
0.707	0.999	0.977	0.723	0.705	0.979
0.702	0.602	0.631	0.879	0.907	0.974
0.726	0.616	0.635	0.873	0.890	0.985

Table 21: (continued)

HC-HL	HC-SL	HC-SC	HL-SL	HL-SC	SL-SC
0.686	0.444	0.464	0.701	0.723	0.981
0.734	0.580	0.603	0.828	0.850	0.981
0.663	0.391	0.413	0.652	0.677	0.978
0.711	0.246	0.261	0.428	0.447	0.981
0.712	0.630	0.653	0.898	0.922	0.978
0.718	0.486	0.513	0.727	0.756	0.975
0.705	0.996	0.980	0.719	0.701	0.977
0.667	0.362	0.371	0.618	0.629	0.989
0.704	0.488	0.505	0.737	0.755	0.986
0.699	0.432	0.447	0.678	0.695	0.986
0.734	0.552	0.574	0.792	0.815	0.978
0.699	0.489	0.507	0.754	0.772	0.984
0.690	0.471	0.491	0.729	0.751	0.981
0.630	0.529	0.545	0.868	0.882	0.987
0.706	0.668	0.695	0.940	0.967	0.975
0.707	0.813	0.846	0.901	0.873	0.971
0.721	0.400	0.414	0.617	0.632	0.988
0.614	0.435	0.451	0.764	0.782	0.985
0.685	0.329	0.342	0.556	0.572	0.984
0.705	0.346	0.370	0.566	0.595	0.971
0.700	0.609	0.633	0.878	0.903	0.978
0.687	0.517	0.533	0.788	0.804	0.987
0.704	0.589	0.610	0.858	0.878	0.982
0.682	0.369	0.383	0.612	0.628	0.986
0.713	0.308	0.329	0.509	0.536	0.974
0.723	0.343	0.364	0.545	0.570	0.975
0.714	0.305	0.324	0.502	0.525	0.978
0.674	0.386	0.395	0.640	0.651	0.989
0.721	0.656	0.689	0.921	0.954	0.969
0.607	0.451	0.462	0.793	0.803	0.992
0.702	0.223	0.233	0.394	0.408	0.983
0.702	0.424	0.449	0.665	0.692	0.976
0.617	0.434	0.446	0.756	0.768	0.992
0.717	0.587	0.608	0.848	0.867	0.985
0.699	0.495	0.510	0.750	0.765	0.987
0.715	0.869	0.889	0.857	0.842	0.983
0.668	0.422	0.433	0.687	0.699	0.989
0.740	0.400	0.420	0.610	0.633	0.980
0.717	0.433	0.453	0.664	0.686	0.980
0.707	0.436	0.457	0.681	0.703	0.982
0.672	0.533	0.552	0.833	0.852	0.982
0.696	0.726	0.745	0.986	0.972	0.986
0.704	0.333	0.348	0.545	0.563	0.984
0.707	0.586	0.610	0.860	0.885	0.977
0.736	0.683	0.702	0.937	0.954	0.985
0.712	0.613	0.638	0.882	0.907	0.976

Table 21: (continued)

HC-HL	HC-SL	HC-SC	HL-SL	HL-SC	SL-SC
0.713	0.362	0.379	0.583	0.602	0.982
0.708	0.781	0.814	0.939	0.909	0.971
0.699	0.421	0.444	0.660	0.685	0.978
0.716	0.616	0.634	0.877	0.893	0.986
0.633	0.373	0.381	0.665	0.672	0.995
0.709	0.535	0.560	0.792	0.818	0.978
0.673	0.474	0.486	0.749	0.762	0.989
0.709	0.224	0.236	0.392	0.408	0.982
0.712	0.292	0.307	0.483	0.501	0.984
0.702	0.326	0.346	0.540	0.564	0.978
0.713	0.240	0.256	0.412	0.432	0.979
0.725	0.515	0.538	0.759	0.784	0.976
0.700	0.458	0.475	0.706	0.725	0.985
0.706	0.527	0.544	0.785	0.802	0.985
0.711	0.618	0.640	0.886	0.908	0.980
0.706	0.435	0.460	0.673	0.701	0.975
0.731	0.272	0.290	0.448	0.470	0.977
0.689	0.447	0.462	0.705	0.721	0.986
0.724	0.252	0.265	0.428	0.443	0.987
0.672	0.401	0.411	0.669	0.680	0.990

H Cumulative net fluxes of four models in simulation without rain

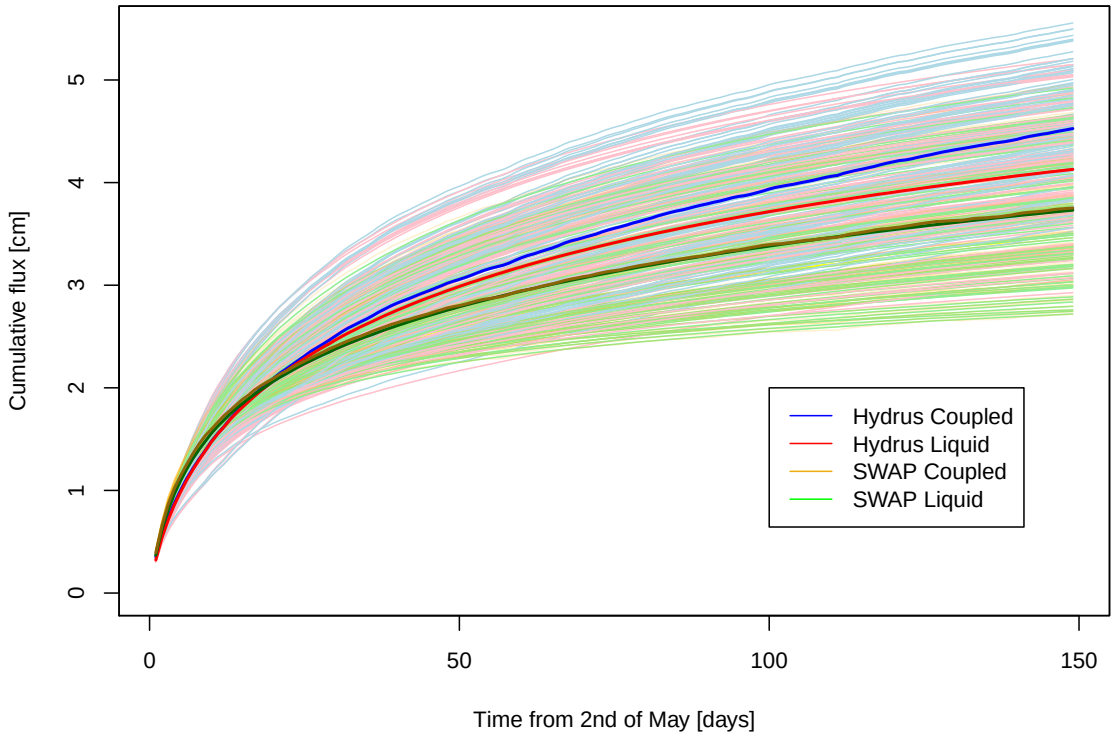

Figure 19: Comparison cumulative fluxes calculated with Hydrus Coupled and Liquid and SWAP Coupled and Liquid in a simulation without rain.

I Cumulative net fluxes of four models in simulation with rain

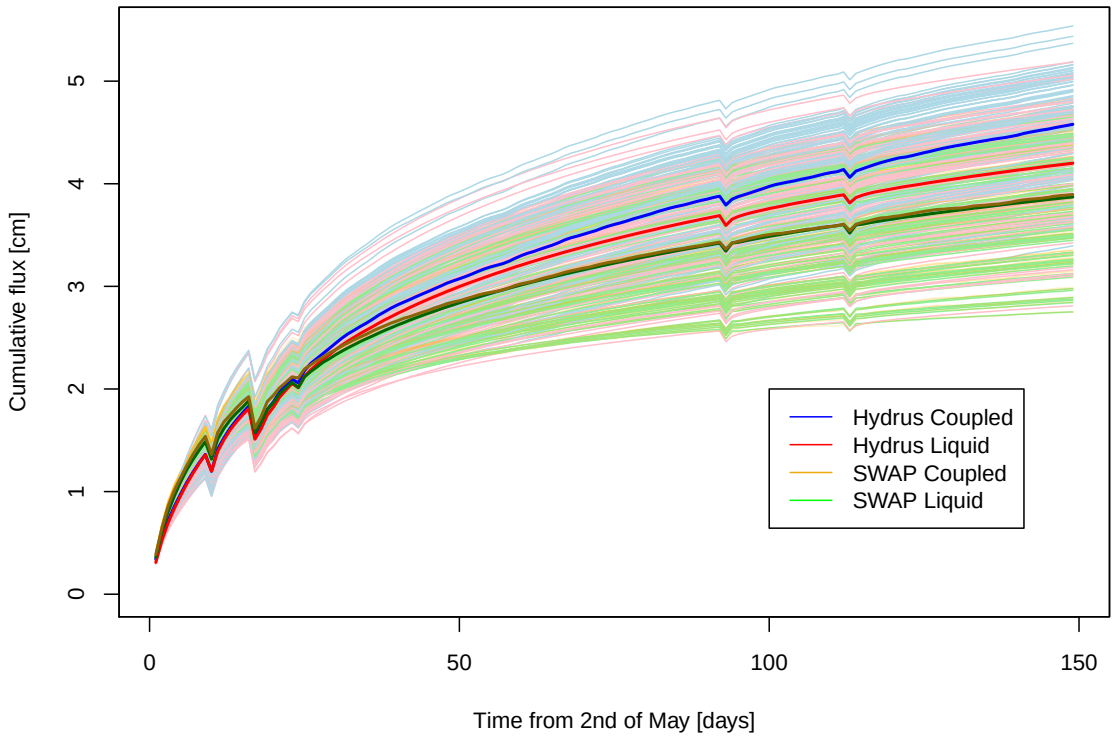

Figure 20: Comparison cumulative fluxes calculated with Hydrus Coupled and Liquid and SWAP Coupled and Liquid in a simulation with rain.

J Cumulative net fluxes of direct simulation 2

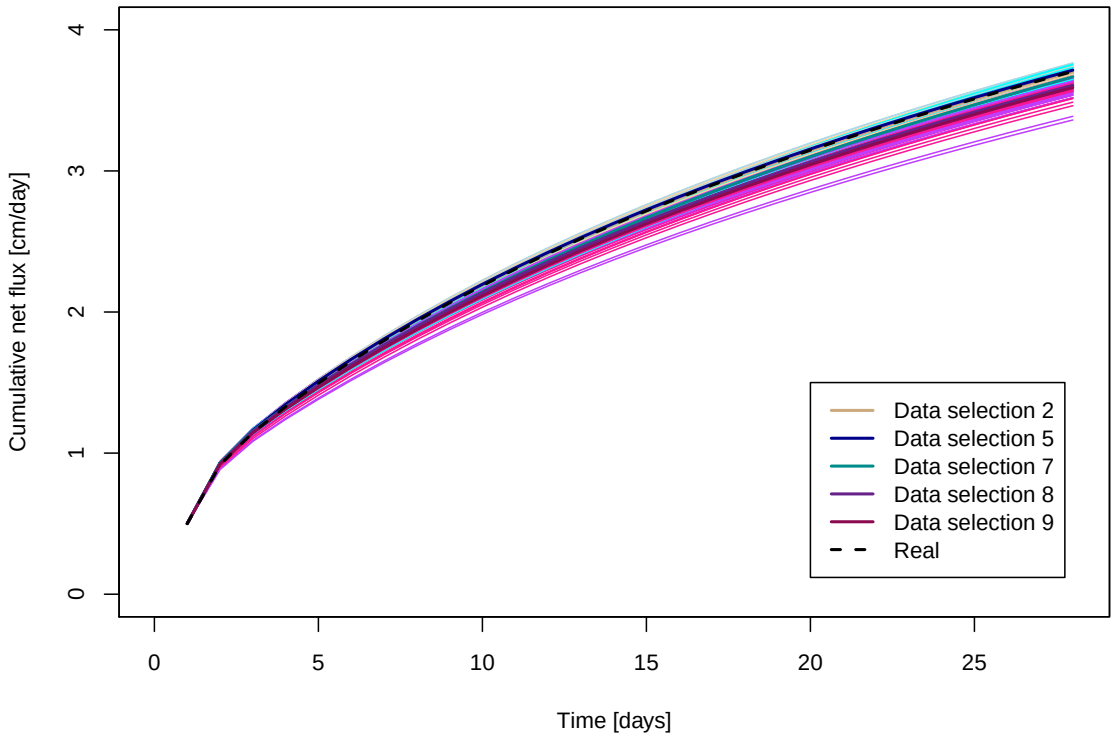

Figure 21: Cumulative net fluxes of direct simulation 2; 1% noise. Black line is the flux with the real parameters, the other lines depict the fluxes from a data selection from table 9.

K Cumulative net fluxes of direct simulation 3

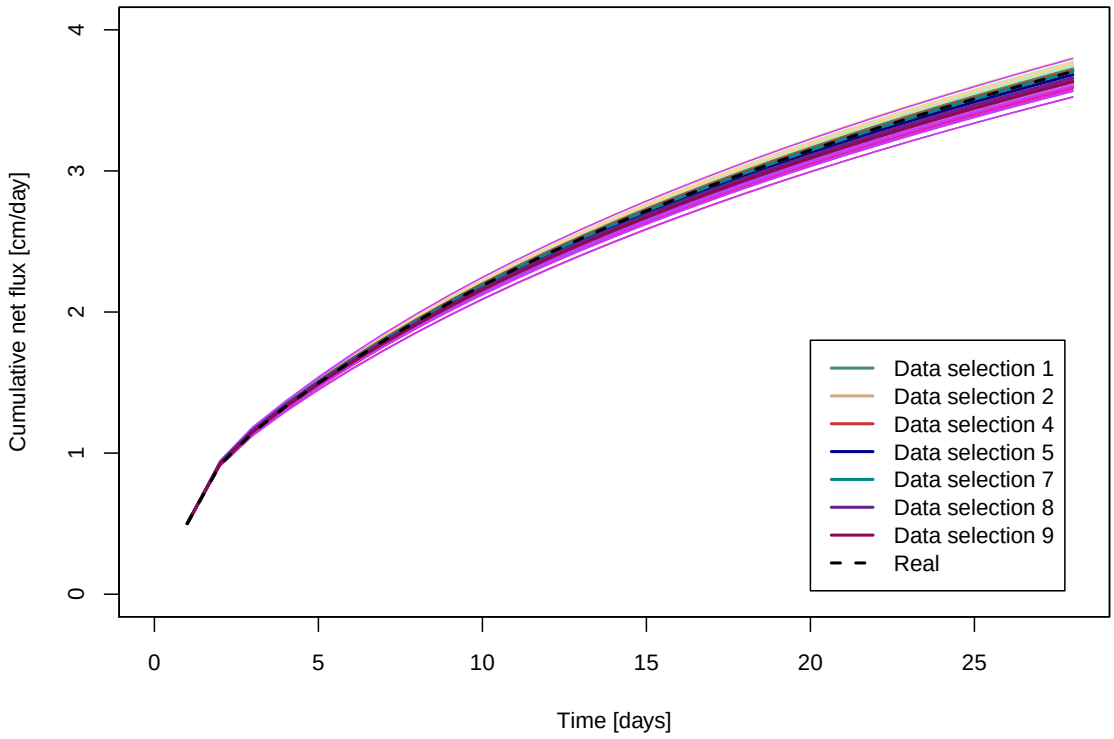

Figure 22: Cumulative net fluxes of direct simulation 3; one estimated soil thermal parameter b_3. Black line is the flux with the real parameters, the other lines depict the fluxes from a data selection from table 9.

L Cumulative net fluxes of direct simulation 4

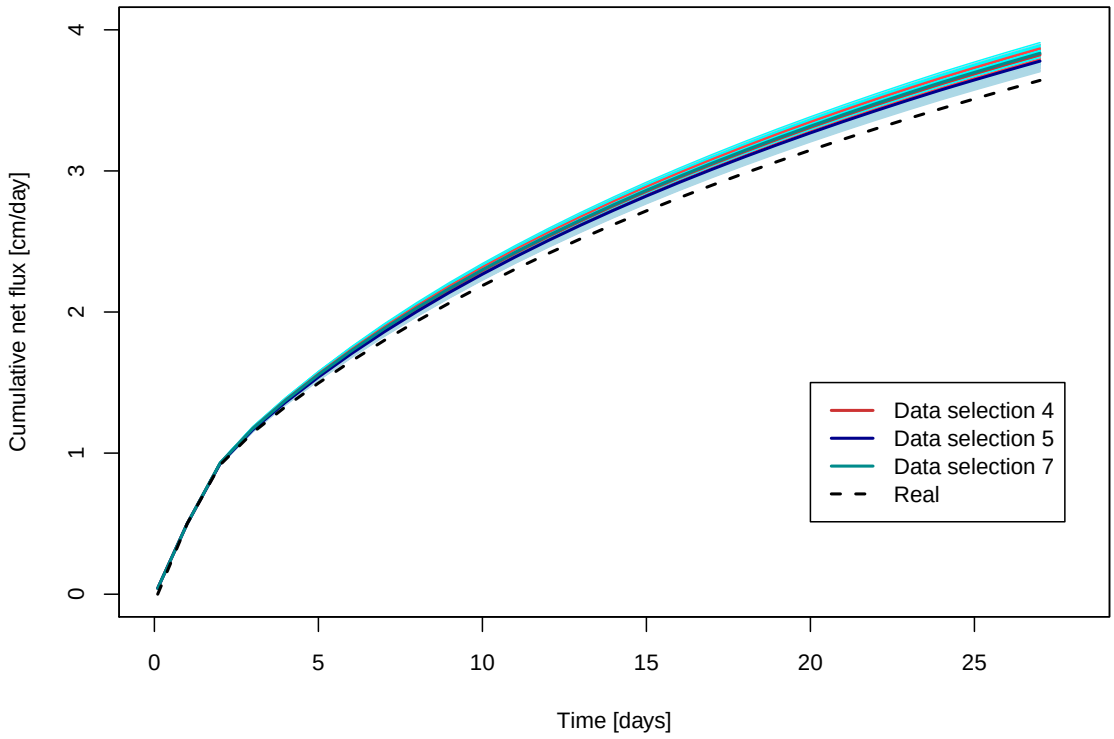

Figure 23: Cumulative net fluxes of direct simulation 4; model in seconds time scale. Black line is the flux with the real parameters, the other lines depict the fluxes from a data selection from table 9.

M Cumulative net fluxes of direct simulation 5

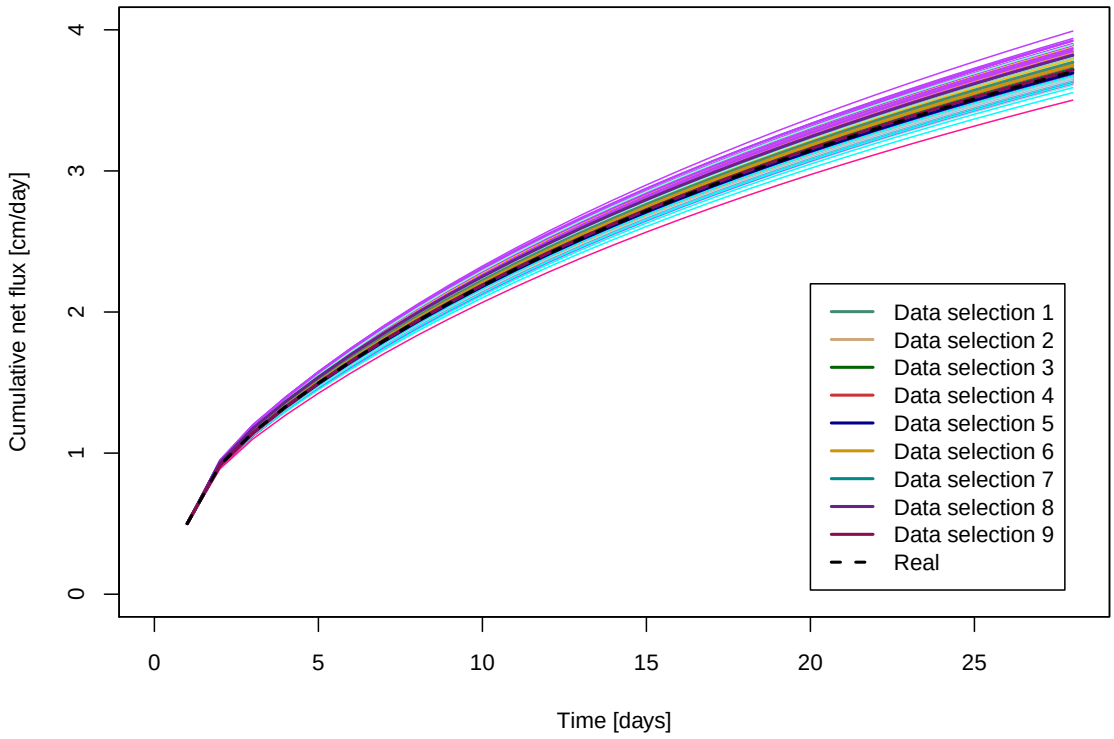

Figure 24: Cumulative net fluxes of direct simulation 5; initial estimate of shp closer to real shp. Black line is the flux with the real parameters, the other lines depict the fluxes from a data selection from table 9.